Thesis presented to the Instituto Tecnológico de Aeronáutica, in partial fulfillment of the requirements for the degree of Doctor of Science in the Graduate Program of Physics, Field of Nuclear Physics.

Everson Henrique Rodrigues

EFFECTS OF DARK MATTER AND SHORT-RANGE CORRELATIONS IN NEUTRON STARS

Thesis approved in its final version by signatories below:

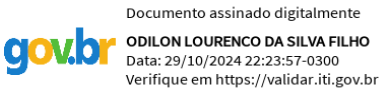

Prof. Dr. Odilon Lourenço da Silva Filho

Advisor

Campo Montenegro
São José dos Campos, SP - Brazil
2024

Cataloging-in Publication Data
Documentation and Information Division

Rodrigues, Everson Henrique
Effects of dark matter and short-range correlations in neutron stars / Everson Henrique Rodrigues.
São José dos Campos, 2024.
96f.

Thesis of Doctor of Science – Course of Physics. Area of Nuclear Physics – Instituto Tecnológico de Aeronáutica, 2024. Advisor: Prof. Dr. Odilon Lourenço da Silva Filho.

1. Neutron Stars. 2. Short-Range Correlations. 3. Dark Matter. 4. Nuclear Physics. I. Instituto Tecnológico de Aeronáutica. II. Title.

BIBLIOGRAPHIC REFERENCE

RODRIGUES, Everson Henrique. **Effects of dark matter and short-range correlations in neutron stars**. 2024. 96f. Thesis of Doctor of Science – Instituto Tecnológico de Aeronáutica, São José dos Campos.

CESSION OF RIGHTS

AUTHOR'S NAME: Everson Henrique Rodrigues
PUBLICATION TITLE: Effects of dark matter and short-range correlations in neutron stars.
PUBLICATION KIND/YEAR: Thesis / 2024

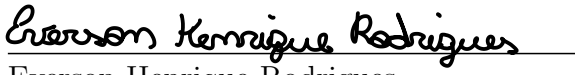

Everson Henrique Rodrigues
Rua Letônia, 573
12.231-150 – São José dos Campos–SP

EFFECTS OF DARK MATTER AND SHORT-RANGE CORRELATIONS IN NEUTRON STARS

Everson Henrique Rodrigues

Thesis Committee Composition:

Prof. Dr.	Brett Vern Carlson		-	ITA
Prof. Dr.	Odilon Lourenço da Silva Filho	Advisor	-	ITA
Prof. Dr.	César Henrique Lenzi		-	ITA
Prof. Dr.	Sidney dos Santos Avancini		-	UFSC
Prof. Dr.	Rodrigo Picanço Negreiros		-	UFF/CIT
Profª. Drª.	Maria Constança Mendes Pinheiro da Providência Santarém e Costa		-	UC

ITA

À minha companheira, aos meus pais, irmãs e sobrinha.

Acknowledgments

To the colleagues of the F2108, thank you all for the talks, coffees and beefs. You helped me to achieve a great sense of belonging. I aspire to meet you again someday. I will never forget you.

To the portuguese colleagues, thank you for teaching me portuguese. I hope some day to pay the debt teaching you the brazilian language. I wish to meet you again for a burrito. A special thanks to Milena, who was incredibly thoughtful and supportive during my days overseas.

I also thank Prof. Odilon for motivating and supporting me throughout the process, and Prof. Constança for advising me during my doctoral internship abroad.

To my parents, a special thank you for doing everything within your power to ensure I never lacked anything. Their hard work is an example of how much the Brazilian working class has to strive to obtain basic rights, such as education for their children. I will never forget the sacrifices you made. To my sisters, I am grateful for making my childhood so much brighter—you also played a part in helping me get here. To my niece, thank you for existing!

I am specially grateful to my wife, who supported me throughout the entire process. Thank you for being comprehensive, reliable and honest. Thank you for all the fun, travels, tips and love. You helped me stay grounded and were the best company anyone could ask for during the challenging times of the pandemic. I will never forget all that we build together. Part of this title is yours. At last, thank you Canela, you are the best ever!

"Ai daqueles e daquelas, entre nós, que pararem com a sua capacidade de sonhar, de inventar a sua coragem de denunciar e de anunciar. Ai daqueles e daquelas que, em lugar de visitar de vez em quando o amanhã, o futuro, pelo profundo engajamento com o hoje, com o aqui e com o agora, ai daqueles que em lugar desta constante viagem ao amanhã, se atrelem a um passado de exploração e de rotina."

— Paulo Freire

Abstract

In this study, we investigate the impact of dark matter (DM) and short-range correlations (SRC) on the physical properties of neutron stars (NS). In the second chapter we enhance a van der Waals-type model by incorporating the effects of short-range correlations (SRC). The attractive and repulsive components of the nucleon-nucleon interaction are treated as density-dependent functions. Specifically, we adopt the Carnahan–Starling (CS) approach for the repulsive term and employ a suitable expression for the attractive term to replicate the Clausius (C) real gas model structure. The resulting model, referred to as the Clausius–Carnahan–Starling (CCS)-SRC model, demonstrates its capability to reproduce the flow constraint at high-density regimes of symmetric nuclear matter, with incompressibility values within the range of $K_0 = (240 \pm 20)$ MeV.

In the context of stellar matter, the CCS-SRC model shows good agreement with recent astrophysical observations, including mass-radius contours and dimensionless tidal deformability constraints obtained from gravitational wave data associated with the GW170817 and GW190425 events, as well as observations from NASA's Neutron Star Interior Composition Explorer (NICER) mission. Furthermore, the slope of the symmetry energy (L_0) predicted by this model aligns with recent results, consistent with those reported by the updated Lead Radius Experiment (PREX-2) collaboration. Our findings indicate that higher values of L_0 are preferred for ensuring simultaneous compatibility with astrophysical data, while lower values of L_0 fail to meet this criterion.

In the third chapter, we incorporate dark matter (DM) and SRC into the relativistic mean-field model FSU2R using the fermionic and bosonic dark matter models. Both models include a repulsive vector interaction, which is particularly crucial for the bosonic model, as it prevents the collapse of the star in the absence of degeneracy pressure. We explore its effects on the mass-radius (MR) diagram. Our findings show that both fermionic and bosonic DM models influence the MR diagram in a similar manner. The inclusion of SRC results in a notable increase in the maximum mass of NS balancing the reduction yielded by the inclusion of DM. Our findings suggest the existence of potentially stable configurations of neutron stars that are consistent with observations from PSR J0030+0451, PSR J0740+6620 and NICER.

List of Figures

List of Tables

List of Abbreviations and Acronyms

NS	neutron Star
EoS	equation of State
RMF	relativistic mean field
SRC	short-range correlations
NM	normal matter
DM	dark matter
TOV	Tolman- Oppenheimer-Volkoff
BHF	Bruenecker-Hartree-Fock
RBHF	Relativistic Bruenecker-Hartree-Fock
QCD	quantum chromodynamic theory
fm	femtometer
GeV	giga-electronvolt
TeV	tera-electronvolt
WIMPs	weakly interacting massive particle
GCE	gran-canonical ensemble
vdW	van der Waals
DD-vdW	density dependent van der Waals
CS	Carnahan-Starling
SNM	symmetric nuclear matter
ANM	asymmetric nuclear matter
CCS	Clausius-Carnahan-Starling
CCS-SRC	Clausius-Clayperon-Starling with short-range correlations
ADM	asymmetric dark matter
FDM	dark matter fraction

Contents

1 Introduction

The universe possesses many kinds of interesting structures and among them compact objects, remnants of massive stars (mass bigger than six to eight times that of our sun) that can be identified as stellar black holes, white dwarfs and neutron stars (NS), with these later system subject of intense studies nowadays. They are one of the densest objects in the universe and their internal structure is not fully known. The high-density environment found in these objects makes them excellent natural laboratories for the study and development of nuclear physics theories. Likewise, progress in theoretical modeling could help to predict and outline the internal content and thermodynamics of NS.

The number of NS is estimated to be around one billion in Milky Way, but only a few thousand have been already observed (CAMENZIND, 2007). However, this scenario has been changing with advances in observational technologies of gravitational waves and high-frequency telescopes. The operating missions such as the Neutron Star Interior Composition Explorer Mission (NICER) and interferometers such as the Laser Interferometer Gravitational-Wave Observatory (Abbott *et al.*, 2009, LIGO), VIRGO (Accadia *et al.*, 2012) and KAGRA collaboration have increased on a daily basis the number of detected objects. The fourth LIGO observation run started in the middle of 2023 with a sensitivity of 160-190 megaparsecs (Mpc) for binary neutron star mergers. That means an increase in sensitivity of 35%, and certainly, a large amount of data (LIGO-CALLTECH, 2022).

With the NS data increasing and the constraints brought by modern telescopes and interferometers, theoretical research in nuclear physics is more than ever a prominent field, from which many scientific developments are expected to come.

1.1 Neutron Stars

Initially, it is indispensable that one understands what is a neutron star and how it is formed. Neutron stars are the final evolutive stage of stars with masses greater than 8-10 solar masses (CAMENZIND, 2007). Such stars, in their final moments, such stars have accumulate in their core elements of the iron family. Fe has the highest binding energy, so further fusions do not happen anymore in that region. Immediately outside the core, a

silicon shell is still being converted into iron. That implies in a Fe-rich region expanding until it gets close to the Chandrasekhar mass.

Without producing energy, gravity promotes a contraction in the inert iron core (FOGLIZZO, 2017). Because of the compression, Fe nuclei starts to capture electrons, reducing the outwards electron pressure inside the core and emitting neutrinos. These neutrinos carry energy away from the star, increasing, even more, the inwards pressure and so the density. With high densities (10^{10} g cm^{-3}) (CERDA-DURAN; ELIAS-ROSA, 2018), photons from the electron capture and other sources trigger the photo-disintegration of iron nuclei, which starts to decay into α particles (KIPPENHAHN *et al.*, 2013). The sequence of events that dictates the final of the star's life is now complete. From there on, the star core can not counter the self-gravity, so it will collapse in the next few minutes.

The processes of cooling and the loss of leptons by the star's core speed up the star's collapse by decreasing its temperature (NEGREIROS *et al.*, 2018; FISCHER *et al.*, 2016). Density increases up to 10^{12} g cm^{-3}. With such high density, not even neutrinos escape from the core, the deleptonization stops and the temperature stagnates. Rapidly the beta-equilibrium is achieved, which means that no more neutrinos are generated and the net number of electrons remains stable. With no more energy escaping, the core keeps shrinking to the point that atomic nuclei are disintegrated into their nucleon components (HANSEN *et al.*, 2012). This process will stop when the densities reach nuclear values, with repulsive short-range forces starting to act and matter becoming almost incompressible. At a certain point, the interaction between nucleons is the most significant source of pressure and the contraction stops (JANKA, 2012).

After stopping the contraction, external parts of the core that are shrinking to centre shock with the 10 kilometers radius stiffened region, rebounding towards the outer parts which are still falling. When the collision happens, a shock wave is formed. The kinetic energy transmitted by the shock photo-dissociates the softer core parts, and as a consequence shock weakens, stalling about 100 kilometers from the centre, propagating now in a non-radial direction. In that way, the shock wave is not sufficient enough to expel the other layers of the onion-structured star (JANKA, 2012; CERDA-DURAN; ELIAS-ROSA, 2018).

What happens next is uncertain. The more accepted theory, supported by modern computational simulations says that under specific conditions a small fraction of the energetic neutrinos coming from the photo-dissociation can be retained behind the shock. Neutrino's energy will then revive the shock, promoting its expansion through the outer core and other strata of the star. This mechanism is called delayed neutrino heating, it will explode the star, expelling most of the star's core together with all external layers (JANKA; MÜLLER, 1996; BURROWS *et al.*, 1995; BETHE; WILSON, 1985). The about 10 kilometers core remnants, a super-dense region composed basically by nucleons and other

fundamental particles, become the so-called neutron star. It is worth mentioning that if the neutrino heating fails for whatever reason, the mass excess will promote a gravitational collapse that will break even the short-range repulsion, what emerges then is a stellar black hole (CERDA-DURAN; ELIAS-ROSA, 2018).

The neutron star is usually divided into five structures, from innermost to outermost, they are inner core, outer core, inner crust, outer crust and atmosphere. Some authors consider another region between the crust and the atmosphere, called envelope or ocean. In this work, we will not use this division, but we consider the ocean as a part of the outer crust.

The atmosphere is the NS's thinnest part, with a few centimeters thick. It has as main component ionized hydrogen atoms and a plasma of electrons, once heavier elements will probably be gravitationally attracted to the star's interior. In despite of the fact that the atmosphere is thin, it is fundamental to the modeling of the electromagnetic spectrum. From observations of the X-ray spectra emitted by this region, one can deduce properties of the star such as effective temperature and magnetic field pattern (POTEKHIN *et al.*, 2015). Furthermore, in a non-trivial and under specific conditions (e.g. being in a binary system), one can obtain pieces of information from the atmosphere about neutron star's radius and temperature. (DEGENAAR; SULEIMANOV, 2018)

Innermost to the atmosphere, one may find the outer crust. In this region, the relatively low density still allows nucleons to group as heavy atomic nuclei. Thence, the outer crust is composed of ions and electrons. Its typical densities go from 10^4 g/cm^3 to 10^{11} g/cm^3 (Piekarewicz, 2022). At the lower density areas, the nucleons are grouped mainly as ^{56}Fe. Moving to densest regions, one may also find, for example, ions of ^{62}Ni, ^{66}Ni, ^{84}Se and even ^{97}Kr (Rüster *et al.*, 2006; Antić *et al.*, 2020). As matter of fact, several other elements and isotopes exist within the outer crust and this topic has been largely investigated with advances in computational methods such as neural networks, machine and deep learning (NEUFCOURT *et al.*, 2020; LOVELL *et al.*, 2022).

The third NS region is the inner crust. There the density has grown to the point that atoms suffer inverse β-decay becoming neutron-rich. With density continuously growing, the permanence of nucleons inside nuclei is no more energetically favorable, so the neutrons start to drip off the nuclei. The density in which such a phenomenon happens is known as neutron drip density and the region where it first occurs is the beginning of the inner crust. As one goes to most internal regions the medium is even more neutron-rich. At this region's top places, the atomic nuclei are still relatively well organized in a lattice, but now with a neutron gas filling the structure. The neutrons inside the gas will form Cooper pairs, analogously to what happens with electrons in terrestrial superconductors (PAGE *et al.*, 2009; GRABER *et al.*, 2017).

At the bottom of the inner crust, nucleons are dissolved in the environment, so the long-range Coulomb repulsion amidst nuclei does not exist anymore. In that regime, the pressure is enough to sufficiently approach nucleons in a way that the short-range attraction is comparable to the long-range Coulomb force. That will lead to the called "Coulomb frustration". The matter then organizes itself as a "nuclear pasta", a complicated and without terrestrial counterpart structure (Piekarewicz, 2022; DEGENAAR; SULEIMANOV, 2018). With densities of one to two times the nuclear saturation density (ρ_0), no more atomic nuclei will be found. The nuclear pasta decomposes into neutrons, a small fraction of protons and electrons marking the beginning of the outer core. Muons will also be found and all these nucleons (and muons) are in beta and chemical equilibrium. Neutrons are expected to be in a super-fluid state, behaving as a superconductor (Sauls, 2019; Lopez *et al.*, 2022).

Inwards to the outer core, densities will surpass ten times the saturation density, marking the transition to the inner core (DEGENAAR; SULEIMANOV, 2018). Above $10\rho_0$, due to the high Fermi energies, it is energetically favorable to form hyperons than keep adding protons and neutrons to the medium (OERTEL *et al.*, 2015). Apart from hyperons, other exotic matter states are also believed to exist, such as pions, kaons and deconfined quarks. However, our poor knowledge of the strong interaction behavior under high densities restricts the theoretical calculations and so further conclusions. (Piekarewicz, 2022)

Our knowledge about regions such as the atmosphere and the outer crust of neutron stars is relatively well established. Direct observations from electromagnetic spectra (e.g. X-ray) and the use of constraints from terrestrial laboratories (as finite nuclei experiments) (Carlson *et al.*, 2022) allow us to set with some certainty its micro-physics and compositions. In another way, if one is treating the inner core, outer core and bottom layers of the inner crust, the description of its phenomenona relies mainly on theoretical models constrained by astronomical or nuclear observations. Those models are expected to reproduce the nuclear properties observed in finite nuclei. Some properties to be obtained are the binding energy, the saturation density, and the symmetry energy, also called bulk parameters. Furthermore, one should also obtain consistent thermodynamics, summarized in the equations of state (EoS).

The equations of state are essential quantities used to determine the mass and radius of NS, found by solving a set of coupled differential equations, named as Tolman-Oppenheimer-Volkoff (TOV) equations (OPPENHEIMER; VOLKOFF, 1939a; TOLMAN, 1939a). They are a direct consequence of general relativity. In the NS, the matter is so concentrated that Newton's gravity is no longer enough to describe the massive interaction, so one must consider the correction into the hydrostatic equilibrium equations. For a star static, spherically symmetric and with a negligible magnetic field the TOV are given by

$$\frac{dP(r)}{dr} = -\frac{[\epsilon(r) + P(r)][m(r) + 4\pi r^3 P(r)]}{r^2\left[1 - \frac{2m(r)}{r}\right]}, \qquad \frac{dm(r)}{dr} = 4\pi r^2 \epsilon(r). \tag{1.1}$$

The relationship between pressure $P(r)$, energy density $\epsilon(r)$ and density ρ is dictated by the EoS. It is worth mentioning that EoS are not unique for a neutron star. For instance, it is common to describe a single neutron star writing different EoS for its different regions. As EoS are related to energy density and pressure, it is natural to expect that its form is linked to the description of the system microphysics, or at least reproduce its observable in a satisfactory way. Many approaches are possible to construct the EoS. There are multiple types of models and treatments. They may be relativistic or not, phenomenological or not, with hadrons only or also including quarks, and so on. Some of models will be discussed in the next section. Those used in this work will be described in a more specific and complete way in the next chapters.

1.2 Main models and treatments

1.2.1 Brueckner-Hartree-Fock Treatment

An important class of methods is the *ab initio* methods, in which realistic interactions are considered. The most used in this context is the Brueckner–Hartree–Fock (BHF). In this approach, the interaction of every particle is considered. The effective potential acting in one particle is taken as a combination of the potential generated by all others. The effective interactions are concentrated in the G-matrices, which arise from the solutions of the Bethe-Goldstone equation (BETHE, 1971), written in a first chosen basis. The G-matrices will compose the Hartree–Fock equations, becoming from the energy minimization using the variational principle.

In this way, for a n-particle system, an *ansatz* state is proposed as a set of n single-particle functions. Another set should be found by using the first one applied into the Hartree–Fock equation. This new set will generate new G-matrices, which should generate another set of solutions. This procedure is taken iteratively until one achieves the desired convergence. By using this procedure one should find the individual energies of each particle (RING; SCHUCK, 2004). From the obtained G-Matrix, the thermodynamics and bulk parameters emerge. Although this method was conceived as a quantum method, a three decades old relativist treatment (RBHF) also has been used in several works (TONG

et al., 2022; ZHANG *et al.*, 2022; SHEN *et al.*, 2016), increasing the range of applications as well as the model's quality in terms of experimental data reproduction.

A work done using the BHF is the one by Fan *et al.* (2022). In their study, the called extended BHF was applied to finite nuclei. The authors modified the model to include in it the proton-neutron short-range correlations. This kind of correlation receives a detailed discussion forward in this work. Once with the theoretical results, they compared it with data from nuclear experiments, finding a satisfactory correspondence. Afterward, they applied the constructed model to several isotones of multiple elements, finding that the number of correlated pairs for a same element increases with the number of neutrons in it.

The BHF or the RBHF are powerful treatments, however, multiple problems can arise. The G-Matrices are frequently energy-dependent and this energy dependency is not uniquely defined. This can lead to a difficulty that is choosing the most satisfactory dependence form. Besides, if one is treating very large and complex systems with the RBHF, G-Matrices will certainly generate unfriendly math. Another usual problem is the change of basis in each iteration. Once G-Matrices have been changed after iteration, the initial basis also has to be changed. That sequence of required changes leads to a considerable numerical effort. (SHEN *et al.*, 2016; Oertel *et al.*, 2017)

1.2.2 Skyrme and Gogny Models

First proposed by T.H.R. Skyrme (1958), the Skyrme model belongs to a class of the non-relativistic phenomenological models, in which a set of parameters is fitted to reproduce the nuclear matter and/or finite nuclei properties. This approach no longer can be understood as an *ab-initio* one.

Nuclear forces are known to be of a short range. If one is using a realistic description the acting forces should have a finite range. In that way, some phenomenological models assume that particles only interact if they are in contact, that is, the force only acts if the distance between particles is zero. This kind of treatment is called zero-range treatment. This is the approach taken by the Skyrme model, in which the effective potential carries a dependence on Dirac's function. Once the potential depends on the delta function instead of more complicated ones, the model is very simple to be treated (SKYRME, 1958; RING; SCHUCK, 2004).

In its original form, the Skyrme potential presents a three-body term added to a two-body interaction term written as a short-range momentum expansion. The three-body interaction term contributes with a parameter to be settled and the two-body with seven. Vautherin e Brink (1972) shown that the three-body interaction term is equivalent to

a density-dependent two-body term. Such formalism is powerful because it allows the inclusion of the microscopic density dependence, as a phenomenological representation, into the Skyrme model. One may notice that it is usual to treat Skyrme potential under mean field approximations (which will be discussed in more detail later) and was used by Vautherin e Brink (1972). Several notorious applications of Skyrme-like models have been done in the past century. Vautherin e Brink (1972) have calculated the binding energy and the nuclear radii of multiple chemical elements. Beiner *et al.* (1975) have studied the effects of pairing and deformation correlations on the binding energy.

As may be clear now, calculations using the Skyrme potential will generate density-dependent equations of state. For that reason, if one uses it in systems with high densities, divergences can appear. Recently, authors have proposed many extensions to the original Skyrme model over the years, intending to use this kind of model in systems such as Neutron Stars. A detailed review of a huge collection of models can be found in Dutra *et al.* (2012). Besides, successful applications in NS are described in works such as Tsang *et al.* (2019) and Zhang e Chen (2016).

Zero-range models such as the Skyrme model can lead to divergences when describing some phenomena such as pairing correlations. To solve problems related to contact-only interaction, Gogny proposed a model similar to the Skyrme one, but instead of Dirac's delta functions, he proposed functions with a finite acting range. As an advantage, one may notice the possibility of describing the realistic medium and long-range part of the interactions with this kind of representation (DECHARGÉ; GOGNY, 1980).

As Gogny-like models use finite range functions, it is more laborious to construct and apply it. The expressions generated are more sophisticated and demand more effort to do the numerical calculations. Being so, very few alternative Gogny models have been proposed since the original one, although, some recent applications can be seen in the context of neutron stars. Mondal *et al.* (2020) constructed in his work an EoS for the inner crust using three finite range Gogny forces, considering pairing correlations and their influence in the global properties of the NS as mass and radius. Another prominent work is (Viñas *et al.*, 2021) in which a new Gogny model was built aiming to generate stiffer EoS for NS, keeping the already good description of finite nuclei. With the model ready, they compared the results achieved to other well-settled models, finding a good agreement with observational data.

Even being powerful methods, Skyrme and Gogny models have some limitations. The first and more obvious one is the fact that they are non-relativistic. A huge analysis done by Dutra *et al.* (2012) has shown that for more than 200 different Skyrme-like models, only half a dozen satisfy all the required constraints. In another hand, 66 of them satisfy all except one, which is still a good result for a relatively simple model.

1.2.3 Other models

Models such as the Skyrme and Gogny or treatments such as the (Dirac-)Brueckner-Hartree-Fock are the most famous used to describe finite or infinite nuclear matter, as well as NS. Many other models exist, though. Within the class of *ab initio* methods, we highlight some: Green's function, variational, quantum Monte Carlo and perturbative quantum chromodynamics methods(Oertel *et al.*, 2017). Within the class of the phenomenological, the remnant fundamental type of model is the one with meson-exchange in the relativistic mean-field approximation. These models are called RMF and will be discussed in the next section.

Some models can arise directly from adaptations of thermodynamical descriptions of real or quantum gases. This class of model is useful due to its simplicity. With a relatively simple form, one can try to incorporate complex phenomena present in the nuclear matter such as the so-called short-range correlations (SRC).

1.3 Short-range correlations

To understand the SRC, one must first look into a specific way of describing nuclear matter. Inside the atomic nuclei, nucleons can be considered Fermi particles. Being so, it is valid to describe the core as a bound system composed of interacting fermions. Within this context, each component particle must be restricted to a maximum momentum and energy, the Fermi ones. To obtain the complete form of energy, one must solve the N-body Schrödinger equations considering the potential outcoming from each one of the other nucleons.

An alternative approach is the called "shell model". In this treatment, the nucleon is supposed to move independently of all others, under an average potential from the remaining nucleons and generated by the strong interaction (HEYDE, 1994). The shell model is successful to describe many atomic nuclei, predicting shells filled for atoms with 2, 8, 20, 28, 50, 82 or 126 protons or nucleons. (Souza *et al.*, 2020).

Disagreeing with the shell model, studies from the late years of the twentieth century and modern scattering experiments have shown that of all nucleons, only 75 to 80% are in the independent state. The other 25 to 20% are linked in pairs to other nucleons. An important work regarding this matter is the one by Ramos *et al.* (1989). In their study, the authors investigated the role of short-range correlations in shaping the single-particle properties of nuclear matter, employing the self-consistent Green function (SCGF) method within the ladder approximation. Unlike conventional Brueckner-Hartree-Fock (BHF) approaches, the SCGF framework treated particle-particle (pp) and hole-hole (hh)

propagations symmetrically, capturing both attractive and repulsive contributions to the self-energy. They used Reid's soft-core interaction, a semi-realistic nuclear potential, to avoid pairing instabilities and ensure numerical stability. The primary objective of the study was to compute the self-energy, spectral functions, and momentum distributions at various densities, offering a detailed view of how short-range forces modified nucleon interactions. This method provided refined predictions of quasi-particle properties, such as effective masses, which are essential for understanding nuclear dynamics.

The findings revealed that short-range correlations redistributed a significant fraction of the single-particle strength to high-energy states, contradicting the traditional assumption that most nucleon strength is concentrated near the Fermi surface. The study reported a depletion of approximately 13% in the momentum distribution at normal nuclear densities, caused by the inclusion of high-momentum components stemming from short-range repulsions. Additionally, by incorporating both pp and hh propagations, the model captured critical contributions to the nucleon self-energy, particularly at high densities, where hole-hole correlations became increasingly relevant. Ensuring consistency between these interactions enabled accurate calculations of the real and imaginary components of the self-energy, providing deeper insights into the energy broadening of nuclear states.

The results suggested that the quasi-particle model remained relevant across a broader range of energies in nuclear matter compared to simple Fermi liquids. The authors emphasized that while the shell model remained effective for describing nuclear structure at low excitation energies, it had to be supplemented with corrections for short-range correlations to align with experimental observations. This integration of quasi-particle theory with advanced correlation treatments allowed for a more accurate description of phenomena such as partial shell occupancy and quenching of transition strengths.

In the beginning of the twentieth one century, an experiment using electron-induced quasi-elastic knockout shed light on the effects of short-range correlations. In these experiments, a nuclear target was hit by electrons expelling a nucleon from the core. Surprisingly, in 20 to 25% of the cases another nucleon was also expelled, leading to the conclusion of some kind of correlation. (CLAS Collaboration, 2018)

Experiments also have shown that the correlated pairs possess relative momentum higher than the Fermi one, but with centre-of-mass momentum smaller. The graphics of the distribution function of the nucleons versus the Fermi momentum is now modified due to the inclusion of SRC. The high-momentum nucleons will originate a tail beyond the Fermi momentum k_F. That tail is known as the high-momentum tail, or shortly, HMT. (CLAS Collaboration, 2018; CAI; LI, 2015a)

It is worth mentioning that SRC act in intermediate to short distances (< 1.2 fm). In this way, the study of SRC is fundamental to help improving our knowledge about the

dynamics of the quantum chromodynamic theory (QCD). In so short distances, interesting subnuclear effects could appear and phenomena such as quark interchanges and chiral symmetry probably have an important role. Indeed, Fomin *et al.* (2017) have argued that superfast quarks could be probed by the short-range correlations if it was explored with higher energy colliders. More than that, the authors argued that studies in this direction will probe the QCD under extreme conditions, opening many possibilities to explore the nuclear medium with the chromodynamics theory.

In addition to applications in subnuclear physics, the SRC also has been applied within the context of high-density physics, more explicitly, in NS modeling. Recent works have shown that this correlation strongly influences NS properties and its EoS. In recent work, Hen *et al.* (2015a) have calculated, using many-body theories, the correction to the symmetry energy promoted by the insertion of SRC. The value found was very smaller than the symmetry energy for the matter without correlations. The significant difference between values with and without SRC changes considerably the slope and skewness of the system. The slope is proportional to the first derivative of the symmetry energy and the skewness to the second.

Another rich discussion was done by Souza *et al.* (2020). In their work, SRC were included in an RMF modeling, named as RMF-SRC. From this model, they obtained the corresponding EoS and mass-radius diagram. For a mass of $1.4M_{\odot}$ they found a radius value compatible with the NICER data (Miller *et al.*, 2019). Comparing the cases with and without SRC, it was clear that the EoS with the effect included become stiffer. They also showed that the inclusion of SRC favors the tidal deformability (TD) to be in accordance with observational data. Tidal deformability (Λ) measures how prone a star is to deform due to tidal force. Higher tidal deformability means that a star is more prone to deform. The value of TD for a $1.4M_{\odot}$ neutron star must be of $\Lambda_{1.4} = 190^{+390}_{-120}$ (Abbott *et al.*, 2018) and authors have found a value of $\Lambda_{1.4}$ inside the confidence interval, what did not happen without SRC. In general, authors have demonstrated that the inclusion of SRC could help to find mass-radius diagrams and tidal deformability in agreement with observational data.

Several other works have included SRC in treatments of finite or infinite nuclear matter, as the reader can found in Souza *et al.* (2020), Guo *et al.* (2021a), Lu *et al.* (2021) and Dutra *et al.* (2022),for instance. Due to the importance of inclusion and utilization of SRC in NS description, we will consider this phenomenon in the next sections, since the comprehension of its effects in hadronic models and NS properties is the main objective of this study.

1.4 Dark matter content in neutron stars

The term "dark matter" was first used by Zwicky (1937) in his study of clusters of nebulae, which are now identified as galaxies. Zwicky's initial aim was to propose new methods for determining the masses of these nebulae. By applying the virial theorem to the cluster, he anticipated that the average kinetic energy of the group would equal minus half of the average potential energy, assuming the system was stable and gravitationally bound. However, based solely on gravitational effects, he found that the mass required to satisfy the virial theorem was significantly greater than that inferred from galaxy components luminosity. This indicated the presence of an unseen mass component, which he called dark matter.

Approximately thirty years after Zwicky's work, another seminal study by Rubin e Ford (1970) demonstrated that visible matter alone could not sufficiently explain the rotational patterns of galaxies. In this study, which was focused on the Andromeda Galaxy (M31), they discovered that M31's rotational velocity does not decrease in its outer regions. A decrease in velocity was expected because the luminosity is significantly lower in the galaxy's most distant parts. Therefore, the conclusion once again, was that visible matter alone could not account for the dynamics of these large celestial structures, so another undetectable kind of matter should exist.

These two works laid the foundations for the definition of dark matter (DM): a type of matter that does not emit, absorb, or reflect light, being detectable only by its gravitational effects. Nowadays, we believe that visible matter represents only 10% to 20% of galaxy clusters, result found by the use of gravitational lensing (Natarajan *et al.*, 2024). Besides, studies in the context of X-ray emission have contributed to understanding the nature of dark matter. Regarding this topic, the work by Clowe *et al.* (2006) can be considered a milestone. Their analysis of X-ray emission revealed that most of its mass is separated from the gas region, indicating that dark matter and baryonic matter are distinct entities. Finally, the Planck Collaboration results obtained from the Planck satellite, indicates that considering large-scale structures: galaxy filaments, super-clusters, and others with sizes of tens of Mega-parsecs, the amount of normal matter is approximately 15% of the total matter (Planck Collaboration, 2020).

Considering the presence of dark matter in large and medium-scale astrophysical structures and its interaction with normal matter, it is reasonable to expect its presence among other massive objects. A probable candidate to concentrated DM would be neutron stars. This scenario is particularly favored by the description of dark matter as weakly interacting massive particles (WIMPs), which are massive, stable, electrically neutral particles with masses typically ranging from 10 GeV to several TeV (SCHUMANN, 2019; ROSZKOWSKI *et al.*, 2018; GRIEST; KAMIONKOWSKI, 1990). Due to the high densities and strong grav-

itational fields, neutron stars could capture and accumulate DM. Such accumulation is possible because WIMPs constitute cold dark matter, meaning that the dark particles travels at relative low velocities and can be trapped by neutron stars (GOLDMAN; NUSSINOV, 1989), leading to several observational effects such as changes in thermal evolution, mass-radius relations, and tidal deformability of neutron stars (YOUNG, 2016; DELIYERGIYEV *et al.*, 2019; LOURENÇO *et al.*, 2022).

To describe the influence of dark matter in the neutron star environment, one must rely on modeling. This necessity arises mainly due to the unknown composition and interaction mechanisms of dark matter, both with itself and with normal matter. Regarding the interaction mechanisms, two primary descriptions can be employed for dark matter studies in neutron stars. One approach involves the usage of Lagrangian with the Higgs portal mechanism. This mechanism posits that fields related to the dark particles, often assumed to be scalar, interacts with the ordinary matter particles by coupling with the standard model Higgs field. Within this formalism, to describe a neutron star in the presence of DM, usually are inserted in the Lagrangian a coupled term that contains both, the DM field and the Higgs field. That changes the star equation of state, resulting, among several other effects, in consequent changes in the relation between mass and radius of the star (LOURENÇO *et al.*, 2022).

Another approach possible to describe the DM in the NS is to consider DM as independent of the ordinary matter, coupling with it only gravitationally. This is a coherent choice if one considers that much of the dark matter properties are still unknown. For example, one can not precise the way that the dark matter field interacts with the standard model fields, hence, is reasonable to treat only the gravitational interaction of both matters, what is done by altering the TOV equations. It now becomes a system of four coupled equations, taking into account the dark matter energy density and the dark matter pressure, in addition to the ordinary ones. These set of equations can lead to quantities that are already constrained by observations, to cite some, tidal deformability and mass-radius relations.

This approach has been widely used, Xiang *et al.* (2014) for example, use it to study the possible presence o dark matter halos in neutron stars, that is, the surpass of the dark matter radius in relation to the ordinary matter radius. Das *et al.* (2022) used it to find a range of possible values for the dark mass particle by applying a Bayesian analysis. Miao *et al.* (2022) used it to study the influence of the dark halos on the pulsar profiles. In this work, we the two fluid formalism was also chosen rather than the Higgs portal description.

Similarly to what happens in the presence of only ordinary matter, to solve the set of Tolman-Oppenheimer-Volkoff (TOV) equations, one must provide the relation between pressure and energy for dark matter, its equation of state. Once that the DM particle is not known, it could be described by both: a bosonic or a fermionic equation of state.

In the bosonic description, the dark matter particles are treated as bosons, which means that they can share the same quantum state and form the Bose-Einstein condensate. The last is particularly interesting, because it can form dense cores and halos leading to specific observational signatures (SAIKAWA; YANAGIDA, 2020; NELSON *et al.*, 2019). Futhermore, the lack of degeneracy pressure could lead a bosonic dark matter to accumulate, affecting the stability of the NS, even bringing about the collapse of the star in a black hole (CHAVANIS, 2015).

In contrast, the fermionic description assumes that the dark matter particles obey Fermi-Dirac statistics, meaning they cannot occupy the same quantum state. The Pauli exclusion principle generates a degeneracy pressure, which can lead to an increase in the maximum mass of a stable star. This is a significant result because it could lead to the existence of over-massive stars, which may be observed in merger phenomena (POPOLO *et al.*, 2018; DAS *et al.*, 2018). Evidently, the two types of DM description, at the level of EoS, lead to different consequences in the NS. Considering that, this work use both descriptions.

The present work is divided into three chapters. In the second chapter, the van der Waals model will be introduced with a brief discussion about its construction, recent uses, its weakness and strengths. In sequence, short-range correlations will be introduced to the model and unpublished results from this research will be presented. Finally, applications of this model to the study of NS will be shown, with results obtained for NS quantities such as mass, radius and tidal deformability.

In the third chapter, we will discuss the relativistic mean field model. After the introductory explanation, this model will be used to describe nuclear matter under the presence of short-range correlations. Additionally, we will add on it the bosonic and fermionic dark matter models to study the effects on NS structure.

2 Van der Waals models with short-range correlations

2.1 Initial propositions of van der Waals models

The van der Waals model was first conceived in as an option to study real gases. Proposed by Johannes Diderik van der Waals, his model introduced into the equation of state of a real gas an additional ingredient coming from the supposition that molecular gas components are not point-like but in the form of hard and impenetrable particles, with a finite dimension. Being so, the effective volume available V_{AV} to one of the composite molecules will be the total volume V minus the volume occupied by all other molecules

$$V_{AV} = V - bN \tag{2.1}$$

This altered volume should be included into the equation of state. In addition, Van der Waals proposed the inclusion of a term regulates the systems tendency to form bound states, reducing the pressure exerted over the boundaries (HUANG, 2008). With this new phenomenology, the pressure of the model is written as

$$p(T, \rho) = \frac{\rho\, T}{1 - b\, \rho} - a\, \rho^2 \tag{2.2}$$

with b being called the excluded volume constant and a the constant gibing the strenght of the attractive part. Notice that (2.2) is the form of the vdW equation in the Canonical Ensemble.

Aiming to apply the vdW equation of state in nuclear matter, a pioneering treatment was done by Vovchenko *et al.* (2015a), with the EoS being first written in the Gran-Canonical ensemble (GCE). The vdW in GCE does not possess a simple form such as (2.2), far from that, the pressure considering the excluded volume $P(T, \mu)$ is written as a transcendental equation in terms of the ideal pressure $P^{\star}_{id}(T, \mu^{\star})$ which is a function of the chemical potential

$$\begin{aligned} p(T,\ \mu) &= p^{\star}_{id}(T,\ \mu^{\star}) - a\rho^2, \\ \mu^{\star} &= \mu - bP(T,\ \mu) - ab\rho^2 + 2a\rho. \end{aligned} \tag{2.3}$$

With μ being the chemical potential of the ideal gas, $\mu^{\star}$ the chemical potential of the VdW gas, T the temperature.

Another way to write the vdW EoS is in terms of the density of particles (VOVCHENKO *et al.*, 2015a). In this form, the transcendental equations becomes from the chemical potential and the particle's density

$$\begin{aligned} \rho(T,\ \mu) &= \frac{\rho^{\star}_{id}(T,\ \mu^{\star})}{1 + b\rho^{\star}_{id}(T,\ \mu^{\star})}, \\ \mu^{\star} &= \mu - T\ \frac{b\rho}{1-\rho} + 2a\rho. \end{aligned} \tag{2.4}$$

To describe nuclear matter one must treat the gas particles in the quantum regime. To do that, Vovchenko *et al.* (2015b) introduced the pressure of a quantum ideal gas

$$p_{id}(T,\ \mu) = \frac{\gamma}{6\pi^2}\int dk \frac{k^4}{\sqrt{M^2+k^2}}\left[\exp\left(\frac{\sqrt{M^2+k^2}-\mu}{T}\right)+\eta\right]^{-1} \tag{2.5}$$

where η is chosen depending on what system one aims to study. For a system with Fermi statistics ($\eta = 1$), for the Bose statistics ($\eta = -1$) or in the Boltzman approximation ($\eta = 0$). Using the thermodynamic relation between pressure and chemical potential $\rho(T,\mu) = (\partial p/\partial\mu)_T$ one may obtain the equation for the density

$$\rho_{id}(T,\ \mu) = \frac{\gamma}{2\pi^2}\int_{\infty}^{\infty} dk k^2 \left[\exp\left(\frac{\sqrt{M^2+k^2}-\mu}{T}\right)+\eta\right]^{-1}, \tag{2.6}$$

with ρ_{id} standing for the ideal density of the quantum ideal gas. After the use of the thermodynamic relation that writes energy density as a function of pressure and chemical potential, one must find

$$\epsilon_{id}(T,\mu) = \frac{\gamma}{2\pi^2}\int dk\ k^2\sqrt{M^{\star 2}+k^2}\left[\exp\left(\frac{\sqrt{M^2+\mathbf{k}^2}-\mu}{T}\right)+\eta\right]^{-1}, \tag{2.7}$$

where M is the mass of the particles. For Fermi gas of nucleons, $M \approx 938$ MeV.

The final form for the pressure becomes from the insertion of expression (2.5) into (2.3). If one takes the limit to the Boltzmann statistics with the appropriate values of $\mu^\star$ and T, the classical vdW gas is recovered. Alternatively, taking $a = b = 0$ the EoS for the quantum ideal gas is recovered (VOVCHENKO *et al.*, 2015b).

With the consistency verified, it was possible to apply the vdW model to describe nuclear matter. Vovchenko *et al.* (2015b) considered in its application only regimes of small temperatures, in which the effects of pion production could be ignored. At zero temperature, the expressions (2.5) and (2.6) must be modified, and one may find that the dependence on the exponential term disappears in both equations. As one is treating nuclear matter, the system is composed of a Fermi gas of nucleons, so $\eta = 1$. Besides, it was considered only symmetric matter, what means $\gamma = 4$. In the zero-temperature regime, the authors have successfully settled numerical values for the constants a and b. Using as a constraint the binding energy of $B_0 = -16$ MeV and saturation density of $\rho_0 = 0.16$ fm^{-3}, the values found was $a \approx 329$ MeV fm^3 and $b \approx 3.42$ fm^3. With these a and b, some basic properties of phase transition in nuclear matter were explored at finite temperatures.

The vdW as presented by Vovchenko *et al.* (2015b) can not be used at high densities. If one intends to apply the model to dense astrophysical objects, the sound velocity should remain lower than the light velocity for the typical densities of these objects. As previously mentioned, density inside the NS can easily reach values of $5\rho_0$ to $10\rho_0$. However, the vdW model is limited to densities of $\rho_{\max} = b^{-1}$, as one may see directly from (2.4). Furthermore, the NS interior is composed of asymmetric matter, which this vdW version does not cover.

To circumvent the restriction over the maximum density, an alteration was proposed in the excluded volume term of the vdW model. This alteration comes from a mathematical expansion (called Starling-Carnahan approximation) first proposed by Carnahan e Starling (1969) to describe a dense fluid composed of rigid spheres. The work Vovchenko (2017a) uses this approximation in the van der Walls model, increasing the model's density range. The name is also changed to vdW-CS model. From now on, we will discuss only the vdW-CS model, and for simplicity, call it only vdW. The pressure now becomes

$$P(T,\ n) = T\ \rho\ \frac{1+\eta+\eta^2-\eta^3}{1-\eta^3} - a\rho^2, \tag{2.8}$$

with $\eta = b\rho/4$ being the packing fraction. With this modified pressure, they were able to find the value of $K_0 = 9(\partial P/\partial\rho)_{\rho_0} = 333$ MeV for incompressibility. This value is still far from the empirical range of 240 ± 20 MeV (Shlomo *et al.*, 2006; GARG; COLò, 2018). Even if one considers a wider range such as the one found by Stone *et al.* (2014) of $250 - 315$

MeV, their result is still unsatisfactory.

Vovchenko *et al.* (2017b) changed again the vdW model to consider the asymmetric matter. In their work, the pressure and chemical potential (2.4) becomes a sum of the individual quantities for each of the species taken into account. In addition to the study of asymmetric matter with nucleons only, they also did a treatment with α particles in the system. Considering only protons and neutrons, pressure becomes

$$p(\rho) = p_p^\star(\rho_p^\star) + p_n^\star(\rho_n^\star) - a_{pp}\rho^2 - a_{nn}\rho^2 - a_{np}\rho_p\rho_n - a_{pn}\rho_p\rho_n, \tag{2.9}$$

with $\rho_{p,n}^\star = \rho_{p,n}/(1 - b_{pp,nn}\ \rho_{p,n} - b_{np,pn}\ \rho_{p,n})$. The constants a_{pn},a_{np}, b_{pn}, b_{np}, in equation (2.9) are the attractive and repulsive vdW parameters for different species, but a_{nn} and b_{pp} stands for the interaction between same particle species. With this modified vdW model, considering only protons and neutrons, the authors found the value of 18 MeV for the symmetry energy at saturation density. This value underestimates the empirical range of 31.7 ± 3.2 MeV (Oertel *et al.*, 2017).

2.2 Density dependent van der Waals model

Summarizing, the works with symmetric or asymmetric vdW and vdW-CS previously cited, fail in achieving satisfactory results for empirical symmetry energy, incompressibility or both.

In Lourenço *et al.* (2019) is proposed a generalization of the vdW model and a possible solution to the mentioned problems. More specifically, possible density dependence in the attractive contribution is taken into account. For the term containing the excluded volume, the aforementioned CS procedure is used as well. The EoS for energy density and pressure are given, respectively, by

$$\epsilon(\rho, y_p) = [1 - \rho\mathcal{B}(\rho)]\,(\epsilon_{\rm kin}^{\star p} + \epsilon_{\rm kin}^{\star n}) - \rho^2\mathcal{A}(\rho) + d(2y_p - 1)^2\rho^2, \tag{2.10}$$

and

$$p(\rho, y_p) = p_{\rm kin}^{\star p} + p_{\rm kin}^{\star n} - \rho^2\mathcal{A}(\rho) + \rho\Sigma(\rho, y_p) + d(2y_p - 1)^2\rho^2, \tag{2.11}$$

with $\Sigma(\rho, y_p) = \rho\mathcal{B}'(P_{\rm kin}^{\star p} + P_{\rm kin}^{\star n}) - \rho^2\mathcal{A}'$ being the rearrangement term with $\mathcal{A}' \equiv d\mathcal{A}/d\rho$, and $\mathcal{B}' \equiv d\mathcal{B}/d\rho$. The kinetic contributions are

$$\epsilon_{\rm kin}^{\star p,n} = \frac{\gamma}{2\pi^2}\int_0^{k_F^{\star p,n}} dk\, k^2\sqrt{k^2 + M^2}, \tag{2.12}$$

and

$$p_{\rm kin}^{\star p,n} = \frac{\gamma}{6\pi^2}\int_0^{k_F^{\star p,n}} \frac{dk\, k^4}{\sqrt{k^2+M^2}}. \tag{2.13}$$

The Fermi momentum of the nucleon of mass $M = 939$ MeV and degeneracy factor $\gamma = 2$ is related to its respective density as $k_F^{\star p,n} = (6\pi^2\rho_{p,n}^{\star}/\gamma)^{1/3}$, where

$$\begin{aligned} \rho_p^{\star} &= \frac{y_p\rho}{1-\rho\mathcal{B}(\rho)} = \frac{\rho_p}{1-\rho\mathcal{B}(\rho)}, \\ \rho_n^{\star} &= \frac{(1-y_p)\rho}{1-\rho\mathcal{B}(\rho)} = \frac{\rho_n}{1-\rho\mathcal{B}(\rho)}. \end{aligned} \tag{2.14}$$

Finally, the density-dependent functions $\mathcal{A}$ and $\mathcal{B}$ are

$$\mathcal{A}(\rho) = \frac{a}{(1+b\rho)^n}, \tag{2.15}$$

and

$$\mathcal{B}(\rho) = \frac{1}{\rho} - \frac{1}{\rho}\exp\left[-\frac{b\rho}{4}\frac{\left(4-\frac{3b\rho}{4}\right)}{\left(1-\frac{b\rho}{4}\right)^2}\right], \tag{2.16}$$

with this last one determined through the CS approach for the repulsive interaction (excluded volume). It is worth noticing that from this general structure, it is possible to recover the other real gases studied in Vovchenko (2017a) for the $y_p = 0.5$ case, as for instance the vdW-CS model itself, by using $n = 0$, and the Clausius-CS one, for which $n = 1$. The traditional versions of these models regarding the excluded volume method are obtained by making $\mathcal{B}(\rho) \to b$ in addition. Another formulation involving a vdW model in which induced surface tension is taken into account was implemented in Sagun *et al.* (2018), Bugaev *et al.* (2019).

The terms $\epsilon_{kin}^{\star p,n}(\rho_{p,n}^{\star})$ in Eq. (2.12) comes from a Fermi gas of nucleons at zero temperature. So, it comes from (2.7) by taking the limit of $T \to 0$.

The last term of (2.11) considers the matter's asymmetry. The parameter d was added by the authors as an adjustment to reproduce the symmetry energy correctly. The expression for the symmetry energy is, as a good approximation (Baldo; Burgio, 2016; LOURENÇO *et al.*, 2019), given by

$$E_{\rm sym}(\rho) \simeq \frac{1}{8}\frac{\partial^2(\epsilon/\rho)}{\partial y_p^2} = E_{\rm sym}^{\star kin}(\rho) + d\rho. \tag{2.17}$$

Thus, using as a constraint the value for symmetry energy expected in stellar environments, one could find d by using

$$d = \frac{(E_{\rm sym}(\rho) - E_{\rm sym}^{\star kin}(\rho))}{\rho} \tag{2.18}$$

with $S(\rho_0) = J$, that is, the desired symmetry energy and $S^{\star}_{kin}(\rho) = k^{\star}_F/(6\sqrt{k^{\star}_F + M^2})$.

One could derive the chemical potential for the asymmetric matter from the expression for the energy density. Lourenço *et al.* (2019) have done it, finding

$$\mu_{p,n} = \mu^{\star}_{p,n} + \mathcal{B}(\rho)(p^{\star p}_{\rm kin} + p^{\star n}_{\rm kin}) \ + \Sigma(\rho) - 2\mathcal{A}(\rho)\rho \pm 2d(2y_p - 1)\rho. \tag{2.19}$$

This new model, named the density-dependent vdW (DD-vdW) model, has shown to preserve causality in a density regime capable of producing mass-radius diagrams consistent with data obtained from the PSR J0348+0432 pulsar (ANTONIADIS *et al.*, 2013), as well as those from the GW170817 neutron-star merger event. It is also compatible with the flow constraint established in Danielewicz *et al.* (2002). The four free parameters (a, b, d and n) are determined by imposing specific values for ρ_0, B_0, K_0 and J (symmetry energy at ρ_0). Furthermore, it also produces some clear correlations in SNM as one can see in Dutra *et al.* (2020).

To apply the newborn DD-vdW model to the Neutron Stars modeling, it was necessary to consider some of the nuclear processes inside the star. One process that must be regarded is the inverse and ordinary beta decay. The star is said to be in beta-equilibrium if the inverse and ordinary processes happen with equal rate. That condition is imposed in many models and it implies

$$\begin{aligned} n \ &\rightarrow \ p + e^- + \bar{\nu_e} \\ p + e^- \ &\rightarrow \ n + \nu_e. \end{aligned} \tag{2.20}$$

The stellar interior also favors the formation of muons. Muons are leptons of charge equal to the electron, with spin 1/2 and a mass approximately 200 greater than the electron's mass. Muons can be formed if the chemical potential of electrons becomes larger than the muon mass. With their formation, pressure and energy density will change to total quantities

$$p_T(\rho, \rho_e, y_p) = p(\rho, y_p) + \frac{\mu^4_e(\rho_e)}{12\pi^2} + \frac{1}{3\pi^2}\int_0^{\sqrt{\mu^2_\mu(\rho_e) - m^2_\mu}} \frac{dk\ k^4}{\sqrt{k^2 + m^2_\mu}} \tag{2.21}$$

and

$$\epsilon_T(\rho, \rho_e, y_p) = \epsilon(\rho, y_p) + \frac{\mu^4_e(\rho_e)}{4\pi^2} + \frac{1}{\pi^2}\int_0^{\sqrt{\mu^2_\mu(\rho_e) - m^2_\mu}} dk\ k^2\sqrt{k^2 + m^2_\mu}. \tag{2.22}$$

From the energy density expression, it is possible to calculate the chemichal potential. This quantity is important once it helps to establishing a quantitative relation between

the species in the system. The ordinary and inverse beta-decay process demands equality between the chemical potential of the initial species and of the formed species

$$\mu_n(\rho, y) = \mu_p(\rho, y) + \mu_e(\rho_e). \tag{2.23}$$

Another condition to be fulfilled is charge neutrality

$$\rho_p(\rho, y) = \rho_\mu(\rho_e) + \rho_e, \tag{2.24}$$

with $\rho_\mu = (\mu_\mu^2 - m_\mu^2)^{3/2}/(3\pi^2)$, $\mu_\mu = \mu_e = (3\pi^2\rho_e)^{1/3}$ and $\rho_p = y_p\ \rho$. The terms ρ_e, ρ_μ and m_μ are the density of electrons , the density of muons, and the mass of muons, respectively. The equations (2.23) and (2.24) are coupled. Those equations must be solved for the electron density and the proton fraction y, for inputs of density ρ.

Using the previous formalism, Lourenço *et al.* (2019) have analyzed several properties of NS. The first compelling result was the agreement between the maximum mass obtained with the DD-vdW model and experimental observations. Data from the electromagnetic spectrum obtained by the Very Large Telescope (VLT) of the European Southern Telescope (ESO) found a mass of $2.01\pm0.04M_\odot$ for a pulsar in an orbit with a white dwarf (Antoniadis *et al.*, 2013). Data from the PSR J0740+6620 by Fonseca *et al.* (2021b), suggests a similar mass of $2.08\pm0.07M_\odot$, with 68.3% of credibility. Thus, even with contemporary information, the mass-radius relation from DD-vdW model is still satisfactory for describing the mass of a NS in a pulsar-white dwarf orbital system.

One should notice that of two calculations for maximum masses by the authors, only one is inside the symmetry energy range of 31.7 ± 3.2 MeV (Oertel *et al.*, 2017). But the two were done considering the incompressibility between the observational constraints of 240 ± 20 MeV (GARG; COLò, 2018). Besides, the authors argue that their maximum mass was obtained with the causal limit being broken in the maximum density of $\rho_{max} = 5.66\rho_0$ for calculation using the symmetry energy out of 31.7 ± 3.2 MeV, and $\rho_{max} = 5.00\rho_0$ using the energy within the limits. These values for ρ_{max} show that, compared with the constant parameters version of the model, the inclusion of density-dependent parameters on the vdW by Lourenço *et al.* (2019) substantially increases the model maximum density, keeping the other bulk parameters with satisfactory values.

However, values from the NICER collaboration have brought a maximum mass of $2.35\pm0.17M_\odot$ for a 20 km radius pulsar (ROMANI *et al.*, 2022). The discrepancies between the measured masses from the observations of Fonseca *et al.* (2021b) and Romani *et al.* (2022) are probably caused by the NS formation process. In any case, one should notice the model DD-vdW underestimates the NS maximum mass in comparison with the new measurement.

Lourenço *et al.* (2019) also calculated the tidal deformability of a single NS. Pieces of information about TD can be obtained directly from the gravitational waveform. Comparing a merger of two NS and a pair of black holes it is possible to trace differences between the gravitational wave signal phases of these two kinds of events. The phase difference from NS to BHs mergers appears in the expansions that describe the inspiral dynamics of each event. The leading order of the different terms is proportional to the star tidal deformability parameter (GRALLA, 2018; Abbott *et al.*, 2018). In this way, measurements of TD are free from modeling and usually used as a constraint to models. Using data from the GW170817 event, Abbott *et al.* (2018) found for a star with a mass of $1.4M\odot$ the tidal deformability of $\Lambda_{1.4} = 190^{+390}_{-120}$. The value obtained by the authors was $\Lambda_{1.4} = 527$, that is, consistent with the previously mentioned range (Abbott *et al.*, 2018).

The tidal deformability can also be calculated if the NS is in a binary system. In this case, the gravitational force that one exerts on another will provoke a TD on each other. The phenomenon now is provoked by the gravitational attraction between the two bodies and no more by an intrinsic quantity of the isolated star, such as the spin. One way to calculate the TD of the set consists in varying one mass of the two stars, with the other varying with a given proportion to keep the chirp mass always constant. For each pair of masses, one calculates the two deformability for that set. The values of TD for the pairs should satisfy the observable constraints within the diagrams of Λ_1 by Λ_2 in some confidence interval. The calculations by Lourenço *et al.* (2019) were inside the 90% confidence interval for all chosen parameters. This shows the strong capability of the model to reproduce the observed TD. Thus, with the NS properties reproduced, the authors have shown that the DD-vdW model is a powerful and promising method to describe NS high-density environments.

2.3 Density dependent van der Waals with short-range correlations

The above model has proved its efficiency. Now, due to its simplicity, one could improve it by including modifications related to observed nuclear phenomena. The focus of this work is to develop a model with short-range correlations using a formalism similar to the one used by Vovchenko *et al.* (2017b) and Lourenço *et al.* (2019) with the DD-vdW model proposed by the last one. Basically, I will show in this chapter the results presented and discussed in Rodrigues *et al.* (2023).

Experimental research in short-range correlation establishes that a fraction of fermions is in a high momentum state which leads to a change in the functional form of pressure and energy density. That happens because the energy density of a fermionic gas is related

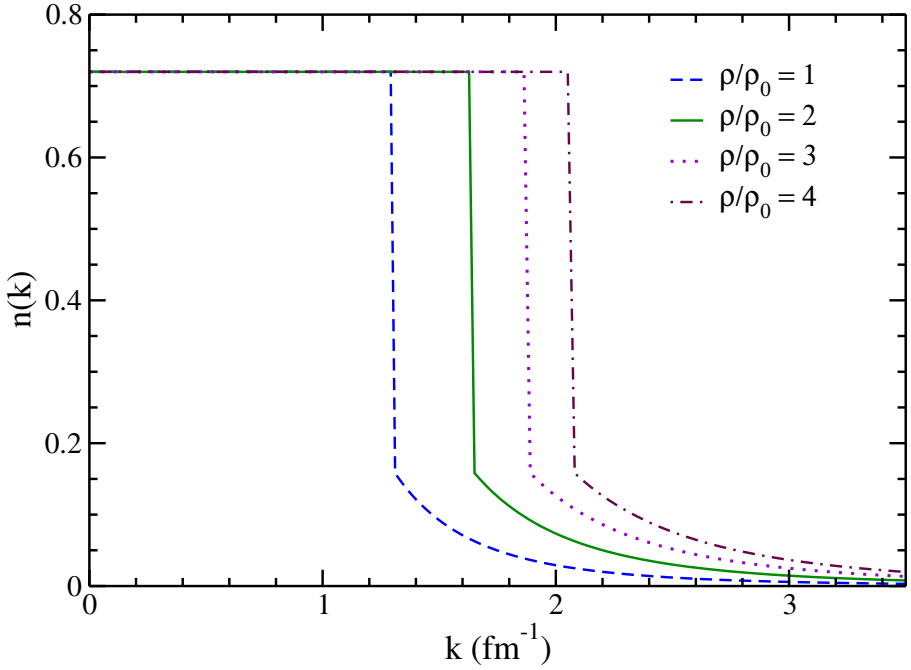

FIGURE 2.1 – Momentum distribution with HMT included for symmetric nuclear matter. Curves for $\rho/\rho_0 = 1, 2, 3$ and 4, with $\rho_0 = 0.15$ fm^{-3}.

to the occupation of those fermions and so to its momentum distribuition. The inclusion of the short-range correlation is done by modifying the single-nucleon momentum distributions, from the usual Fermi step functions to those encompassing the high-momentum tail (HMT) that read

$$n_{p,n}(k) = \begin{cases} \Delta_{p,n}, & 0 < k < k_F^{p,n} \\ \\ C_{p,n}\dfrac{(k_F^{p,n})^4}{k^4}, & k_F^{p,n} < k < \phi_{p,n} k_F^{p,n}, \end{cases} \tag{2.25}$$

with $\Delta_{p,n} = 1 - 3C_{p,n}(1 - 1/\phi_{p,n})$, $C_p = C_0[1 - C_1(1 - 2y_p)]$, $C_n = C_0[1 + C_1(1 - 2y_p)]$, $\phi_p = \phi_0[1 - \phi_1(1 - 2y_p)]$ and $\phi_n = \phi_0[1 + \phi_1(1 - 2y_p)]$. The values $C_0 = 0.161$, $C_1 = -0.25$, $\phi_0 = 2.38$, and $\phi_1 = -0.56$ are determined (CAI; LI, 2015b; CAI; LI, 2016b; CAI; LI, 2016a) by taking experimental data concerning $d(e, e', p)$ and two-nucleon knockout reactions, medium-energy photonuclear absorption, as well as by using the normalization condition

$$\frac{1}{\pi^2}\int_0^\infty dk\, k^2\, n_{p,n}(k) = \rho_{p,n} = \frac{(k_F^{p,n})^3}{3\pi^2}. \tag{2.26}$$

Furthermore, the fraction of nucleons in the HMT given by $x^{\rm HMT} = 3C_{p,n}(1 - \phi_{p,n}^{-1})$ is also used in this determination, namely, $x_{\rm SNM}^{\rm HMT} = 28\%$ and $x_{\rm PNM}^{\rm HMT} = 1.5\%$: numbers obtained for symmetric nuclear matter and pure neutron matter, respectively (CAI; LI, 2015b; CAI; LI, 2016b; CAI; LI, 2016a). In Fig. 2.1 we depict the $n(k)$ distribution in SNM for some values of ρ/ρ_0.

Some papers have explored possible modifications in Eq. (3.15) and their consequences. In Cai e Li (2022), for instance, it was studied the effect of generalizing $n_{p,n}(k)$ to arbitrary dimensions. In Guo *et al.* (2021b), on the other hand, the authors investigated three different shapes for the SRC HMT, namely, proportional to k^4, k^6, and k^9. A study of these high order tails is done in appendix A. There, the constants C_0, C_1, ϕ_0, and ϕ_1 are calculated for each case. Besides, the new functional forms of $\Delta_{p,n}$, $C_{n,p}$ and $\phi_{p,n}$ are also found for a generic tail order m, resulting in a generalization of the expressions.

In this work, the further analysis is based on hard photons emissions due to the reactions ^{14}N+^{12}C and ^{48}Ca+^{124}Se at beam energies around the Fermi energy. From the reactions, they analyzed the yields, angular distribution, and energy spectra of the hard photons, leading them to important conclusions. The first is related to the yields, which increase equally for all different powers of k. The second is that the shape of the HMT does not affect the angular distribution of the produced hard photons. In this way, if one looks only at the yields or at the angular distribution, the shape seems not to be relevant. The two first conclusions make the third one the most meaningful. The authors have calculated the effects of the HMT shape in the hard photons spectra, finding that this effect is considerable and should not be ignored. The effects are greater as greater are the energy of the photons. We address the reader to appendix B for more details regarding SRC.

Here we use the expression given in Eq. (3.15) adapted to the case in which excluded volume effects are implemented in the system, namely, taking $k_F^{p,n} \to k_F^{\star p,n}$, in order to generate new EoS for the vdW-type model presented before. This procedure leads to generalized thermodynamical quantities, such as energy density and pressure, given respectively by,

$$\epsilon(\rho, y_p) = [1 - \rho\mathcal{B}(\rho)]\left[\epsilon^{\star p}_{\mathrm{kin(SRC)}} + \epsilon^{\star n}_{\mathrm{kin(SRC)}}\right] - \rho^2\mathcal{A}(\rho) + d(2y_p - 1)^2\rho^2, \tag{2.27}$$

and

$$p(\rho, y_p) = p^{\star p}_{\mathrm{kin(SRC)}} + p^{\star n}_{\mathrm{kin(SRC)}} - \rho^2\mathcal{A}(\rho) + \rho\Sigma_{\mathrm{SRC}}(\rho, y_p) + d(2y_p - 1)^2\rho^2, \tag{2.28}$$

where

$$\Sigma_{\mathrm{SRC}}(\rho, y_p) = \rho\mathcal{B}'\left[p^{\star p}_{\mathrm{kin(SRC)}} + p^{\star n}_{\mathrm{kin(SRC)}}\right] - \rho^2\mathcal{A}', \tag{2.29}$$

and with modified kinetic terms written as

$$\epsilon^{\star p,n}_{\mathrm{kin(SRC)}} = \frac{\gamma\Delta_{p,n}}{2\pi^2}\int_0^{k_F^{\star p,n}} dk\, k^2\sqrt{k^2 + M^2} + \frac{\gamma C_{p,n}(k_F^{\star p,n})^4}{2\pi^2}\int_{k_F^{\star p,n}}^{\phi_{p,n}k_F^{\star p,n}} dk\, \frac{\sqrt{k^2 + M^2}}{k^2}, \tag{2.30}$$

and

$$p^{\star p,n}_{\rm kin(SRC)} = \frac{\gamma\Delta_{p,n}}{6\pi^2}\int_0^{k_F^{\star p,n}} \frac{dk\,k^4}{\sqrt{k^2+M^2}} + \frac{\gamma C_{p,n}(k_F^{\star p,n})^4}{6\pi^2}\int_{k_F^{\star p,n}}^{\phi_{p,n}k_F^{\star p,n}} \frac{dk}{\sqrt{k^2+M^2}}, \tag{2.31}$$

with the normalization condition, now taken as $\int_0^\infty n_{p,n}(k)\,k^2\,dk = \rho^\star_{p,n} = (k_F^{\star p,n})^3/3$, giving the same numbers for C_0, C_1, ϕ_0, and ϕ_1. Furthermore, we consider the CS excluded volume mechanism for the function $\mathcal{B}(\rho)$, Eq. (2.16). In the case of the attractive density-dependent function $\mathcal{A}(\rho)$, we make $n=1$ and $b\to c$ in Eq. (2.15), namely,

$$\mathcal{A}(\rho) = \frac{a}{1+c\rho}. \tag{2.32}$$

By doing so, we actually assume the three parameters Clausius-CS model applied to the nuclear matter as shown in Vovchenko (2017a), Vovchenko *et al.* (2018), but also generalized to include SRC effects. Hereafter we name it as CCS-SRC model. The four free parameters of the model, a, b, c and d, are determined by imposing $\rho_0 = 0.15$ fm^{-3}, $B_0 = -16$ MeV, $J = E_{\rm sym}(\rho_0) = 32$ MeV, and some values for $K_0 = K(\rho_0, y_p = \frac{1}{2})$. The expression for the incompressibility in SNM is given by

$$K(\rho) = 9\frac{\partial P}{\partial\rho}\Big|_{y_p=\frac{1}{2}} = 9[\Sigma_{\rm SRC}(\rho) + \rho\Sigma'_{\rm SRC}(\rho)] + \frac{1+\mathcal{B}'\rho^2}{[1-\mathcal{B}(\rho)\rho]^2}K^\star_{\rm kin(SRC)} - 9\rho[2\mathcal{A}(\rho)+\mathcal{A}'\rho], \tag{2.33}$$

with $\Sigma_{\rm SRC}(\rho) = \Sigma_{\rm SRC}(\rho, y_p = 1/2)$,

$$\Sigma'_{\rm SRC}(\rho) = (\mathcal{B}''\rho + \mathcal{B}')p^\star_{\rm kin(SRC)} + \frac{(1+\mathcal{B}'\rho^2)\mathcal{B}'\rho}{9[1-\mathcal{B}(\rho)\rho]^2}K^\star_{\rm kin(SRC)} - \mathcal{A}''\rho^2 - 2\mathcal{A}'\rho, \tag{2.34}$$

$$K^\star_{\rm kin(SRC)} = \frac{3\Delta k_F^{\star 2}}{\sqrt{k_F^{\star 2}+M^2}} + 3C_0k_F^{\star 2}\left[\frac{\phi_0}{\sqrt{\phi_0^2k_F^{\star 2}+M^2}} - \frac{1}{\sqrt{k_F^{\star 2}+M^2}} + \frac{4}{k_F^\star}\ln\left(\frac{\phi_0k_F^\star + \sqrt{\phi_0^2k_F^{\star 2}+M^2}}{k_F^\star + \sqrt{k_F^{\star 2}+M^2}}\right)\right], \tag{2.35}$$

and $\Delta = 1 - 3C_0(1-1/\phi_0)$. For $p^\star_{\rm kin(SRC)}$ shown in Eq. (2.34), we use the expression given in Eq. (2.31) with $k_F^{\star p,n}$ replaced by $k_F^\star$ and $\gamma = 4$.

The symmetry energy reads

$$
\begin{aligned}
E_{\rm sym}(\rho) = \frac{1}{8}\frac{\partial^2(\epsilon/\rho)}{\partial y_p^2}\Big|_{y_p=\frac{1}{2}} &= \frac{k_F^{\star 2}}{6E_F^\star}\left[1-3C_0\left(1-\frac{1}{\phi_0}\right)\right] - 3C_0E_F^\star\left[C_1\left(1-\frac{1}{\phi_0}\right)+\frac{\phi_1}{\phi_0}\right] \\
&- \frac{9M^4}{8k_F^{\star 3}}\frac{C_0\phi_1(C_1-\phi_1)}{\phi_0}\left[\frac{2k_F^\star}{M}\left(1+\frac{k_F^{\star 2}}{M^2}\right)^{3/2} - \frac{k_F^\star}{M}\sqrt{1+\frac{k_F^{\star 2}}{M^2}} - \operatorname{arcsinh}\left(\frac{k_F^\star}{M}\right)\right] \\
&+ \frac{2C_0k_F^\star(6C_1+1)}{3}\left[\sqrt{1+\frac{M^2}{k_F^{\star 2}}} - \sqrt{1+\frac{M^2}{k_F^{\star 2}\phi_0^2}} + \operatorname{arcsinh}\left(\frac{k_F^\star\phi_0}{M}\right) - \operatorname{arcsinh}\left(\frac{k_F^\star}{M}\right)\right] \\
&+ \frac{3C_0k_F^\star}{2}\left[\frac{4E_F^\star}{9k_F^\star} - \frac{k_F^\star}{9E_F^\star} + \frac{1}{9}(3\phi_1+1)^2\left(\frac{k_F^\star\phi_0}{F_F^\star} - \frac{2F_F^\star}{k_F^\star\phi_0}\right) + \frac{2F_F^\star(3\phi_1-1)}{9k_F^\star\phi_0}\right] \\
&+ \frac{C_0(3C_1+4)}{3}\left[\frac{F_F^\star(3\phi_1+1)}{\phi_0} - E_F^\star\right] + d\rho, \qquad (2.36)
\end{aligned}
$$

with $E_F^\star = \sqrt{k_F^{\star 2}+M^2}$ and $F_F^\star = \sqrt{\phi_0^2k_F^{\star 2}+M^2}$.

It is worth mentioning that Eq. (2.33) reduces to that one related to the DD-vdW model (LOURENÇO *et al.*, 2019) when SRC are turned off, by taking $\phi_0 = 1$ and $\phi_1 = 0$, and when Eq. (2.15) is used instead of Eq. (2.32). With regard to the symmetry energy, notice that its kinetic part, given by $E_{\rm sym}^{\star\rm kin}(\rho) = E_{\rm sym}(\rho) - d\rho$, is exactly the same presented in Cai e Li (2016b) for the case in which no excluded volume effects are considered in the system, i.e., for $k_F^\star = k_F$. Furthermore, we find $E_{\rm sym}^{\star\rm kin}(\rho_0) = -14.7$ MeV for the kinetic part of the symmetry energy at the saturation density. This value is compatible with respective numbers obtained in Cai e Li (2016b) from a nonlinear relativistic mean-field (RMF) model, and from a nonrelativistic calculation, both including SRC effects.

For the sake of completeness, we also investigate how the symmetry energy and its slope, obtained through $L = 3\rho(\partial E_{\rm sym}/\partial\rho)$, correlates with each other (both quantities evaluated at the saturation density: J and $L_0 = L(\rho_0)$). Such a relationship is depicted in Fig. 2.2. From the figure, it is verified a strong linear correlation between these quantities, in accordance with many other approaches performed in the literature, as can be seen, in Drischler *et al.* (2020), Li *et al.* (2021), Santos *et al.* (2015), for example. Another feature exhibited in the figure is that SRC significantly increase the values of L_0 for the same J. It is also observed that there is no big impact in L_0 for K_0 changing in the range of $K_0 = (240 \pm 20)$ MeV.

Applications in SNM and stellar matter

We show in Figs. 2.3a and 2.3b the effect of the SRC applied to the CCS-SRC model in the energy per particle and pressure of the system in SNM. From these figures, we notice that SRC mainly affects such thermodynamical quantities especially for densities greater than 0.2 fm^{-3}, approximately. In this case, it is important to verify the results

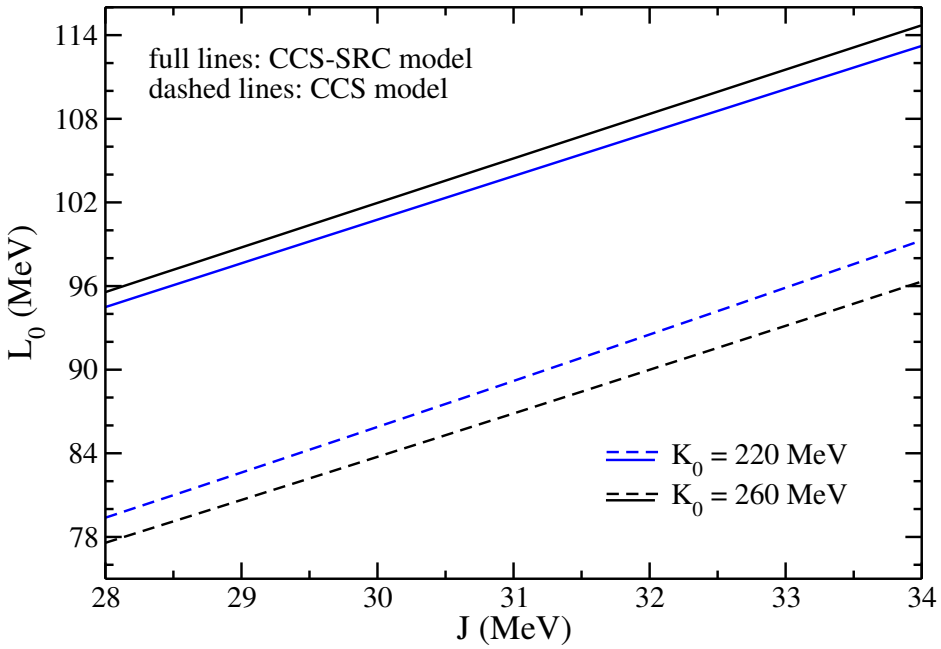

FIGURE 2.2 – L_0 as a function of J for the CCS model with (full lines) and without (dashed lines) SRC included. Curves constructed by using $\rho_0 = 0.15$ fm^{-3}, $B_0 = -16$ MeV.

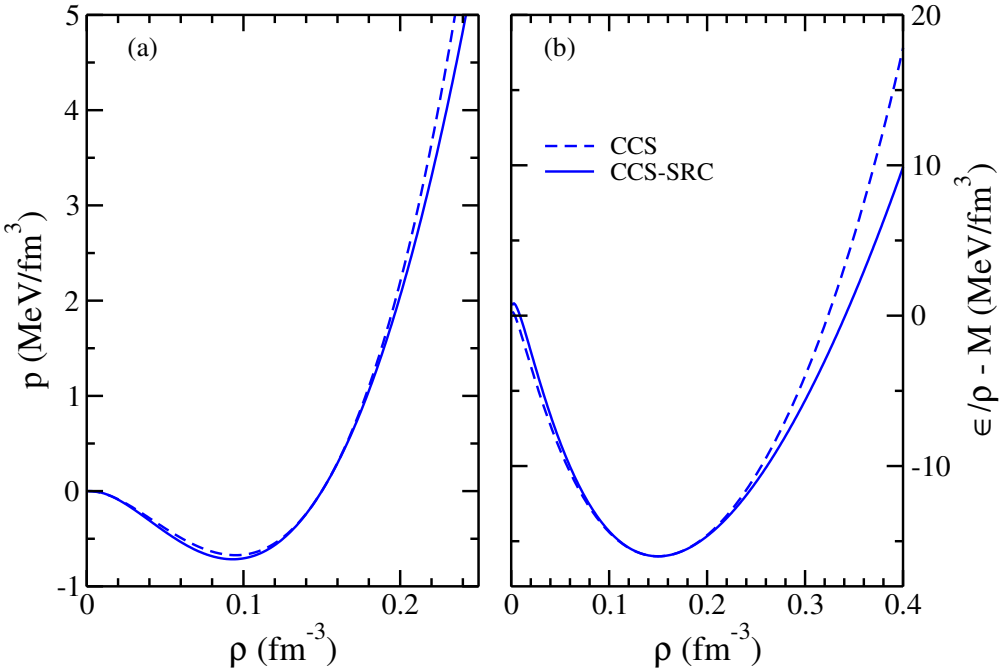

FIGURE 2.3 – CCS model with (full lines) and without (dashed lines) SRC included: (a) pressure and (b) energy per particle as a function of the density. Curves for symmetric nuclear matter with $\rho_0 = 0.15$ fm^{-3}, $B_0 = -16$ MeV, and $K_0 = 240$ MeV.

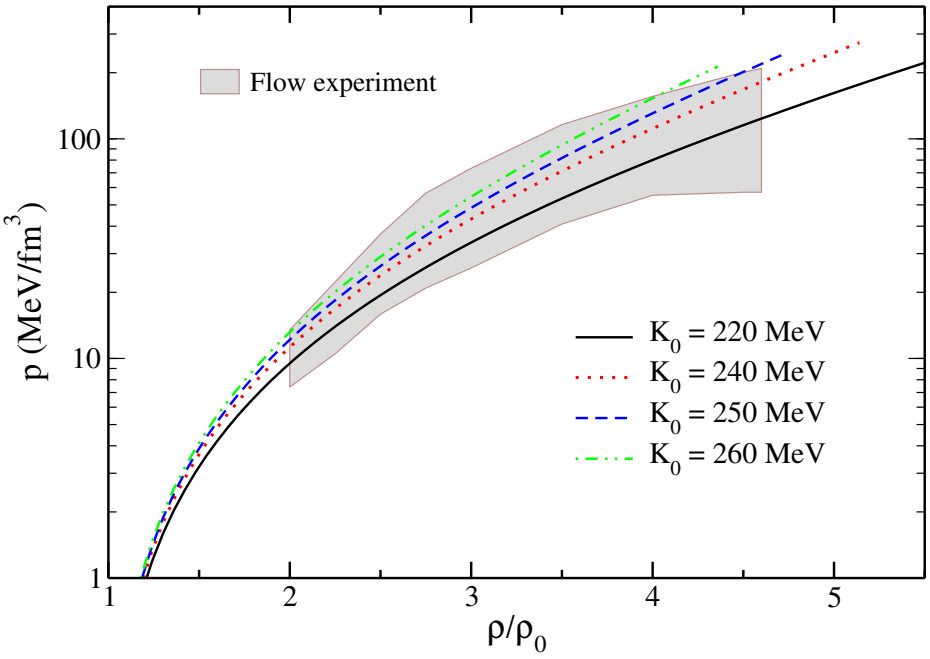

FIGURE 2.4 – Pressure versus ρ/ρ_0 for different parametrizations of the CCS-SRC model. Curves for symmetric nuclear matter with $\rho_0 = 0.15$ fm^{-3} and $B_0 = -16$ MeV. Band: flow constraint extracted from Danielewicz *et al.* (2002).

of the model regarding the high-density regime. For this purpose, we also investigate how it behaves against the so-called flow constraint. It is based on the study performed in Danielewicz *et al.* (2002) in which limits on the pressure of SNM (zero temperature case) at high densities were established from experimental data related to the motion of ejected matter in energetic nucleus–nucleus collisions, more specifically, particle flow in the collisions of ^{197}Au nucleus at incident kinetic energy per nucleon running from about 0.15 GeV to 10 GeV.

The comparison of the model with the flow constraint is displayed in Fig. 2.4. It is verified that parametrizations of the CCS-SRC model constructed by fixing K_0 in the range of $K_0 = (240 \pm 20)$ MeV (GARG; COLÒ, 2018) are completely in agreement with the band provided by the flow constraint. All these curves were generated in a density range that ensures causality to the system. In the case of excluded volume models, like the one we are presenting here, nucleons are treated as finite-size objects and therefore a suitable Lorentz contraction should be taken into account for relativistic frameworks in order to avoid causality violation for any density (BUGAEV, 2008). An alternative to this procedure is the implementation of the CS excluded volume treatment, since this mechanism effectively produces an excluded volume depending on the density, more specifically, as a decreasing function. In the case of the model proposed in this work, we verify that SRC moves the density in which causality is broken to higher values in comparison with the model without this phenomenology implemented. This feature is observed in Fig. 2.5.

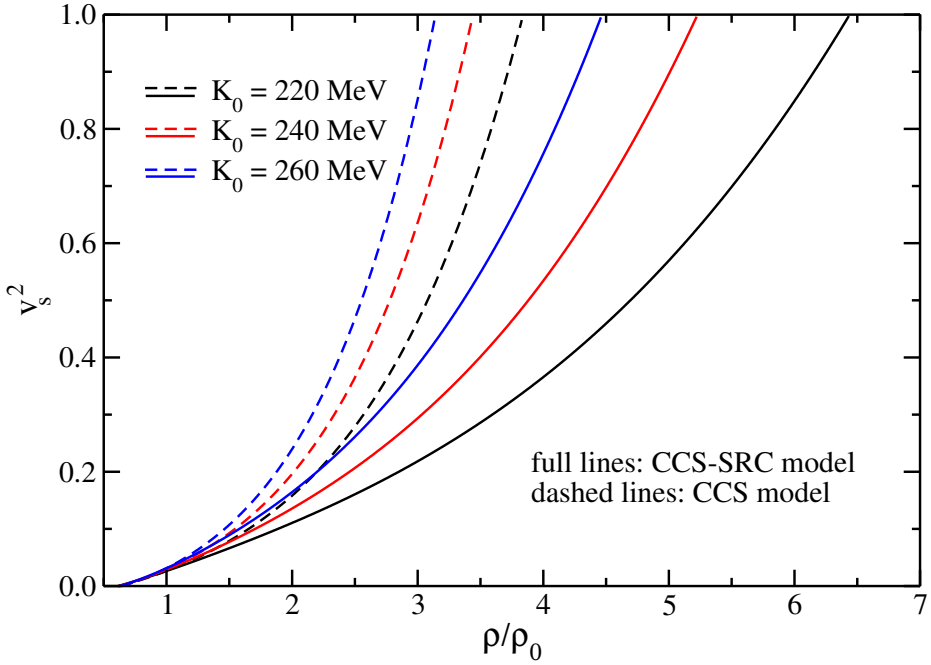

FIGURE 2.5 – Squared sound velocity as a function of ρ/ρ_0 for different parametrizations of the CCS model with (full lines) and without (dashed lines) SRC included. Curves for symmetric nuclear matter with $\rho_0 = 0.15$ fm^{-3} and $B_0 = -16$ MeV.

We also investigate the capability of the CCS-SRC model in describing stellar matter in general, and some recent astrophysical observations in particular. In order to do that, it is necessary to solve the Tolman-Oppnheimer-Volkoff (TOV) equations (TOLMAN, 1939b; OPPENHEIMER; VOLKOFF, 1939b), given by $dP(r)/dr = -[\varepsilon(r) + P(r)][m(r) + 4\pi r^3 P(r)]/[r^2 g(r)]$ and $dm(r)/dr = 4\pi r^2 \varepsilon(r)$, where $g(r) = 1 - 2m(r)/r$. The solution of these equations is constrained to $P(0) = P_c$ (central pressure) and $m(0) = 0$, with the conditions $P(R) = 0$ and $m(R) = M_{\rm NS}$ satisfied at the star surface. Here R defines the radius of the respective neutron star of mass $M_{\rm NS}$.

To construct the EoS of the star, some considerations must be done. In the outer layers of the Neutron Stars such as the outer crust and outer parts of the inner crust, atoms still are expected to be found (Piekarewicz, 2022). Furthermore, the β-equilibrium has not yet been reached and so it can not be described by the CCS-SRC. In this work, we have used the model proposed by Baym *et al.* (1971) to describe the outer crust (hereafter referred to as BPS model). The BPS model takes into account the presence of decoupled nucleons, atomic nuclei, and atoms themselves in the calculation.

Despite being useful in the outer crust, the BPS model can not be applied in a satisfactory way to the innermost star regions. If one does that, the NS radius will be hugely underestimated. So, in its original form, it is applied in the density range of $6.3 \times 10^{-12}\,\text{fm}^{-3} \leqslant \rho_{\rm outer} \leqslant 2.5 \times 10^{-4}\,\text{fm}^{-3}$, being the higher limit the beginning of the inner crust (Baym *et al.*, 1971).

Two options arise from the use of the BPS model. One could simply connect the hadronic model to it. But that could lead to imprecise calculations on the tidal deformability (PIEKAREWICZ; FATTOYEV, 2019). An alternative approach consists add another model to describe the inner crust, linking it to the liquid core. This is the procedure chosen. But the inner crust is a heterogeneous structure with many complex constituents such as the nuclear pasta. That makes precise modeling of this region a herculean task. Besides, the role of pasta in nuclear systems is still unknown, what has led some to choose a simple polytropic interpolation of the form (LINK *et al.*, 1999; Xu *et al.*, 2009; PIEKAREWICZ; FATTOYEV, 2019)

$$P(\epsilon) = A + B\epsilon^{4/3}. \tag{2.37}$$

The polytropic is connected to the BPS model in the density of $\rho = 2.50 \times 10^{-3}$ fm^{-3}. The connection of the polytropic with our hadronic model is done in a transition density ρ_t. This density is defined using the concepts of the thermodynamical instability region which is the region where the uniform liquid becomes unstable against small density amplitude fluctuations, in such region, nuclear clusters start to be formed. The density at which that happens is the transition density. Using this concept and expressions brought by Xu *et al.* (2009) and Gonzalez-Boquera *et al.* (2019), one is able to find the ρ_t by solving the system of equations

$$\begin{aligned} V_{ther}(\rho, y_p) &= 2\rho\frac{\partial E_b(\rho, y_p)}{\partial \rho^2} + \rho^2\frac{\partial^2 E_b(\rho, y_p)}{\partial \rho^2} - \left(\frac{\partial^2 E_b(\rho, y_p)}{\partial \rho\, \partial y_p}\right)^2 \left(\frac{\partial^2 E_b(\rho, y_p)}{\partial y_p^2}\right)^{-1} = 0 \\ \mu_n(\rho, y_p) &= \mu_p(\rho, y_p) + \mu_e(y_p\rho). \end{aligned} \tag{2.38}$$

Where we are using for $E_b(\rho, y_p)$ the parabolic approximation (GONZALEZ-BOQUERA *et al.*, 2017). The values of ρ and y_p that solve the above set of equations are respectively the transition density ρ_t and the transition proton fraction y_{pt}.

Now, all three domains of the three component models are defined. The BPS model acts in the outer crust to the beginning of the polytropic modeling in the inner crust. This polytropic is connected to the CCS-SRC model at the transition density ρ_t. For values of density greater than ρ_t, the physics is described by the CCS-SRC model.

The total energy density and total pressure of the system composed of protons, neutrons, electrons, and muons are written as

$$\varepsilon = \epsilon + \frac{\mu_e^4}{4\pi^2} + \frac{1}{\pi^2}\int_0^{\sqrt{\mu_\mu^2(\rho_e) - m_\mu^2}} dk\, k^2 (k^2 + m_\mu^2)^{1/2} \tag{2.39}$$

and

$$P = p + \frac{\mu_e^4}{12\pi^2} + \frac{1}{3\pi^2}\int_0^{\sqrt{\mu_\mu^2 - m_\mu^2}} \frac{dk\, k^4}{(k^2 + m_\mu^2)^{1/2}}, \tag{2.40}$$

where, by chemical equilibrium and charge neutrality conditions, both imposed in an NS, one has $\mu_n - \mu_p = \mu_e$ and $\rho_p - \rho_e = \rho_\mu$, with $\mu_e = (3\pi^2\rho_e)^{1/3}$, $\rho_\mu = [(\mu_\mu^2 - m_\mu^2)^{3/2}]/(3\pi^2)$, and $\mu_\mu = \mu_e$, for $m_\mu = 105.7$ MeV (muon mass) and massless electrons. ϵ, and p are determined from the CCS-SRC model, as well as the chemical potentials for, namely,

$$\begin{aligned}\mu_{p,n} = \frac{\partial \epsilon}{\partial \rho_{p,n}} &= \Delta_{p,n}\mu^{\star p,n}_{\rm kin} + \mu^{\star p,n}_{\rm kin(SRC)} + \mathcal{B}(\rho)[P^{\star p}_{\rm kin(SRC)} + P^{\star n}_{\rm kin(SRC)}] \\ &+ \Sigma_{\rm SRC}(\rho, y_p) - 2\mathcal{A}(\rho)\rho \pm 2d(2y_p - 1)\rho \end{aligned} \tag{2.41}$$

for protons (upper sign) and neutrons (lower sign).

Regarding the chemical potential, two different approaches are done, firstly we considered the full form of it

$$\begin{aligned}\mu^{\star p,n}_{\rm kin(SRC)} &= 3C_{p,n}\left[\mu^{\star p,n}_{\rm kin} - \frac{(\phi^2_{p,n}k^{\star 2}_{Fp,n} + M^2)^{1/2}}{\phi_{p,n}}\right] + 4C_{p,n}k^\star_{Fp,n}\ln\left[\frac{\phi^2_{p,n}k^{\star 2}_{Fp,n} + (\phi^2_{p,n}k^{\star 2}_{Fp,n} + M^2)^{1/2}}{k^\star_{Fp,n} + (k^{\star 2}_{Fp,n} + M^2)^{1/2}}\right] \\ &+ \frac{2}{\pi^2}\frac{\rho_{p,n}}{\rho^2}[1 - \mathcal{B}(\rho)\rho\,]\eta_{p,n}, \end{aligned} \tag{2.42}$$

and $\mu^{\star p,n}_{\rm kin} = (k^{\star 2}_{Fp,n} + M^2)^{1/2}$. The term $\eta_{p,n}$ is given by

$$\begin{aligned}\eta_{p,n} &= \phi_0\phi_1\frac{C_{p,n}}{\phi^2_{p,n}}k^{\star 3}_{F_{p,n}}\left(\phi^2_{p,n}k^{\star 2}_{F_{p,n}} + M^2\right)^{1/2} - \phi_0\phi_1\frac{C_{n,p}}{\phi^2_{n,p}}k^{\star 3}_{F_{n,p}}\left(\phi^2_{n,p}k^{\star 2}_{F_{n,p}} + M^2\right)^{1/2} \\ &+ C_0C_1\int_{k_{F_{p,n}}}^{\phi_{p,n}k^\star_{F_{p,n}}} dk\frac{k^{\star 4}_{F_{p,n}}}{k^2\left(k^2 + M^2\right)^{1/2}} - C_0C_1\int_{k_{F_{n,p}}}^{\phi_{n,p}k^\star_{F_{n,p}}} dk\frac{k^{\star 4}_{F_{n,p}}}{k^2\left(k^2 + M^2\right)^{1/2}} \\ &- 3\left[C_0C_1\left(1 - \frac{1}{\phi_{p,n}}\right) + \phi_0\phi_1\frac{C_{p,n}}{\phi^2_{p,n}}\right]\int_0^{k^\star_{F_{p,n}}} dk\left(k^2 + M^2\right)^{1/2}k^2 \\ &+ 3\left[C_0C_1\left(1 - \frac{1}{\phi_{n,p}}\right) + \phi_0\phi_1\frac{C_{n,p}}{\phi^2_{n,p}}\right]\int_0^{k^\star_{F_{n,p}}} dk\left(k^2 + M^2\right)^{1/2}k^2 \end{aligned} \tag{2.43}$$

We also considered an approximation $\mu^{(a)}_{p,n}$ to the chemical potential in which $\Delta_{p,n}$ $C_{p,n}$ and $\Phi_{p,n}$ are made independent of y_p in equation (2.30) leading to $\eta_{p,n} = 0$. This approach also ensures the validity of the Euler relation. Both cases, the exact and the approximated one, are presented in this work. The results and diagrams for astrophysical quantities are constructed for each case.

Notice that Eqs. (2.41) reduce to the chemical potentials of the DD-vdW model when

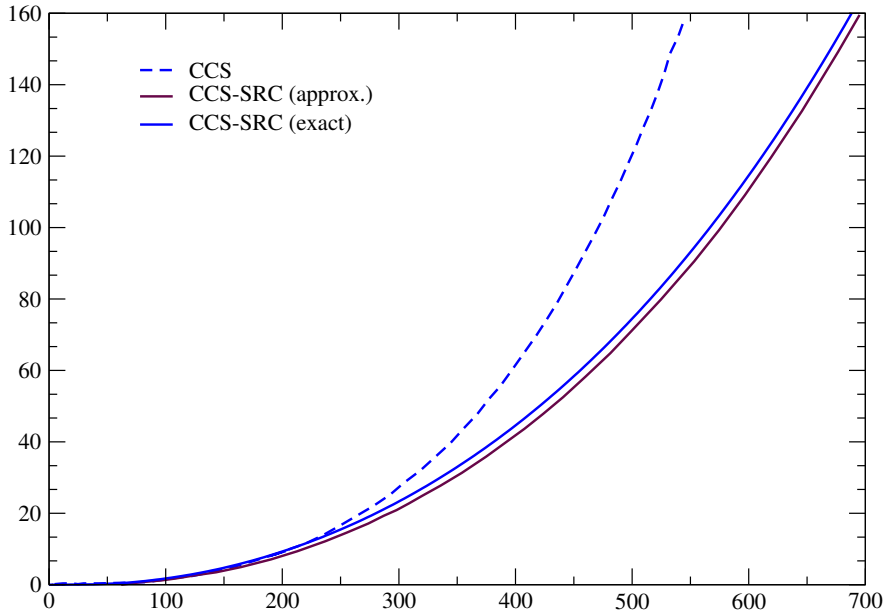

FIGURE 2.6 – Total pressure vs total energy for the CCS model with (full lines) and without (dashed lines) SRC included. Both cases are shown, the case with approximated chemical potential (maroon) and the case with exact chemical potential (blue). Curves for stellar matter with $\rho_0 = 0.15$ fm^{-3}, $B_0 = -16$ MeV, $K_0 = 240$ MeV, and $J = 32$ MeV.

SRC are turned off ($\phi_0 = 1$ and $\phi_1 = 0$ case). Furthermore, in the case of no excluded volume implemented in the model, i.e., for $\mathcal{B}(\rho) \to 0$, the first two terms of Eqs. (2.41) become identical to ones related to the relativistic model studied in Souza *et al.* (2020), for $M \to M^*$, see Eqs. 6 to 8 of that reference.

Before presenting the outcomes of the model concerning the mass-radius diagrams, we first discuss the effect of SRC in the EoS used as input to the TOV equations, by analyzing the outcomes presented in Fig. 2.6. As already mentioned, SRC move the break of causality to higher densities, or equivalently, to higher energy densities. Moreover, one can also notice that SRC make softer the EoS since the pressure is lower for the same value of ϵ in comparison with the case in which no SRC are included. This is not the case for RMF models that present quartic interaction in the vector field ω_μ, i.e., a term given by $C_\omega(\omega_\mu\omega^\mu)^2$ in its Lagrangian density, where C_ω is a constant free parameter, namely Li *et al.* (2008), Dutra *et al.* (2014),

$$\mathcal{L} = \overline{\psi}(i\gamma^\mu\partial_\mu - M)\psi + g_\sigma\sigma\overline{\psi}\psi - g_\omega\overline{\psi}\gamma^\mu\omega_\mu\psi - \frac{g_\rho}{2}\overline{\psi}\gamma^\mu\vec{\rho}_\mu\vec{\tau}\psi + \frac{1}{2}(\partial^\mu\sigma\partial_\mu\sigma - m_\sigma^2\sigma^2)$$
$$- \frac{A}{3}\sigma^3 - \frac{B}{4}\sigma^4 - \frac{1}{4}F^{\mu\nu}F_{\mu\nu} + \frac{1}{2}m_\omega^2\omega_\mu\omega^\mu + C_\omega(\omega_\mu\omega^\mu)^2 - \frac{1}{4}\vec{B}^{\mu\nu}\vec{B}_{\mu\nu} + \frac{1}{2}\alpha_3' g_\omega^2 g_\rho^2\omega_\mu\omega^\mu\vec{\rho}_\mu\vec{\rho}^\mu + \frac{1}{2}m_\rho^2\vec{\rho}_\mu\vec{\rho}^\mu. \tag{2.44}$$

For models with this structure, it is verified that SRC make stiffer the EoS (the pressure is higher for the same energy density). For instance, we display in Fig. 2.7a this finding for the FSU2R parametrization (TOLOS *et al.*, 2017b) with and without SRC.

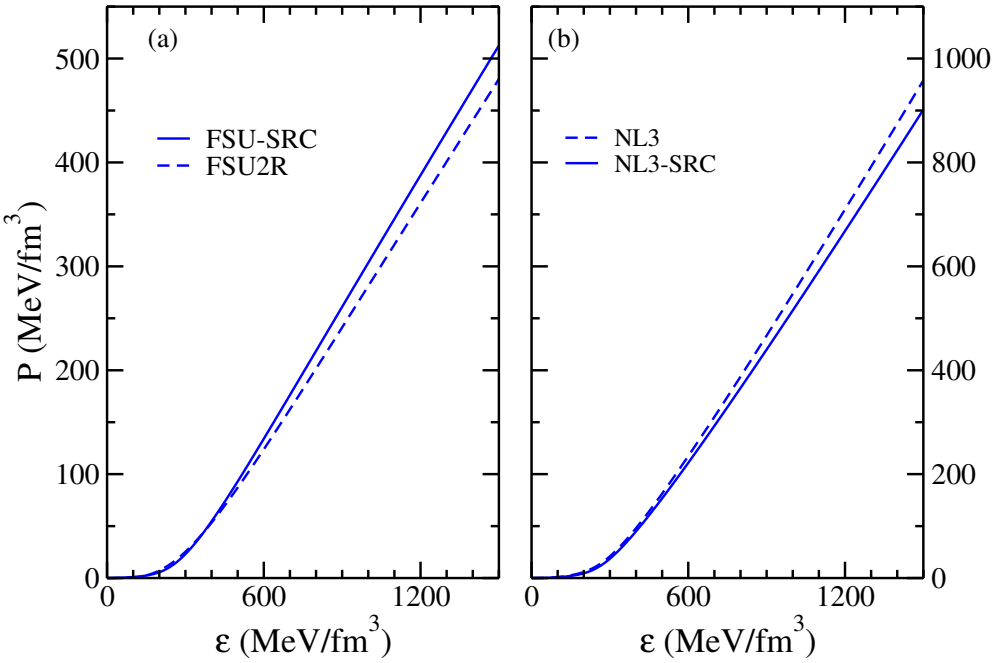

FIGURE 2.7 – Total pressure as a function of total energy density (stellar matter) for the (a) FSU and (b) NL3 parametrizations with (full lines) and without (dashed lines) SRC included.

For the construction of the 2.7a curves, the bulk parameters were kept the same for both approaches (with and without SRC) as well as the value of the constant C_ω, the procedure also adopted in Cai e Li (2016b), Souza *et al.* (2020). Despite this result, it is worth mentioning that SRC can also soften the EoS even for RMF models. This is the case for parametrizations with $C_\omega = 0$. As an example, we plot in Fig. 2.7b total pressure as a function of total energy density for the NL3 (LALAZISSIS *et al.*, 1997; SILVA *et al.*, 2008) parametrization, for which there is no quartic self-interaction in the repulsive vector channel. As we see, the effect of including SRC is exactly the opposite of that verified for the FSU2R parametrization, but the same as the one presented by the CCS-SRC model. It is known that hadronic models with stiffer EoS produce more massive neutron stars. This is a direct consequence of introducing SRC in RMF models with $C_\omega \neq 0$, as verified in Cai e Li (2016b), Souza *et al.* (2020), Lourenço *et al.* (2022), for instance. For the case of models with softer EoS, the opposite is expected. In our case, despite SRC generating softer EoS, we still find possible parametrizations of the CCS-SRC model capable of reproducing recent astrophysical observational data, as presented in Fig. 2.8.

Notice that the model produces mass-radius diagrams in agreement with the following astrophysical constraints: gravitational waves data related to the GW170817 (ABBOTT *et al.*, 2017; ABBOTT *et al.*, 2018) and GW190425 (ABBOTT *et al.*, 2020) events, some of them provided by the LIGO and Virgo Collaboration; data from the NICER mission regarding the pulsars PSR J0030+0451 (RILEY *et al.*, 2019; MILLER *et al.*, 2019) and PSR J0740+6620 (RILEY *et al.*, 2021; MILLER *et al.*, 2021); and data from the latter pulsar extracted from (FONSECA *et al.*, 2021a). Such agreement is true for both, the approxi-

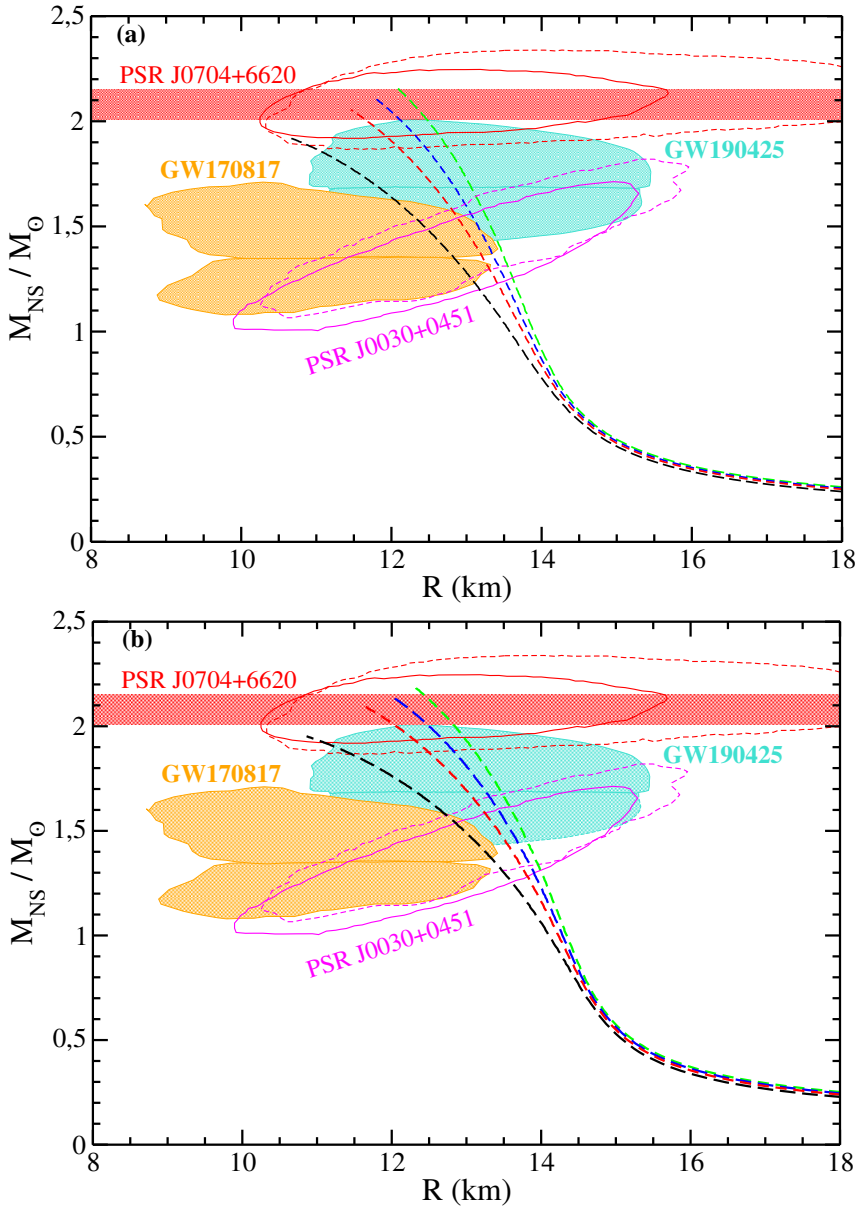

FIGURE 2.8 – Mass-radius diagrams constructed from the CCS-SRC model with different values of K_0, for **(a)** - approximated chemical potential and **(b)** - complete form of the chemical potential. The contours are related to data from the NICER mission, namely, PSR J0030+0451 (RILEY *et al.*, 2019; MILLER *et al.*, 2019) and PSR J0740+6620 (RILEY *et al.*, 2021; MILLER *et al.*, 2021), the GW170817 (ABBOTT *et al.*, 2017; ABBOTT *et al.*, 2018) and the GW190425 events (ABBOTT *et al.*, 2020), all of them at 90% credible level. The red horizontal lines are also related to the PSR J0740+6620 pulsar (FONSECA *et al.*, 2021a).

mated and the exact form of the chemical potential, depicted in the Figs. 2.8a and 2.8b, respectively.

For the sake of completeness, we present in Fig. 2.9b the plot of the stellar mass as a function of the central density for the different CCS-SRC parametrizations used here.

In addition, we show in Fig. 2.9a the squared sound velocity for beta-equilibrated matter, $v_s^2 = \partial P/\partial\varepsilon$, also as a function of the density. By comparing the results of both panels, it is possible to confirm that a break of causality is not observed for the

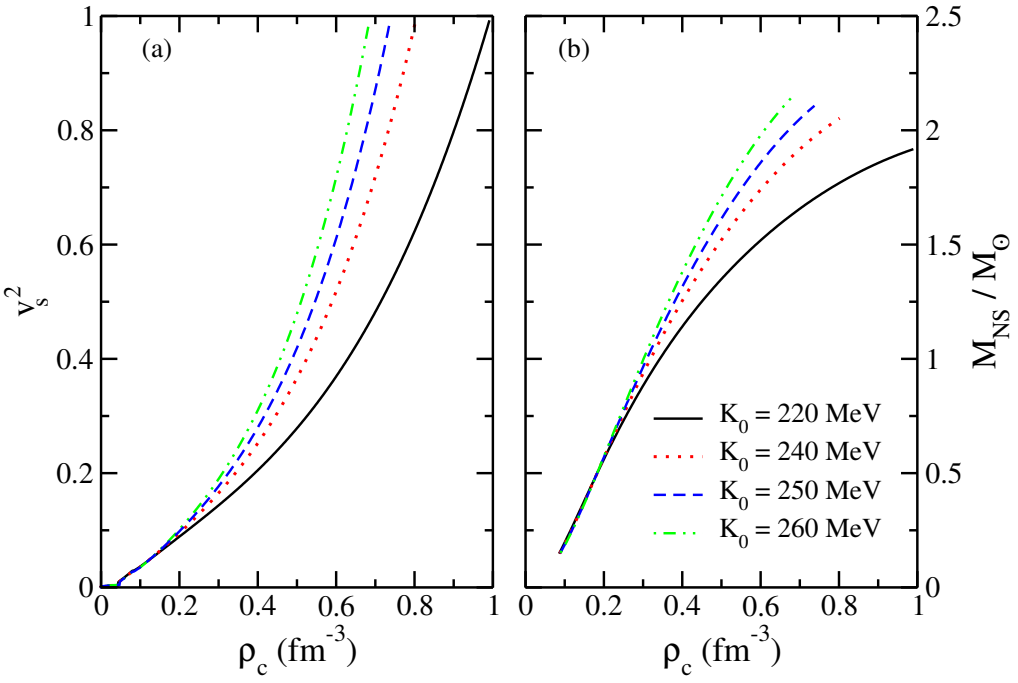

FIGURE 2.9 – (a) Squared sound velocity for beta-equilibrated matter, and (b) stellar mass in units of $M_\odot$, both as a function of the central density for the CCS-SRC model. All curves constructed by using $\rho_0 = 0.15$ fm^{-3}, $B_0 = -16$ MeV, $J = 32$ MeV, and different values of K_0, considering the approximate form of chemical potential.

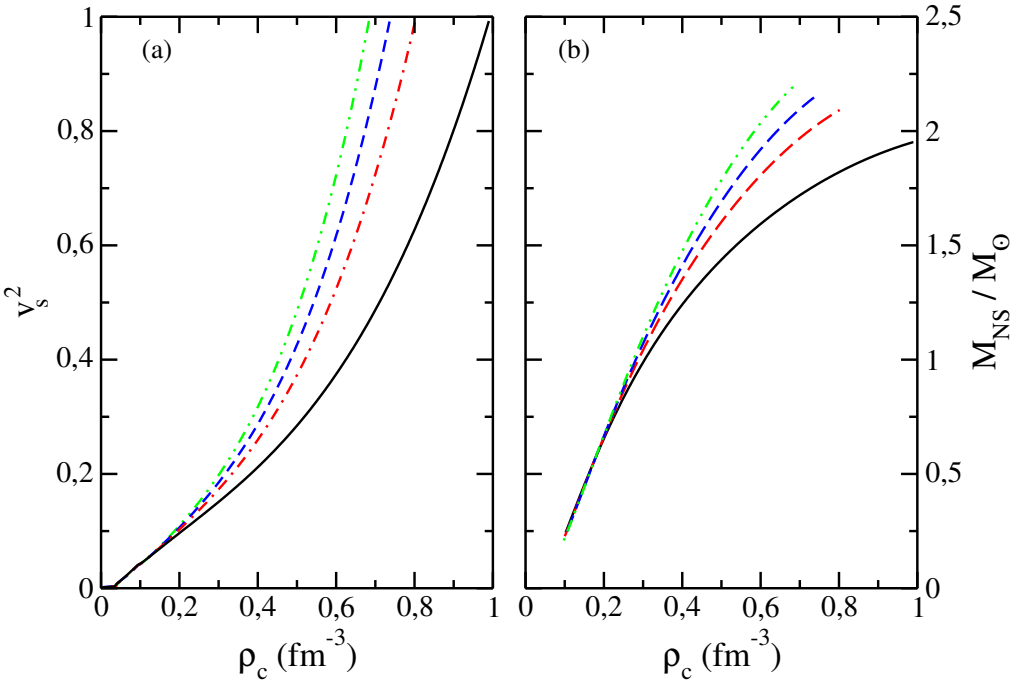

FIGURE 2.10 – (a) Squared sound velocity for beta-equilibrated matter, and (b) stellar mass in units of $M_\odot$, for the same parameters in Fig. 2.9, but for the complete form of chemical potential.

configurations of the stars generated by the model.

We also verify the results obtained through the model with regard to the dimensionless tidal deformability. This quantity is defined as $\Lambda = 2k_2/(3C^5)$, with $C = M_{\rm NS}/R$, and the second Love number given by

$$\begin{aligned} k_2 \;=\; & \tfrac{8C^5}{5}(1-2C)^2[2+2C(y_R-1)-y_R \times \Big\{2C[6-3y_R+3C(5y_R-8)] \\ & +4C^3[13-11y_R+C(3y_R-2)+2C^2(1+y_R)] \\ & +3(1-2C)^2[2-y_R+2C(y_R-1)]\ln(1-2C)\Big\}^{-1}, \end{aligned} \tag{2.45}$$

with $y_R = y(R)$. The quantity $y(r)$ is determined from the solution of the differential equation $r(dy/dr) + y^2 + yF(r) + r^2Q(r) = 0$, solved simultaneously with the TOV ones. The expressions for the functions $F(r)$ and $Q(r)$ are

$$F(r) \;=\; \frac{1-4\pi r^2[\epsilon(r)-p(r)]}{g(r)}, \tag{2.46}$$

(2.47)

$$\begin{aligned} Q(r) \;=\; & \frac{4\pi}{g(r)}\left[5\epsilon(r)+9p(r)+\frac{\epsilon(r)+p(r)}{v_s^2(r)}-\frac{6}{4\pi r^2}\right] \\ - \; & 4\left[\frac{m(r)+4\pi r^3 p(r)}{r^2 g(r)}\right]^2, \end{aligned} \tag{2.48}$$

with $v_s^2(r) = \partial p(r)/\partial\epsilon(r)$ being the squared sound velocity (POSTNIKOV *et al.*, 2010; HINDERER, 2008; DAMOUR; NAGAR, 2010; BINNINGTON; POISSON, 2009). We show the results concerning Λ in Fig. 2.11. From this figure, one notices that the inclusion of SRC in the system favors the model to attain the constraint of $\Lambda_{1.4} = 190^{+390}_{-120}$ (ABBOTT *et al.*, 2018) for both forms of the chemical potential.

For the model presented here, it is also clear that the inclusion of SRC systematically decreases Λ in all cases. The physical reason for this effect comes from the fact that SRC soften the EoS, as already discussed. In this case, the NS radius is also reduced by these correlations, and due to the relation given by $\Lambda \sim R^\alpha$, verified in different hadronic models for a 1.4 $M_\odot$ star for instance (Lourenço *et al.*, 2019; Lourenço *et al.*, 2020), it is straightforward to conclude that Λ decreases with the radius decreasing. For the CCS model, this decrease makes the model compatible with the astrophysical data analyzed.

Finally, we plot in Fig. 2.12 the tidal deformabilities Λ_1 and Λ_2 of the binary neutron stars system with component masses m_1 and m_2 ($m_1 > m_2$), related to the GW170817 event, and taking into account the range for m_1 given by $1.365 \leqslant m_1/M_\odot \leqslant 1.60$ (ABBOTT *et al.*, 2017). The mass of the companion star m_2, is obtained from the relationship between

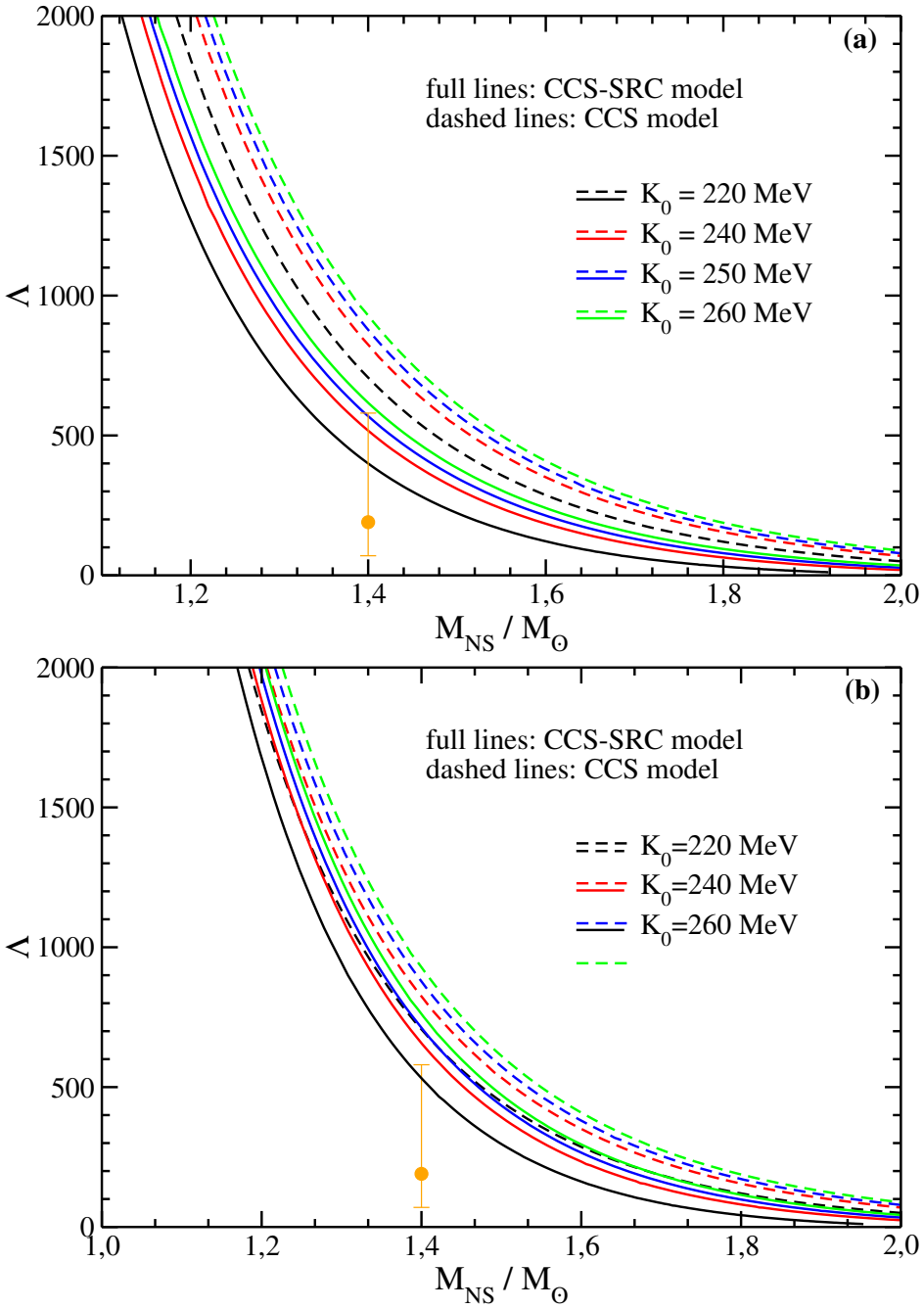

FIGURE 2.11 – Λ versus $M_{\rm NS}/M_{\odot}$ for the CCS model with $\rho_0 = 0.15$ fm^{-3}, $B_0 = -16$ MeV, $J = 32$ MeV, and different values of K_0 with (full lines) and without (dashed lines) SRC included. The panel stands for **(a)** - approximated chemical potential and **(b)** - complete form of the chemical potential. Full circle with error bars: result of $\Lambda_{1.4} = 190^{+390}_{-120}$ obtained in Abbott *et al.* (2018).

m_1, m_2, and the chirp mass, that reads

$$\mathcal{M}_c = \frac{(m_1 m_2)^{3/5}}{(m_1 + m_2)^{1/5}}, \tag{2.49}$$

and is fixed at the observed value of $1.188 M_\odot$, according to (ABBOTT *et al.*, 2017). Upper and lower orange dashed lines correspond to the 90% and 50% confidence limits, respectively, provided by LIGO and Virgo Collaboration (ABBOTT *et al.*, 2018). It is clear that the effect of SRC is to move the $\Lambda_1 \times \Lambda_2$ curves of our excluded volume model to the region of compatibility with the LIGO and Virgo Collaboration data regarding the GW170817 event, due to the fact that SRC decreases the values of both dimensionless tidal deformabilities. In the figure, we also furnish a band with results obtained through the relativistic mean field models studied in Lourenço *et al.* (2019) that are consistent with constraints from nuclear matter, pure neutron matter, symmetry energy, and its derivatives analyzed in Dutra *et al.* (2014). Notice that the parametrizations of the CCS-SRC model also have a good intersection with this band.

It is also worth to noting that the CCS-SRC parametrizations used to construct Figs. 2.8, 2.11, and 2.12 have the symmetry energy slope at the saturation density around 108 MeV. This value is inside the range of $L_0 = (106 \pm 37)$ MeV, claimed in Reed *et al.* (2021) to be in full agreement with the updated results provided by the lead radius experiment (PREX-2) collaboration concerning the neutron skin thickness of ^{208}Pb (ADHIKARI *et al.*, 2021). Nevertheless, it is also important to mention that there are other studies pointing out smaller ranges for L_0. In Reinhard *et al.* (2021), for instance, the interval of $L_0 = (54 \pm 8)$ MeV was determined from an analysis that takes into account theoretical uncertainties of the parity-violating asymmetry in ^{208}Pb. Ab initio calculations performed in Hu *et al.* (2022), also for the ^{208}Pb nucleus, predict the range of $L_0 = (37 - 66)$ MeV for the slope parameter. Furthermore, according to (LATTIMER, 2023), the range of $L_0 = (-5 \pm 40)$ MeV is related to the results of the neutron skin thickness of ^{48}Ca provided by CREX Collaboration (ADHIKARI *et al.*, 2022). Another analysis in Zhang e Chen (2022) combined the results from PREX-2 and CREX and found $L_0 = 15.3^{+46.8}_{-41.5}$ MeV through a Bayesian inference. However, another combination of the PREX-2 and CREX results produced, through a covariance analysis, higher values for this isovector quantity: $L_0 = (82.32 \pm 22.93)$ MeV (KUMAR *et al.*, 2023).

We verified that for lower values of L_0, the CCS-SRC parametrizations are not simultaneously compatible with all astrophysical constraints depicted in Fig. 2.8. Moreover, in this case, the model produces extremely low values of J, for example, $J \sim 19$ MeV for $L_0 = 66$ MeV. This feature leads the bulk parameter space of the model with SRC to the direction of higher values of L_0. A more complete description, namely, the one in which lower values of L_0 are also allowed, necessarily imposes a suitable modification

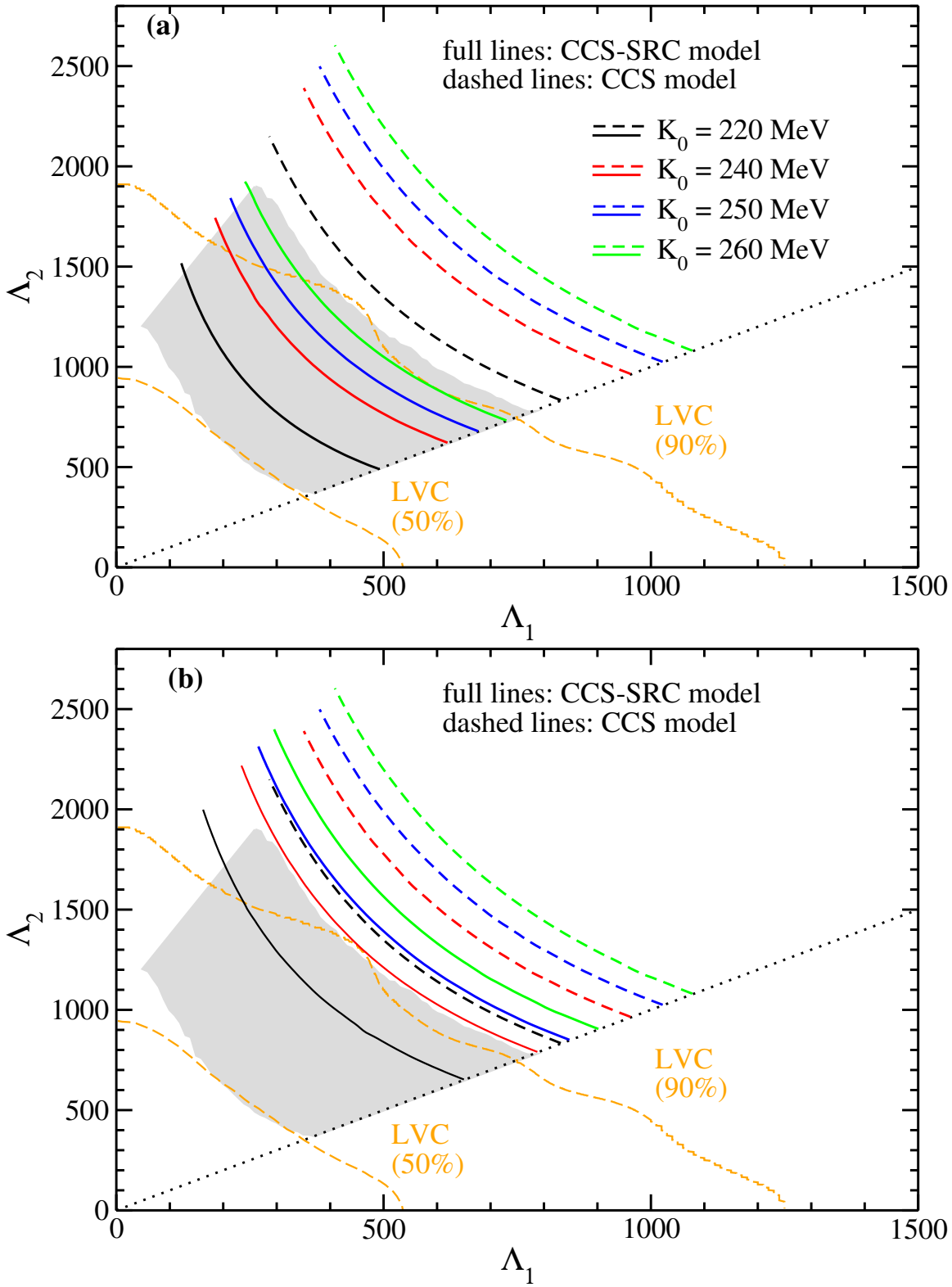

FIGURE 2.12 – Λ_2 versus Λ_1 for the CCS model with $\rho_0 = 0.15$ fm^{-3}, $B_0 = -16$ MeV, $J = 32$ MeV, and different values of K_0 with (full lines) and without (dashed lines) SRC included. The panel stands for **(a)** - approximated chemical potential and **(b)** - complete form of the chemical potential. The orange dashed lines correspond to the 90% and 50% confidence limits given by the LIGO and Virgo Collaboration (LVC) (ABBOTT *et al.*, 2018). The gray band represents the results obtained through the relativistic mean field models studied in Lourenço *et al.* (2019).

in the isovector sector. This specific study is already been performed for the CCS-SRC model.

2.4 Final remarks

We verified that one of the effects of including SRC in the model is the shift of the break of causality to a higher-density region. It is important to mention that this kind of relativistic models suffer from this issue, namely, the break of causality due to the lack of a complete treatment of the Lorentz contraction for the finite-size nucleons. As we have shown, SRC helps to circumvent this problem in an effective way. We also observed that SRC did not destroy the linear relationship between symmetry energy and its slope (L_0), a correlation often found in the literature (DRISCHLER *et al.*, 2020; LI *et al.*, 2021; SANTOS *et al.*, 2015). Furthermore, SRC increase the value of L_0 in comparison with the model without this phenomenology implemented. At higher density regime, another important finding shown in Fig. 2.4 is that the CCS-SRC model completely satisfies the flow constraint, a wide constraint used to validate and select hadronic models (DUTRA *et al.*, 2014), for parametrizations constructed by running K_0 in the range of $K_0 = (240 \pm 20)$ MeV (GARG; COLò, 2018).

With regard to the stellar matter, the inclusion of SRC in the CCS model softens the EoS generated as input to the TOV equations used to construct the mass-radius profiles. This softness is slightly greater if the exact chemical potential is used instead of the approximated one. Looking only to the mass-radius diagram, one may notice that the difference between the curves generated by the exact and approximated chemical potential is very small.

For RMF models presenting quartic self-interaction in the repulsive vector field, that is, models in which the Lagrangian density presents a term given by $C_\omega(\omega^\mu\omega_\mu)^2$, the effect of the SRC inclusion in the EoS is opposite to the one suffered by the CCS model. For these models, SRC make the EoS stiffer and consequently capable of producing more massive neutron stars. However, RMF models in which $C_\omega = 0$ exhibit the same behavior as the one found here, i.e., softer EoS in comparison with the ones without SRC added. Nevertheless, the CCS-SRC model still generates mass-radius diagrams compatible with recent astrophysical constraints, such as those coming from gravitational waves data related to the GW170817 (ABBOTT *et al.*, 2017; ABBOTT *et al.*, 2018) and GW190425 (ABBOTT *et al.*, 2020) events, data from the NICER mission regarding the pulsars PSR J0030+0451 (RILEY *et al.*, 2019; MILLER *et al.*, 2019) and PSR J0740+6620 (RILEY *et al.*, 2021; MILLER *et al.*, 2021); and data from the latter pulsar extracted from (FONSECA *et al.*, 2021a).

Our results show that SRC also favor the model to be consistent with the constraints

regarding the dimensionless tidal deformability, namely, the one related to the $1.4M_{\odot}$, namely, $\Lambda_{1.4} = 190^{+390}_{-120}$ (ABBOTT *et al.*, 2018), and those from the binary neutron stars system (ABBOTT *et al.*, 2017), both of them provided by the LIGO and Virgo Collaboration through the analysis of gravitational waves detected in the GW170817 event. In this particular case, it was observed that SRC decrease the value of Λ due to the reduction of the neutron star radius caused by the softening of the EoS.

Finally, the values found for L_0 are inside the range of $L_0 = (106 \pm 37)$ MeV, pointed out in Reed *et al.* (2021) as compatible with data from the PREX-2 collaboration with regard to the ^{208}Pb neutron skin thickness (ADHIKARI *et al.*, 2021). We also mention that, for the case in which lower values of L_0 are considered, the model is not able to simultaneously reconcile with all astrophysical constraints. Furthermore, very low values of J are also found in this case. This feature has motivated us to investigate a possible improvement in the isovector sector of the model in order to make it suitable to also reach this particular region of the parameter space.

3 Hadronic model with short-range correlations admixed with dark matter

3.1 Dark matter models in a two fluid formalism

As previously discussed in section the introduction, it is reasonable to consider dark matter in the Neutron Stars. The effects of the dark matter are observed in the NS if one takes the case of the non-self-annihilating DM. Non-self-annihilating DM stands for the class of theories that propose that these particles do not annihilate itself, so its interactions could lead not only to indirect effects, such as imprints in charged cosmic rays, but to most direct effects as effects on the NS structure. A prominent type of non-self-annihilating DM is the asymmetric DM. The asymmetric DM states that the process of formation of DM in the early universe could result into a discrepancy between the quantity of DM and anti-DM, similar to what happens to the baryonic matter (normal matter) . Therefore, there is a net excess of dark matter that does not significantly self-annihilate nowadays. (ZUREK, 2014)

One proposed model for describing asymmetric dark matter is the mirror dark matter scenario, where each particle in the visible sector has a corresponding counterpart in the dark sector. In this framework, an asymmetry in mirror baryons—analogous to the baryon asymmetry in the visible sector—results in a relic abundance of mirror matter that can account for dark matter in the universe. This asymmetry prevents mirror matter from annihilating completely in the early universe, ensuring its survival. The interactions between the mirror and visible sectors are primarily mediated through gravity, making mirror matter difficult to detect directly. Nevertheless, it can still influence cosmological processes, such as the formation of large-scale structures and the evolution of the universe (PETRAKI; VOLKAS, 2013).

If the mirror modelling for the DM is considered, the description of this kind of matter must be exactly equal to that used for the NM. In this context, in an ideal scenario for treatment of a system with DM, one must use the same Lagrangian used for the baryonic sector. This could be unachievable given that there is no sufficient observational data to

constraint every mirrored constant present in the dark sector. The mirrored Lagrangian is then customarily approximated, that meaning that some terms present in the Lagrangian are neglected, a handling that has been extensively done recently (DAS *et al.*, 2022; THAKUR *et al.*, 2024).

Regarding the interaction between sectors, one possible procedure is to take the interaction as purely gravitational. Being so, there is no Lagrangian cross term that relates or link both sectors. The linking happens only in the gravitational field, that modifies the TOV equations. Previously, the gravitational field for the normal matter was written as a set of equations for a single fluid as in (1.1). The inclusion of an additional type of matter, that is, a new fluid, give rise to a set of two additional equations (CIARCELLUT; SANDIN, 2011; XIANG *et al.*, 2014; ELLIS *et al.*, 2018; THAKUR *et al.*, 2024). In this approach, each fluid satisfies conservation of energy-momentum separately, that is equivalent to have $P(r) = P_{\rm vis}(r) + P_{\rm DM}(r)$ and $\mathcal{E}(r) = \mathcal{E}_{\rm vis}(r) + \mathcal{E}_{\rm DM}(r)$, with r being the radial coordinate from the center of the star. This consideration leads to the following differential TOV equations to be solved,

$$\frac{dP_{\rm vis}(r)}{dr} = -\frac{[\mathcal{E}_{\rm vis}(r) + P_{\rm vis}(r)]\,[m(r) + 4\pi r^3 P(r)]}{r\,[r - 2m(r)]}, \tag{3.1}$$

$$\frac{dP_{\rm DM}(r)}{dr} = -\frac{[\mathcal{E}_{\rm DM}(r) + P_{\rm DM}(r)]\,[m(r) + 4\pi r^3 P(r)]}{r\,[r - 2m(r)]}, \tag{3.2}$$

$$\frac{dm_{\rm vis}(r)}{dr} = 4\pi r^2 \mathcal{E}_{\rm vis}(r), \tag{3.3}$$

$$\frac{dm_{\rm DM}(r)}{dr} = 4\pi r^2 \mathcal{E}_{\rm DM}(r), \tag{3.4}$$

where $m(r) = m_{\rm vis}(r) + m_{\rm DM}(r)$ is the total mass contained in the sphere of radius r. The visible matter mass is $m_{\rm vis}(r)$, and the dark matter mass is $m_{\rm DM}(r)$. This set of coupled equations can be obtained from the stationary condition of the star mass (XIANG *et al.*, 2014).

Technically, the procedure adopted to solve Eqs. (3.1)-(3.4) is the following. First we define the four initial conditions as $m_{\rm vis}(0) = m_{\rm DM}(0) = 0$, $P_{\rm vis}(0) = P^c_{\rm vis}$, and $P_{\rm DM}(0) = P^c_{\rm DM}$, where $P^c_{\rm vis}$ and $P^c_{\rm DM}$ are the central pressures related to visible and dark matter, respectively, given by the equations of state presented in the previous sections. Then, for each set of initial conditions we use the fourth order Runge–Kutta method in order to obtain pressures and masses as functions of r. The radii $R_{\rm vis}$ and $R_{\rm DM}$ are defined as being the quantities that lead to $P_{\rm vis}(R_{\rm vis})/P^c_{\rm vis} = 0$ and $P_{\rm DM}(R_{\rm DM})/P^c_{\rm DM} = 0$, within a certain tolerance. The radii $R_{\rm vis}$ and $R_{\rm DM}$ are used to determine $M_{\rm vis} \equiv m_{\rm vis}(R_{\rm vis})$, and $M_{\rm DM} \equiv m_{\rm DM}(R_{\rm DM})$. Therefore, the total mass of the respective star is $M = M_{\rm vis} + M_{\rm DM}$, and its radius is $R = R_{\rm vis}$ if $R_{\rm vis} > R_{\rm DM}$, or $R = R_{\rm DM}$ if $R_{\rm DM} > R_{\rm vis}$. This latter case

identifies dark matter halo configurations for the star of mass M and radius R.

In order to satisfy this restriction, we proceed as follows. First one needs to construct all the inputs for the TOV equations, namely, $P^c_{\rm vis}$, $\mathcal{E}^c_{\rm vis}$, $P^c_{\rm DM}$ and $\mathcal{E}^c_{\rm DM}$ (despite not directly used as initial conditions, the energy densities have also to be furnished since their relationships with the pressures are used to replace $\mathcal{E}$'s by P's in the TOV equations).

To obtain the visible pressure and energy density, one should now define the kind of description used to construct the EoS. For the visible sector, the hadrons should obbey the Fermi-Dirac statistic and so, it must depicted by a Fermionic model. The question that remains is what kind of interaction should be taken into account? In a previous work, Dutra *et al.* (2014) explored an extensive description of the hadronic interaction within the RMF formalism. We used a similar, but simplified description for the Lagrangian, that is pointed out in the next section.

If the mirror dark matter framework is used, DM consists of fermionic particles that are counterparts to ordinary baryonic matter. Within the RMF formalism, modeling such fermionic dark matter requires constructing a Lagrangian density that includes mass terms for the dark fermions, ensuring they have well-defined masses analogous to their visible-sector counterparts. Moreover, the DM Lagrangian density must incorporate interactions mediated by dark analogues of mesons—mirror mesons such as the dark scalar, vector, and isovector meson fields. These interactions are characterized by coupling parameters that determine the strength of the coupling between dark fermions and dark meson fields. Including these coupling constants is essential, as they dictate the dynamics of the dark matter particles within the RMF framework, influencing properties like the equation of state, particle interactions, and ultimately the macroscopic behavior of dark matter in astrophysical systems. However, the lack of observational constraints, leaves the choice for the couplings parameters relatively free. Such constants are very often constrained by astrophysical observational data.

This substantial flexibility in the choice of parameters could lead to difficulties in the choice of an adequate range to reproduced observational data. To tackle this problem, several strategies have been applied, the most prominent one being those that uses large computational analyses. In its paper, Das *et al.* (2022) proposed an sophisticated technique to constraint and find the best choices for the dark counterpart of the coupling constant relative to the scalar and vector mesons. They used a Bayesian analysis, in which the prior was adequately chosen and the likelihood function was taken considering the observational constraints of gravitational waves and X-ray telescopes. Another study using a computational analysis was done by Thakur *et al.* (2024), who used a sampling of 50.000 combinations of parameter that represents the bare dark mass, the vector meson mass and coupling constant and the dark mass fraction composing the star. They chose a initial range for the parameters and used the Kendall ranking correlation to find a distri-

bution of the most probable values for each parameter. The model for the fermionic dark matter used in this work is exactly the one brought by Thakur *et al.* (2024).

Another possible dark matter description is the one considering it as of composed by bosonic WIMP particles. Bosonic WIMPs are bosonic dark matter particles candidates that interacts via weak nuclear force and gravity. Prominent examples include scalar singlet dark matter from Higgs portal models, where a spin-0 scalar particle interacts with the Standard Model Higgs boson through a coupling term in the Lagrangian (ARCADI *et al.*, 2018; ATHRON *et al.*, 2019). This interaction allows the scalar particle to interact weakly with ordinary matter. Another example is vector dark matter like dark photons, which are spin-1 particles associated with a hidden U(1) gauge symmetry. Dark photons kinetically mix with Standard Model photons, enabling weak interactions with normal matter (FABBRICHESI *et al.*, 2021; CAPUTO *et al.*, 2021). Additionally, Kaluza-Klein photons from theories with universal extra dimensions act as massive spin-1 bosonic WIMPs. These higher-dimensional photons interact with Standard Model particles through extensions of electromagnetic interactions (FLACKE *et al.*, 2017; KAKIZAKI *et al.*, 2017).

There is a widely range of possibilities to treat the bosonic dark matter. Here, we use one simple model. The bosonic matter is considered as a self-interacting asymmetric dark matter (ADM), with only the repulsive self-interactions of ADM, the minimal interaction of ADM to gravity, and the interaction of ADM with baryons taken into account. This kind of model was first proposed by Nelson *et al.* (2019). This model was then used by Rutherford *et al.* (2023) to determine the free parameters related to dark matter via a Bayesian analysis. We use exact the same results found by the last, including the pressure and energy density for dark matter therein.

With both dark matter depictions defined, the main objective of this chapter can be achieved, namely, to include the short-range correlations in the visible sector aiming to verify the effect of such phenomenology in neutron stars with dark matter content.

3.2 Hadronic and DM models

For the fermionic dark matter model, we begin with a Lagrangian density that includes a kinetic term (the Dirac Lagrangian density) for a single fermionic component, alongside a vector meson coupled to the Dirac spinor. The complete expression is (XIANG *et al.*, 2014; DAS *et al.*, 2022; THAKUR *et al.*, 2024)

$$\mathcal{L}_{\text{FDM}} = \bar{\chi}\left[\gamma_\mu(i\partial^\mu - g_V V^\mu) - m_\chi\right]\chi - \frac{1}{4}F_{\mu\nu}F^{\mu\nu} + \frac{1}{2}m_V^2 V_\mu V^\mu, \tag{3.5}$$

The dark fermion mass is denoted by m_χ, and m_V represents the mass of the dark vector meson. In this model, we do not include the dark scalar meson in order to simplify the model and avoid an additional free parameter to be fixed. This can be done once that the main effect driving the increase in the final compact star mass comes from repulsive interactions. Introducing a scalar particle would lead to attractive interactions, which would diminish the net repulsion.

Similar to the approach used in relativistic hadronic models, which follow the same mathematical formulation for the Lagrangian density, we apply the mean field approximation to calculate the energy density and pressure of the dark sector. These expressions are given by

$$\mathcal{E}_{\rm FDM} = \frac{1}{\pi^2}\int_0^{k_{F\chi}} dk\, k^2 (k^2 + m_\chi^2)^{1/2} + \frac{1}{2} C_V^2 \rho_\chi^2, \tag{3.6}$$

$$P_{\rm FDM} = \frac{1}{3\pi^2}\int_0^{k_{F\chi}} dk\, \frac{k^4}{(k^2 + m_\chi^2)^{1/2}} + \frac{1}{2} C_V^2 \rho_\chi^2, \tag{3.7}$$

with $C_V = g_V/m_V$ and $\rho_\chi = k_{F\chi}^3/(3\pi^2)$. The Fermi momentum of the dark particle is $k_{F\chi}$. Fermionic self-interacting dark matter models coupled to hadronic matter were used in the description of neutron stars with DM content, as the reader can find in Das *et al.* (2022), for instance.

Regarding the bosonic dark matter, the model by Nelson *et al.* (2019) and Rutherford *et al.* (2023) brings following Lagrangian density for the model

$$\mathcal{L}_{\rm BDM} = -\sqrt{-g}\left(D_\mu^* \sigma^* D^\mu \sigma - m_\sigma^2 \sigma^* \sigma - \frac{1}{2} m_\phi^2 \phi_\mu \phi^\mu - \frac{1}{4} Z_{\mu\nu} Z^{\mu\nu} \right) \tag{3.8}$$

where $D_\mu = \partial_\mu + i g_\sigma \phi_\mu$, g_σ is the interaction strength of the dark scalar complex field σ with the dark vector field ϕ^μ, $Z_{\mu\nu} = \partial_\mu \phi_\nu - \partial_\nu \phi_\mu$, and g is the determinant of the metric. The masses of the dark scalar and dark vector fields are m_σ and m_ϕ, respectively. Usual quantum field theory techniques, along with the mean field approximation, lead to the following energy-momentum tensor

$$T_{\mu\nu} = 2 D_\mu^* \sigma^* D_\nu \sigma - g_{\mu\nu}\left(D_\rho^* \sigma^* D^\rho \sigma + m_\sigma^2 \sigma^* \sigma \right) + m_\sigma^2 \left(\phi_\mu \phi_\nu - \frac{1}{2} g_{\mu\nu} \phi_\rho \phi^\rho \right), \tag{3.9}$$

that is used to find the equations of state for the bosonic DM model given by

$$\mathcal{E}_{\rm BDM} = m_\sigma \rho_\sigma + \frac{1}{2} C_{\sigma\phi}^2 \rho_\sigma^2, \tag{3.10}$$

$$P_{\rm BDM} = \frac{1}{2} C_{\sigma\phi}^2 \rho_\sigma^2, \tag{3.11}$$

with $C_{\sigma\phi} = g_\sigma/m_\phi$. The DM density ρ_σ relates to the zero component of the vector field

ϕ_0, and with the scalar field and its conjugate through $\phi_0 = (g_\sigma/m_\phi^2)\rho_\sigma$, and $\rho_\sigma = 2m_\sigma\sigma^*\sigma$, respectively.

For the visible sector, we used the model studied by Lourenco *et al.* (2022) to describe the hadronic matter, that is, nucleons and mesons, with the Lagrangian reading

$$\begin{aligned}\mathcal{L}_{\rm HAD} = {} & \bar{\psi}(i\gamma^\mu\partial_\mu - M_{\rm nuc})\psi + g_\sigma\bar{\psi}\sigma\psi - g_\omega\bar{\psi}\gamma^\mu\omega_\mu\psi - \frac{g_\rho}{2}\bar{\psi}\gamma^\mu\vec{\rho}_\mu\vec{\tau}\psi + \frac{1}{2}(\partial^\mu\sigma\partial_\mu\sigma - m_\sigma^2\sigma^2) \\ & - \frac{A}{3}\sigma^3 - \frac{B}{4}\sigma^4 - \frac{1}{4}F^{\mu\nu}F_{\mu\nu} + \frac{1}{2}m_\omega^2\omega_\mu\omega^\mu + \frac{C}{4}(g_\omega^2\omega_\mu\omega^\mu)^2 - \frac{1}{4}\vec{B}^{\mu\nu}\vec{B}_{\mu\nu} \\ & + \frac{1}{2}\alpha_3 g_\omega^2 g_\rho^2\omega_\mu\omega^\mu\vec{\rho}_\mu\vec{\rho}^\mu + \frac{1}{2}m_\rho^2\vec{\rho}_\mu\vec{\rho}^\mu. \end{aligned} \tag{3.12}$$

in which ψ is the nucleon field whereas σ, ω^μ, and $\vec{\rho}_\mu$ are the scalar, vector, and isovector-vector fields representing, respectively, mesons σ, ω, and ρ. Furthermore, one has $F_{\mu\nu} = \partial_\nu\omega_\mu - \partial_\mu\omega_\nu$ and $\vec{B}_{\mu\nu} = \partial_\nu\vec{\rho}_\mu - \partial_\mu\vec{\rho}_\nu$. The nucleon rest mass is $M_{\rm nuc}$, and the meson masses are m_σ, m_ω, and m_ρ. Here we consider the meson self-interactions, like the ones whose strengths are given by the constants A, B, C, and the ones between the ω and $\vec{\rho}$, regulated by the constant α_3'.

From the Lagrangian (3.12), if one applies the mean field approximation it is possible to obtain the field equations and then the energy-momentum tensor $T^{\mu\nu}$, in which $\mathcal{E}_{\rm vis} = \langle\mathcal{T}_{00}\rangle$ and $P_{\rm vis=\langle T_{ii}\rangle/3}$. One may find that the form of the density energy reads

$$\begin{aligned}\mathcal{E}_{\rm vis} = {} & \frac{m_\sigma^2\sigma^2}{2} + \frac{A\sigma^3}{3} + \frac{B\sigma^4}{4} - \frac{m_\omega^2\omega_0^2}{2} - \frac{Cg_\omega^4\omega_0^4}{4} - \frac{m_\rho^2\rho_{0(3)}^2}{2} + g_\omega\omega_0\rho + \frac{g_\rho}{2}\bar{\rho}_{0(3)}\rho_3 \\ & - \frac{1}{2}\alpha_3 g_\omega^2 g_\rho^2\omega_0^2\bar{\rho}_{0(3)}^2 + \mathcal{E}_{\rm kin}^p + \mathcal{E}_{\rm kin}^n, \end{aligned} \tag{3.13}$$

and pressure for the visible matter

$$\begin{aligned}P_{\rm vis} = {} & -\frac{m_\sigma^2\sigma^2}{2} - \frac{A\sigma^3}{3} - \frac{B\sigma^4}{4} + \frac{m_\omega^2\omega_0^2}{2} + \frac{Cg_\omega^4\omega_0^4}{4} + \frac{m_\rho^2\rho_{0(3)}^2}{2} + \frac{1}{2}\alpha_3 g_\omega^2 g_\rho^2\omega_0^2\bar{\rho}_{0(3)}^2 \\ & + P_{\rm kin}^p + P_{\rm kin}^n. \end{aligned} \tag{3.14}$$

As in the previous chapter, the inclusion of the short-range correlation is done by modifying the single-nucleon momentum distributions, from the usual Fermi step functions

to those encompassing the high-momentum tail (HMT) that read

$$n_{p,n}(k) = \begin{cases} \Delta_{p,n}, & 0 < k < k_F^{p,n} \\ \\ C_{p,n}\dfrac{(k_F^{p,n})^4}{k^4}, & k_F^{p,n} < k < \phi_{p,n}k_F^{p,n}, \end{cases} \tag{3.15}$$

with $\Delta_{p,n} = 1 - 3C_{p,n}(1 - 1/\phi_{p,n})$, $C_p = C_0[1 - C_1(1 - 2y_p)]$, $C_n = C_0[1 + C_1(1 - 2y_p)]$, $\phi_p = \phi_0[1-\phi_1(1-2y_p)]$ and $\phi_n = \phi_0[1+\phi_1(1-2y_p)]$. The values $C_0 = 0.161$, $C_1 = -0.25$, $\phi_0 = 2.38$, and $\phi_1 = -0.56$ are determined (CAI; LI, 2015b; CAI; LI, 2016b; CAI; LI, 2016a). That steers to the kinetic energy density and pressure

$$\mathcal{E}_{\rm kin}^{p,n} = \frac{\gamma\Delta_{p,n}}{2\pi^2}\int_0^{k_{Fp,n}} k^2dk\left(k^2 + M^{*2}\right)^{1/2} + \frac{\gamma C_{p,n}}{2\pi^2}\int_{k_{Fp,n}}^{\phi_{p,n}k_{Fp,n}} \frac{k_{Fp,n}^4}{k^2}dk\left(k^2 + M^{*2}\right)^{1/2}, \tag{3.16}$$

and

$$P_{\rm kin}^{p,n} = \frac{\gamma\Delta_{p,n}}{6\pi^2}\int_0^{k_{Fp,n}} \frac{k^4dk}{(k^2 + M^{*2})^{1/2}} + \frac{\gamma C_{p,n}}{6\pi^2}\int_{k_{Fp,n}}^{\phi_{p,n}k_{Fp,n}} \frac{k_{Fp,n}^4dk}{(k^2 + M^{*2})^{1/2}}. \tag{3.17}$$

Notice that here we are using the indices p, n for protons and neutrons, respectively. The degeneracy factor is $\gamma = 2$ and the proton fraction is defined as $y_p = \rho_p/\rho$, with proton/neutron densities given by

$$\rho_{p,n} = \gamma\frac{k_{Fp,n}^3}{6\pi^2}. \tag{3.18}$$

The quantity $k_{Fp,n}$ is the Fermi momenta associated with the nucleon (protons and neutrons).

3.3 Results

With the mathematical formalism defined, it is necessary to chose a parametrization for the visible matter. We chose the the FSU2R model (TOLOS *et al.*, 2017b; TOLOS *et al.*, 2017a; LOURENCO *et al.*, 2022), since it considers some of the mesons self-interaction terms, but it is not so complicated that it undermines the study after the inclusion of the short-range correlations.

The value of the coupling parameters for the visible matter are the same as those

used by Lourenco *et al.* (2022), and are shown in table 3.1. We also used $C = 0.004$, $M_{\rm nuc} = 939$ MeV, $m_\sigma = 497.479$ MeV, $m_\omega = 782.5$ MeV, and $m_\rho = 763$ MeV for both versions, with and without short-range correlations. The values of the coupling constants presented in Table I were found by authors by imposing the same bulk parameters for both approaches (model with and without SRC), namely, $\rho_0 = 0.15$ fm^{-3}, $B_0 = -16.0$ MeV (binding energy), $m^* = M_0/M_{\rm nuc} = 0.593$ (M_0^*: effective nucleon mass at $\rho = \rho_0$), $K_0 = 237.7$ MeV (incompressibility at $\rho = \rho_0$), $J = 30.7$ MeV (symmetry energy at $\rho = \rho_0$).

TABLE 3.1 – Coupling constants of the FSU2R parametrization with and without SRC included.

Coupling	**FSU2R**	**FSU2R-SRC**
g_σ	10.3718	10.5174
g_ω	13.5054	12.3648
g_ρ	14.3675	15.5988
$A/M_{\rm nuc}$	1.8365	2.9133
B	-3.2403	-32.4432
α_3'	0.0900	0.0093

We start the study by taking the dark matter as composed of fermions. So, the dark sector energy density and pressure are those described in (3.6) and (3.7). There is two free constants to be fixed C_V and m_χ. To fix these constants we use the results found by Thakur *et al.* (2024) . After the analysis for multiple EoS, the authors constrained the values for each of those parameters for a select group of four different EoS. We chose $C_V = 3.25$ fm and $m_\chi = 1950$ MeV that are close to the central values for the distributions of the selected EoS. Furthermore, one must chose the parameter set for the bosonic model. For this model we must set two parameters, m_σ and $C_{\sigma\phi}$, to be able to completely define equations (3.10) and (3.11). We use the exact same parameters as those chosen as best scenario parameters by Rutherford *et al.* (2023): $m_\sigma = 15$ GeV and the $C_{\sigma\phi} = 0.1$ MeV^{-1}.

The third quantity of interest to be obtained is the relative mass fraction $F_{\rm DM} = M_{\rm DM}/M$. The objective is to compare how different dark mass fractions changes the star in presence of SRC. To construct the mass-radius diagram, one must firstly solve the two fluid TOV equation (3.4) using the total energy density and pressure of the system

$$\epsilon_{\rm vis} = \mathcal{E}_{\rm vis} + \frac{\mu_e^4}{4\pi^2} + \frac{1}{\pi^2}\int_0^{\sqrt{\mu_\mu^2 - m_\mu^2}} dk\, k^2 \left(k^2 + m_\mu^2\right)^{1/2}, \tag{3.19}$$

$$p_{\rm vis} = P_{\rm vis} + \frac{\mu_e^4}{12\pi^2} + \frac{1}{3\pi^2}\int_0^{\sqrt{\mu_\mu^2 - m_\mu^2}} dk\, \frac{k^4}{\left(k^2 + m_\mu^2\right)^{1/2}}, \tag{3.20}$$

in which the first term is the energy density and pressure from the set of equations (3.13) and (3.14). Additionally, in the astrophysical context, more specifically, the de-

scription of neutron stars, one should consider stellar matter under charge neutrality and β-equilibrium, i.e., a system in which the weak process and its inverse reaction, namely, $n \to p + e^- + \bar{\nu}_e$ and $p + e^- \to n + \nu_e$, occur simultaneously. Besides massless electrons, we also consider muons, which appear when the electron chemical potential μ_e exceeds the muon mass ($m_\mu = 105.7$ MeV). In this case, the following conditions hold: $\rho_p - \rho_e = \rho_\mu$ and $\mu_n - \mu_p = \mu_e$, with $\mu_\mu = \mu_e$. ρ_e is the electron density with μ_e and ρ_e related to each other through $\rho_e = \mu_e^3/(3\pi^2)$. The muon density is

$$\rho_\mu = \left[\left(\mu_\mu^2 - m_\mu^2\right)^{3/2}\right]/(3\pi^2).$$

Once the chemical potential is related to the appearing of electrons and muons, if is worth to mentioning explicitly its mathematical form for the case in which short range correlations are included in the visible sector of the system. Its expression for protons and neutrons is

$$\mu_{p,n} = \frac{\partial \epsilon}{\partial \rho_{p,n}} = \Delta_{p,n}\mu_{\rm kin}^{p,n} + \mu_{\rm kin(SRC)}^{p,n} + g_\omega \omega_0 \pm \frac{g_\rho}{2}\bar{\rho}_{0(3)}, \tag{3.21}$$

with

$$\begin{aligned}\mu_{\rm kin(SRC)}^{p,n} = {} & 3C_{p,n}\left[\mu_{\rm kin}^{p,n} - \frac{(\phi_{p,n}^2 k_{Fp,n}^2 + M^{\star 2})^{1/2}}{\phi_{p,n}}\right] \\ & + 4C_{p,n}k_{Fp,n}\ln\left[\frac{\phi_{p,n}^2 k_{Fp,n}^2 + (\phi_{p,n}^2 k_{Fp,n}^2 + M^{\star 2})^{1/2}}{k_{Fp,n} + (k_{Fp,n}^2 + M^{\star 2})^{1/2}}\right] + \frac{2}{\pi^2}\frac{\rho_{p,n}}{\rho^2}\eta_{p,n},\end{aligned} \tag{3.22}$$

and $\mu_{\rm kin}^{p,n} = (k_{Fp,n}^2 + M^2)^{1/2}$. The quantity $\eta_{p,n}$ reads

$$\begin{aligned}\eta_{p,n} = {} & \phi_0\phi_1\frac{C_{p,n}}{\phi_{p,n}^2}k_{F_{p,n}}^3\left(\phi_{p,n}^2 k_{F_{p,n}}^2 + M^{\star 2}\right)^{1/2} - \phi_0\phi_1\frac{C_{n,p}}{\phi_{n,p}^2}k_{F_{n,p}}^3\left(\phi_{n,p}^2 k_{F_{n,p}}^2 + M^{\star 2}\right)^{1/2} \\ & + C_0C_1\int_{k_{F_{p,n}}}^{\phi_{p,n}k_{F_{p,n}}} dk\frac{k_{F_{p,n}}^4}{k^2\left(k^2 + M^{\star 2}\right)^{1/2}} - C_0C_1\int_{k_{F_{n,p}}}^{\phi_{n,p}k_{F_{n,p}}} dk\frac{k_{F_{n,p}}^4}{k^2\left(k^2 + M^{\star 2}\right)^{1/2}} \\ & - 3\left[C_0C_1\left(1 - \frac{1}{\phi_{p,n}}\right) + \phi_0\phi_1\frac{C_{p,n}}{\phi_{p,n}^2}\right]\int_0^{k_{F_{p,n}}} dk\left(k^2 + M^{\star 2}\right)^{1/2}k^2 \\ & + 3\left[C_0C_1\left(1 - \frac{1}{\phi_{n,p}}\right) + \phi_0\phi_1\frac{C_{n,p}}{\phi_{n,p}^2}\right]\int_0^{k_{F_{n,p}}} dk\left(k^2 + M^{\star 2}\right)^{1/2}k^2\end{aligned} \tag{3.23}$$

Now one must define the energy density for the DM. In both cases, bosonic and fermionic DM, it is not completely defined since (3.6) and (3.7) depend on ρ_χ, which is

not known. To determine ρ_χ, we impose that the DM energy density is a fraction of the visible one: $\epsilon_{\rm DM} = f\epsilon_{\rm vis}$. By varying the values of f and calculating the TOV, we select stars that have a particular mass fraction. In this work, the stars selected are those with a mass fraction between 1% and 8%. This limit is inside the range found by Ciancarella *et al.* (2021) and by the sampling of Thakur *et al.* (2024).

To graphycally depict the influence of both, dark matter and SRC in the mass radius digram, we adtopted the folloing approach: for each type of dark matter model we take three different mass fractions. We use those mass fractions to construct four mass-radius diagrams, two for the fermionic dark matter model and two for the bosonic (one with and one without short-range correlations).

As stated, the Figs. 3.1 and 3.2 are direct consequences of the solving of the two fluid TOV equations. In each graph, we take the FDM as equal to 2%, 5% and 8% in addition to the case without DM. The influence of DM is indirectly manifested through its effects on the behavior of the visible matter, which allows us to infer its presence and impact by analyzing the observable properties of the star.

One may realize that the inclusion of DM decreases the maximum mass of the system. This is a result previouly found by other authors and are in agreemente with recent discussions (THAKUR *et al.*, 2024; DAS *et al.*, 2022; BHAT; PAUL, 2020; DAS *et al.*, 2018).

Taking now the inclusion of SRC, we see that such a phenomenon produces more massive stars. That is also in accordance with recent works that discuss the consequence of SRC in RMF models (CAI; LI, 2016c; Souza *et al.*, 2020; LOURENCO *et al.*, 2022). One should remark that the influence of SRC is dependent of the model. In the previous section of this work, for example, the presence of SRC leads to less massive stars. Notice also that the inclusion of SRC helps balancing the decreasing of the neutron star mass caused by DM. This effect becomes more evident when we analyze the results for the fermionic DM model. In the absence of SRC, only the curve without DM falls inside the constraint set by Fonseca *et al.* (2021b). By including SRC, however, an additional curve—specifically, the one with a DM mass fraction of 2%—also fits into this constraint region. For this particular curve, the inclusion of SRC increases the maximum mass from $M = 1.996\ M_\odot$ to $M = 2.055\ M_\odot$, which represents a difference of approximately 3%. A similar effect is observed when considering bosonic DM, as demonstrated in the Fig. 3.2.

A comparison between fermionic and bosonic DM models incorporating SRC reveals that the increase in maximum mass induced by SRC is slightly more pronounced in the fermionic DM scenario. Despite this minor variation, the overall behavior of the MR diagram for visible matter remains largely unaffected by the type of DM present. However, this conclusion may not hold when considering the spatial distribution of DM within the star, as distinct patterns can emerge. In particular, bosonic DM models are more likely

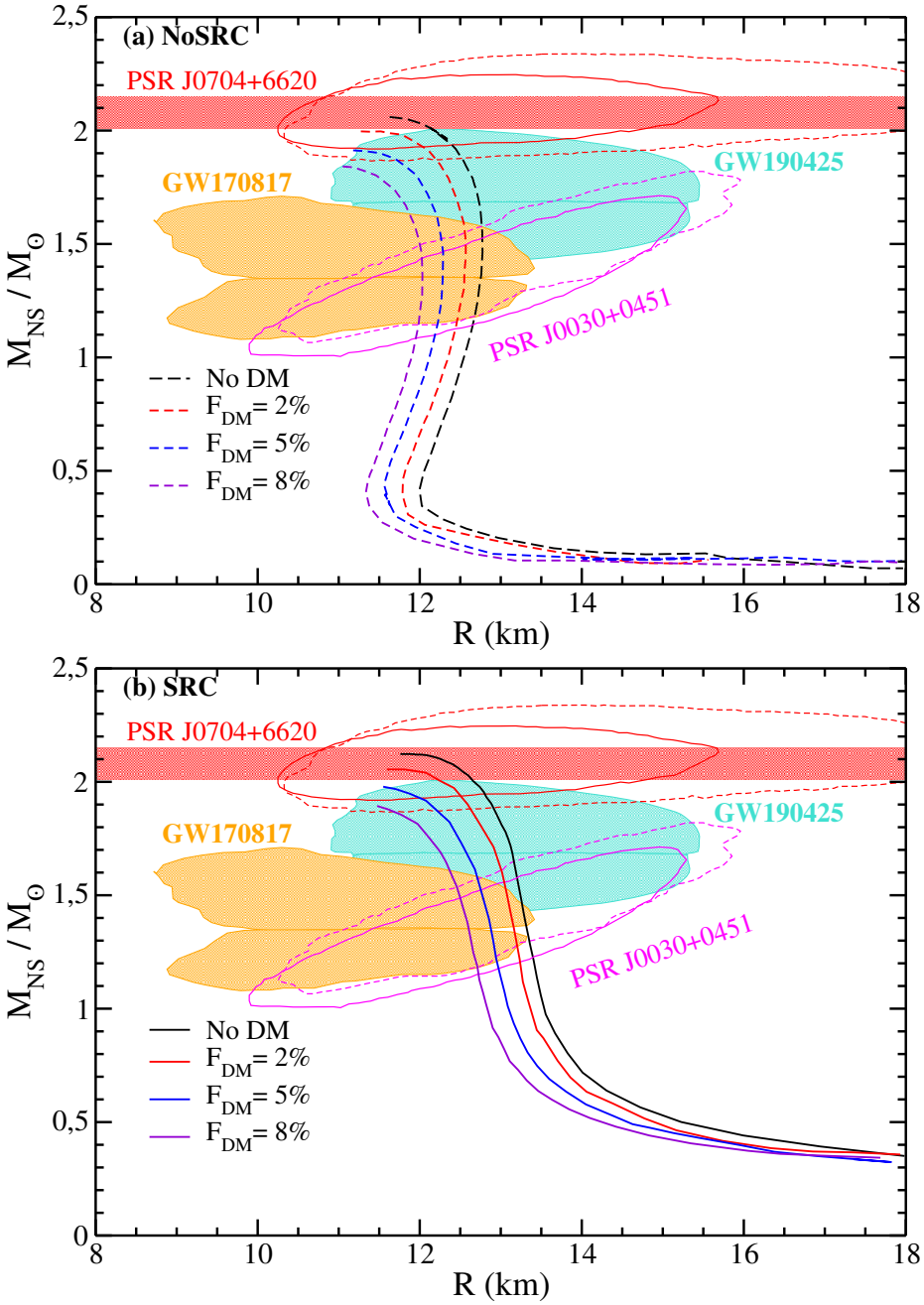

FIGURE 3.1 – Mass-radius diagrams constructed from the FSU2R model with different values of F_{DM} considering the fermionic DM, for (a) - the case without SRC and (b) - the case with SRC. The contours are related to data from the NICER mission, namely, PSR J0030+0451 (RILEY *et al.*, 2019; MILLER *et al.*, 2019) and PSR J0740+6620 (RILEY *et al.*, 2021; MILLER *et al.*, 2021), the GW170817 (ABBOTT *et al.*, 2017; ABBOTT *et al.*, 2018) and the GW190425 events (ABBOTT *et al.*, 2020), all of them at 90% credible level. The red horizontal lines are also related to the PSR J0740+6620 pulsar (FONSECA *et al.*, 2021a).

to lead to the formation of dark matter halos, which could significantly alter the internal structure and the physical properties of neutron stars (MARZOLA *et al.*, 2024; KARKEVANDI *et al.*, 2022).

In summary, the impact of dark matter on the mass-radius relationship of neutron stars was systematically explored by using both fermionic and bosonic DM models within the framework of the FSU2R parametrization with and without the inclusion of short-

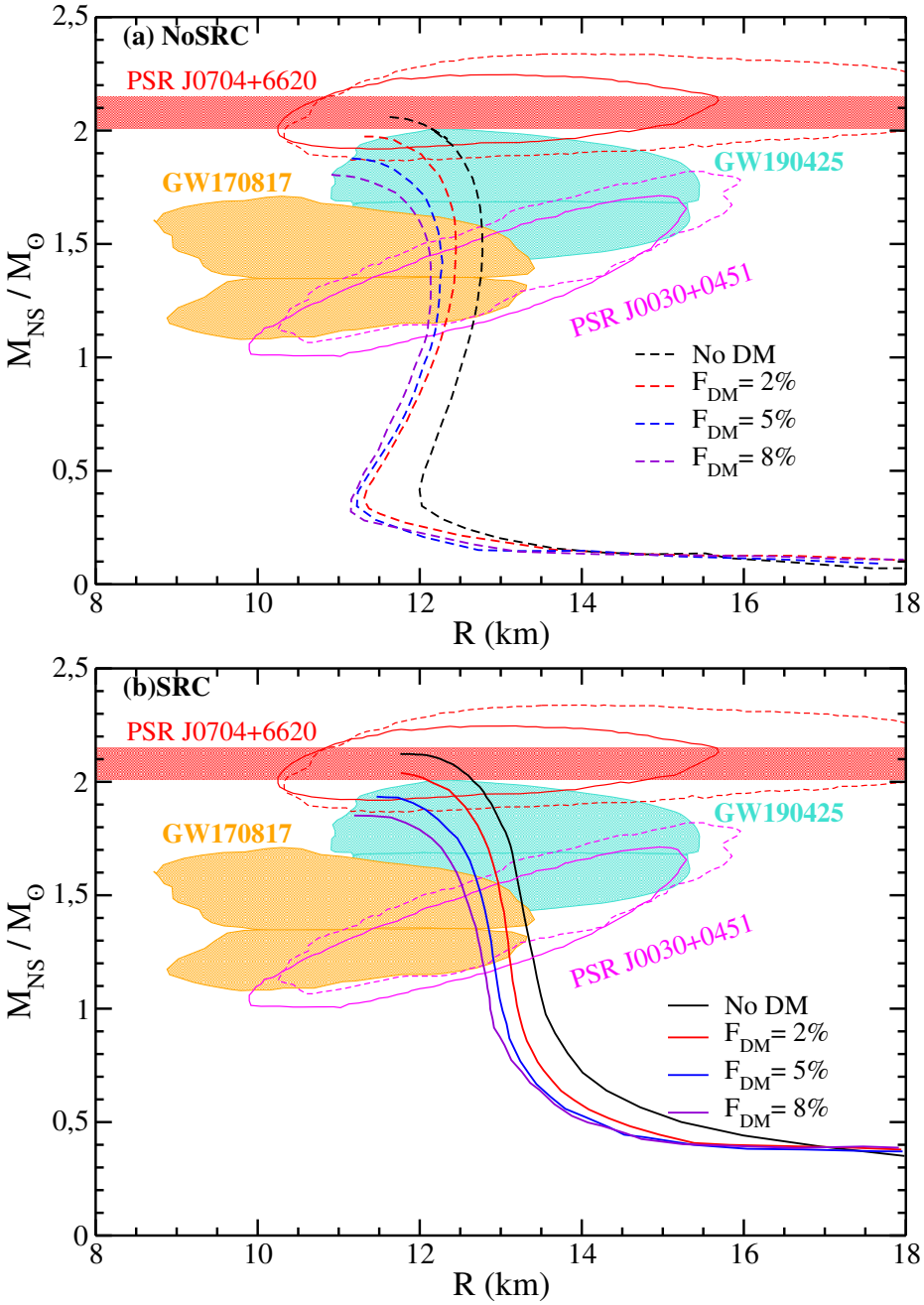

FIGURE 3.2 – Mass-radius diagrams constructed from the FSU2R model with different values of FDM considering the **bosonic** dark matter, for **(a)** - the case without SRC and **(b)** - the case with SRC. The contours are the same described in 3.1.

range correlations. The study shows that SRC increases the stiffness of the equation of state, resulting in more massive stars. This effect partially counterbalances the softening of the EoS introduced by the presence of DM, as observed in both fermionic and bosonic scenarios. While the overall behavior of the MR diagram for visible matter remains relatively unchanged when comparing the two types of DM, bosonic models are more likely to produce distinct dark matter distribution patterns, including the formation of dark matter halos. Such structures can significantly alter the internal properties of neutron stars, offering new insights into the influence of DM on compact astrophysical objects.

3.4 Final remarks

The results presented in this chapter demonstrate that the inclusion of dark matter in relativistic mean-field models can alter the physical properties of neutron stars, such as their mass and radius. Moreover, the inclusion of SRC leads to a notable increase in the maximum mass of neutron stars, making it a crucial factor to consider when modeling stellar configurations that must satisfy observational constraints. The comparison between fermionic and bosonic DM models indicates that while the overall impact on the MR diagram remains similar, bosonic models could be sensitive to variations in the DM distribution, potentially leading to observable differences in structure formation.

In future studies, the detailed profiles of dark matter distribution within neutron stars will be investigated in order to assess the potential formation of dark matter halos. This analysis will include the study of the radial density profiles and their impact on the visible matter, as well as the conditions under which halos are formed. These studies can enlarge the understanding of how dark matter influences the internal structure and observable properties of neutron stars, helping to refine the constraints on dark matter models and the role played by this component in compact objects.

4 Final Remarks and future prospects

This study demonstrates that incorporating dark matter (DM) and short-range correlations (SRC) within relativistic mean-field (RMF) models significantly affects the physical properties of neutron stars, including their mass and radius. Our results show that SRC increase the stiffness of the equation of state (EoS), thereby enhancing the maximum mass of neutron stars. The presence of DM, on the other hand, softens the EoS, reducing the maximum mass achieved by the model. However, the overall mass-radius (MR) diagram remains within the observational constraints provided by recent astrophysical data. When comparing fermionic and bosonic DM models, we found that both exhibit similar trends in the MR diagram.

Regarding the CCS-SRC model, its clear that SRC also helps maintaining the linear relationship between the symmetry energy and its slope (L_0), as observed in various theoretical models, while increasing L_0 compared to models without SRC.Moreover, our study reveals that SRC can reconcile the CCS-SRC model with the flow constraint at high densities, further validating the model's applicability to a broad range of densities and pressures. For stellar configurations, the inclusion of SRC leads to a slight softening of the EoS when compared to models without SRC, yet it still produces stars that comply with observational constraints, including mass-radius profiles derived from the NICER mission and gravitational wave events like GW170817 and GW190425. The effect of SRC on the dimensionless tidal deformability, $\Lambda_{1.4}$, was also investigated, showing a decrease in Λ due to the reduction in neutron star radius, which is consistent with LIGO and Virgo measurements.

These findings underscore the importance of including SRC when modeling the EoS for neutron stars, as it helps to resolve inconsistencies related to causality and enhances agreement with both terrestrial and astrophysical constraints. However, challenges remain, particularly in the isovector sector of the model. Low values of L_0 and J remain problematic for reconciling the model with all observed data simultaneously, suggesting the need for further refinements in future work.

Looking ahead, future studies will construct the MR diagrams, already done for a RMF description in the visible sector, for a case with the CCS-SRC model for normal

matter. We will also analyze the detailed profiles of DM distribution within neutron stars to explore the conditions under which dark matter halos could form. This will be done for both DM descriptions and for the FSU2R-SRC and CCS-SRC models. By investigating the radial dependence of the energy density and pressure using profiles and their impact on visible matter, we aim to gain deeper insights into how the combined effect of DM and SRC influences the structure of NS.

In future studies, we also intend to use a Bayesian analysis to help constrain the parameter space for the fermionic DM model with SRC. By utilizing Bayesian inference techniques, we aim to find the set of parameters that govern the interactions within the dark sector. Besides, we strive to include a negative coupling constant for the $\omega_\mu \omega^\mu$ meson interaction.

Bibliography

ABBOTT, B. P.; ABBOTT, R.; ABBOTT, T. D.; ACERNESE, F.; ACKLEY, K. *et al.* Gw170817: Observation of gravitational waves from a binary neutron star inspiral. **Phys. Rev. Lett.**, American Physical Society, v. 119, p. 161101, Oct 2017. Available at: https://link.aps.org/doi/10.1103/PhysRevLett.119.161101.

ABBOTT, B. P.; ABBOTT, R.; ABBOTT, T. D.; ACERNESE, F.; ACKLEY *et al.* Gw170817: Measurements of neutron star radii and equation of state. **Phys. Rev. Lett.**, American Physical Society, v. 121, p. 161101, Oct 2018. Available at: https://link.aps.org/doi/10.1103/PhysRevLett.121.161101.

ABBOTT, B. P.; ABBOTT, R.; ABBOTT, T. D.; ABRAHAM, S.; ACERNESE, F. *et al.* Gw190425: Observation of a compact binary coalescence with total mass 3.4 m. **The Astrophysical Journal Letters**, The American Astronomical Society, v. 892, n. 1, p. L3, mar 2020. Available at: https://dx.doi.org/10.3847/2041-8213/ab75f5.

Abbott, B. P. *et al.* LIGO: the Laser Interferometer Gravitational-Wave Observatory. **Reports on Progress in Physics**, v. 72, n. 7, p. 076901, jul. 2009.

Abbott, B. P. *et al.* Gw170817: Measurements of neutron star radii and equation of state. **Phys. Rev. Lett.**, American Physical Society, v. 121, p. 161101, Oct 2018. Available at: https://link.aps.org/doi/10.1103/PhysRevLett.121.161101.

ABRAMOWITZ, M.; STEGUN, I. A. **Handbook of mathematical functions with formulas, graphs, and mathematical tables**. [*S.l.*]: US Government printing office, 1964.

Accadia, T. *et al.* Virgo: a laser interferometer to detect gravitational waves. **Journal of Instrumentation**, v. 7, n. 3, p. 3012, mar. 2012.

ADHIKARI, D.; ALBATAINEH, H.; ANDROIC, D.; ANIOL, K.; ARMSTRONG, D. S.; AVERETT, T. *et al.* Accurate determination of the neutron skin thickness of ^{208}Pb through parity-violation in electron scattering. **Phys. Rev. Lett.**, American Physical Society, v. 126, p. 172502, Apr 2021. Available at: https://link.aps.org/doi/10.1103/PhysRevLett.126.172502.

ADHIKARI, D.; ALBATAINEH, H.; ANDROIC, D.; ANIOL, K. A.; ARMSTRONG, D. S.; AVERETT, T.; GAYOSO, C. A.; BARCUS, S. K.; BELLINI, V.; BEMINIWATTHA, R. S.; BENESCH, J. F.; BHATT, H.; PATHAK, D. B.; BHETUWAL, D.; BLAIKIE, B.; BOYD, J.; CAMPAGNA, Q.; CAMSONNE, A.; CATES, G. D.; CHEN, Y.; CLARKE, C.; CORNEJO, J. C.; DUSA, S. C.; DALTON,

M. M.; DATTA, P.; DESHPANDE, A.; DUTTA, D.; FELDMAN, C.; FUCHEY, E.; GAL, C.; GASKELL, D.; GAUTAM, T.; GERICKE, M.; GHOSH, C.; HALILOVIC, I.; HANSEN, J.-O.; HASSAN, O.; HAUENSTEIN, F.; HENRY, W.; HOROWITZ, C. J.; JANTZI, C.; JIAN, S.; JOHNSTON, S.; JONES, D. C.; KAKKAR, S.; KATUGAMPOLA, S.; KEPPEL, C.; KING, P. M.; KING, D. E.; KUMAR, K. S.; KUTZ, T.; LASHLEY-COLTHIRST, N.; LEVERICK, G.; LIU, H.; LIYANAGE, N.; MAMMEI, J.; MAMMEI, R.; MCCAUGHAN, M.; MCNULTY, D.; MEEKINS, D.; METTS, C.; MICHAELS, R.; MIHOVILOVIC, M.; MONDAL, M. M.; NAPOLITANO, J.; NARAYAN, A.; NIKOLAEV, D.; OWEN, V.; PALATCHI, C.; PAN, J.; PANDEY, B.; PARK, S.; PASCHKE, K. D.; PETRUSKY, M.; PITT, M. L.; PREMATHILAKE, S.; QUINN, B.; RADLOFF, R.; RAHMAN, S.; RASHAD, M. N. H.; RATHNAYAKE, A.; REED, B. T.; REIMER, P. E.; RICHARDS, R.; RIORDAN, S.; ROBLIN, Y. R.; SEEDS, S.; SHAHINYAN, A.; SOUDER, P.; THIEL, M.; TIAN, Y.; URCIUOLI, G. M.; WERTZ, E. W.; WOJTSEKHOWSKI, B.; YALE, B.; YE, T.; YOON, A.; XIONG, W.; ZEC, A.; ZHANG, W.; ZHANG, J.; ZHENG, X. Precision determination of the neutral weak form factor of ^{48}Ca. **Phys. Rev. Lett.**, American Physical Society, v. 129, p. 042501, Jul 2022. Available at: https://link.aps.org/doi/10.1103/PhysRevLett.129.042501.

Antić, S.; Stone, J. R.; Miller, J. C.; Martinez, K. L.; Guichon, P. A. M.; Thomas, A. W. Outer crust of a cold, nonaccreting neutron star within the quark-meson-coupling model. , v. 102, n. 6, p. 065801, dez. 2020.

Antoniadis, J.; Freire, P. C. C.; Wex, N.; Tauris, T. M. *et al.* A Massive Pulsar in a Compact Relativistic Binary. **Science**, v. 340, n. 6131, p. 448, abr. 2013.

ANTONIADIS, J.; FREIRE, P. C. C.; WEX, N.; TAURIS, T. M.; LYNCH, R. S.; KERKWIJK, M. H. van; KRAMER, M.; BASSA, C.; DHILLON, V. S.; DRIEBE, T.; HESSELS, J. W. T.; KASPI, V. M.; KONDRATIEV, V. I.; LANGER, N.; MARSH, T. R.; MCLAUGHLIN, M. A.; PENNUCCI, T. T.; RANSOM, S. M.; STAIRS, I. H.; LEEUWEN, J. van; VERBIEST, J. P. W.; WHELAN, D. G. A massive pulsar in a compact relativistic binary. **Science**, v. 340, n. 6131, p. 1233232, 2013. Available at: https://www.science.org/doi/abs/10.1126/science.1233232.

ARCADI, G.; DUTRA, M.; GHOSH, P.; LINDNER, M.; MAMBRINI, Y.; PIERRE, M.; PROFUMO, S.; QUEIROZ, F. S. The waning of the wimp? a review of models, searches, and constraints. **The European Physical Journal C**, v. 78, n. 3, p. 203, 2018. ISSN 1434-6052. Available at: https://doi.org/10.1140/epjc/s10052-018-5662-y.

ARFKEN, G. B.; WEBER, H. J.; HARRIS, F. E. Chapter 18 - more special functions. *In*: ARFKEN, G. B.; WEBER, H. J.; HARRIS, F. E. (Ed.). **Mathematical Methods for Physicists (Seventh Edition)**. Seventh edition. Boston: Academic Press, 2013. p. 871–933. ISBN 978-0-12-384654-9. Available at: https://www.sciencedirect.com/science/article/pii/B9780123846549000189.

ARRINGTON, J.; FOMIN, N.; SCHMIDT, A. Progress in understanding short-range structure in nuclei: An experimental perspective. **Annual Review of Nuclear and Particle Science**, v. 72, n. 1, p. 307–337, 2022. Available at: https://doi.org/10.1146/annurev-nucl-102020-022253.

ATHRON, P. *et al.* Global analyses of higgs portal singlet dark matter models using gambit. **European Physical Journal C**, Springer, v. 79, n. 1, p. 38, 2019.

Baldo, M.; Burgio, G. F. The nuclear symmetry energy. **Progress in Particle and Nuclear Physics**, v. 91, p. 203–258, nov. 2016.

Baym, G.; Pethick, C.; Sutherland, P. The Ground State of Matter at High Densities: Equation of State and Stellar Models. , v. 170, p. 299, dez. 1971.

BEINER, M.; FLOCARD, H.; Van Giai, N.; QUENTIN, P. Nuclear ground-state properties and self-consistent calculations with the skyrme interaction: (i). spherical description. **Nuclear Physics A**, v. 238, n. 1, p. 29–69, 1975. ISSN 0375-9474. Available at: https://www.sciencedirect.com/science/article/pii/0375947475903383.

BETHE, H. **Annu. Rev. Nucl. Sci.** 1971.

BETHE, H. A.; WILSON, J. R. Revival of a stalled supernova shock by neutrino heating. , v. 295, p. 14–23, ago. 1985.

BHAT, S. A.; PAUL, A. Effect of dark matter on neutron star properties within the relativistic mean field framework. **European Physical Journal C**, v. 80, p. 544, 2020.

BINNINGTON, T.; POISSON, E. Relativistic theory of tidal love numbers. **Phys. Rev. D**, American Physical Society, v. 80, p. 084018, Oct 2009. Available at: https://link.aps.org/doi/10.1103/PhysRevD.80.084018.

BUGAEV, K. A. The van der waals gas eos for the lorentz contracted rigid spheres. **Nuclear Physics A**, v. 807, n. 3, p. 251–268, 2008. ISSN 0375-9474. Available at: https://www.sciencedirect.com/science/article/pii/S0375947408005265.

BUGAEV, K. A.; IVANYTSKYI, A. I.; SAGUN, V. V.; GRINYUK, B. E.; SAVCHENKO, D. O.; ZINOVJEV, G. M.; NIKONOV, E. G.; BRAVINA, L. V.; ZABRODIN, E. E.; BLASCHKE, D. B.; TARANENKO, A. V.; TURKO, L. Hard-core radius of nucleons within the induced surface tension approach. **Universe**, v. 5, n. 2, 2019. ISSN 2218-1997. Available at: https://www.mdpi.com/2218-1997/5/2/63.

BURROWS, A.; Hayes, J.; Fryxell, B. A. On the Nature of Core-Collapse Supernova Explosions. , v. 450, p. 830, set. 1995.

CAI, B.-J.; LI, B.-A. Isospin quartic term in the kinetic energy of neutron-rich nucleonic matter. **Phys. Rev. C**, American Physical Society, v. 92, p. 011601, Jul 2015. Available at: https://link.aps.org/doi/10.1103/PhysRevC.92.011601.

CAI, B.-J.; LI, B.-A. Isospin quartic term in the kinetic energy of neutron-rich nucleonic matter. **Phys. Rev. C**, American Physical Society, v. 92, p. 011601, Jul 2015. Available at: https://link.aps.org/doi/10.1103/PhysRevC.92.011601.

CAI, B.-J.; LI, B.-A. Nucleon effective E-mass in neutron-rich matter from the Migdal–Luttinger jump. **Phys. Lett. B**, v. 757, p. 79–83, 2016.

CAI, B.-J.; LI, B.-A. Symmetry energy of cold nucleonic matter within a relativistic mean field model encapsulating effects of high-momentum nucleons induced by short-range correlations. **Phys. Rev. C**, American Physical Society, v. 93, p. 014619, Jan 2016. Available at: https://link.aps.org/doi/10.1103/PhysRevC.93.014619.

CAI, B.-J.; LI, B.-A. Symmetry energy of cold nucleonic matter within a relativistic mean field model encapsulating effects of high-momentum nucleons induced by short-range correlations. **Phys. Rev. C**, American Physical Society, v. 93, p. 014619, Jan 2016. Available at: https://link.aps.org/doi/10.1103/PhysRevC.93.014619.

CAI, B.-J.; LI, B.-A. Equation of state of neutron-rich matter in d-dimensions. **Annals of Physics**, v. 444, p. 169062, 2022. ISSN 0003-4916. Available at: https://www.sciencedirect.com/science/article/pii/S000349162200183X.

CAMENZIND, M. **Compact objects in astrophysics**. [*S.l.*]: Springer, 2007.

CAPUTO, A.; ELOR, G.; HARDY, E. Dark photon limits: A handbook. **Physical Review D**, American Physical Society, v. 104, n. 9, p. 095029, 2021.

Carlson, B. V.; Dutra, M.; Lourenço, O.; Margueron, J. Low-energy nuclear physics and global neutron star properties. **arXiv e-prints**, p. arXiv:2209.03257, set. 2022.

Carnahan, N. F.; Starling, K. E. Equation of State for Nonattracting Rigid Spheres. , v. 51, n. 2, p. 635–636, jul. 1969.

CERDA-DURAN, P.; ELIAS-ROSA, N. Neutron stars formation and core collapse supernovae. *In*: REZZOLLA, L.; PIZZOCHERO, P.; JONES, D. I.; REA, N.; NA, I. V. (Ed.). **The Physics and Astrophysics of Neutron Stars**. [*S.l.*]: Springer, 2018. v. 457.

CHAVANIS, P.-H. Self-gravitating bose-einstein condensates. *In*: _____. **Quantum Aspects of Black Holes**. Cham: Springer International Publishing, 2015. p. 151–194. ISBN 978-3-319-10852-0. Available at: https://doi.org/10.1007/978-3-319-10852-0_6.

CIANCARELLA, R.; PANNARALE, F.; ADDAZI, A.; MARCIANO, A. Neutron star binaries as particle detectors for early dark energy and exotic gravitational waves. **Physics of the Dark Universe**, v. 32, p. 100796, 2021.

CIARCELLUT, P.; SANDIN, F. Phys. lett. b. **Physics Letters B**, v. 695, p. 19, 2011.

CLAS Collaboration. Probing high-momentum protons and neutrons in neutron-rich nuclei. , v. 560, n. 7720, p. 617–621, ago. 2018.

CLOWE, D.; BRADAč, M.; GONZALEZ, A. H.; MARKEVITCH, M.; RANDALL, S. W.; JONES, C.; ZARITSKY, D. A direct empirical proof of the existence of dark matter*. **The Astrophysical Journal**, v. 648, n. 2, p. L109, aug 2006. Available at: https://dx.doi.org/10.1086/508162.

COLLE, C.; HEN, O.; COSYN, W.; KOROVER, I.; PIASETZKY, E.; RYCKEBUSCH, J.; WEINSTEIN, L. B. Extracting the mass dependence and quantum numbers of short-range correlated pairs from $a(e, e'p)$ and $a(e, e'pp)$ scattering. **Phys. Rev. C**, American Physical Society, v. 92, p. 024604, Aug 2015. Available at: https://link.aps.org/doi/10.1103/PhysRevC.92.024604.

DAMOUR, T.; NAGAR, A. Effective one body description of tidal effects in inspiralling compact binaries. **Phys. Rev. D**, American Physical Society, v. 81, p. 084016, Apr 2010. Available at: https://link.aps.org/doi/10.1103/PhysRevD.81.084016.

Danielewicz, P.; Lacey, R.; Lynch, W. G. Determination of the Equation of State of Dense Matter. **Science**, v. 298, n. 5598, p. 1592–1596, nov. 2002.

DANIELEWICZ, P.; LACEY, R.; LYNCH, W. G. Determination of the equation of state of dense matter. **Science**, v. 298, n. 5598, p. 1592–1596, 2002. Available at: https://www.science.org/doi/abs/10.1126/science.1078070.

DAS, A.; MALIK, T.; NAYAK, A. C. Dark matter admixed neutron star properties in light of gravitational wave observations: A two fluid approach. **Phys. Rev. D**, American Physical Society, v. 105, p. 123034, Jun 2022. Available at: https://link.aps.org/doi/10.1103/PhysRevD.105.123034.

DAS, A.; MUKHOPADHYAY, B.; RAO, A. R. Effects of magnetic field and dark matter on neutron star structure. **Journal of Cosmology and Astroparticle Physics**, v. 2018, n. 5, p. 045, 2018.

DECHARGÉ, J.; GOGNY, D. Hartree-fock-bogolyubov calculations with the $d1$ effective interaction on spherical nuclei. **Phys. Rev. C**, American Physical Society, v. 21, p. 1568–1593, Apr 1980. Available at: https://link.aps.org/doi/10.1103/PhysRevC.21.1568.

DEGENAAR, N.; SULEIMANOV, V. F. Testing the equation of state with electromagnetic observations. *In*: REZZOLLA, L.; PIZZOCHERO, P.; JONES, D. I.; REA, N.; NA, I. V. (Ed.). **The Physics and Astrophysics of Neutron Stars**. [*S.l.*]: Springer, 2018. v. 457.

DELIYERGIYEV, M.; POPOLO, A. D.; TOLOS, L.; DELLIOU, M. L.; LEE, X.; BURGIO, F. Dark compact objects: An extensive overview. **Phys. Rev. D**, American Physical Society, v. 99, p. 063015, Mar 2019. Available at: https://link.aps.org/doi/10.1103/PhysRevD.99.063015.

DRISCHLER, C.; FURNSTAHL, R. J.; MELENDEZ, J. A.; PHILLIPS, D. R. How well do we know the neutron-matter equation of state at the densities inside neutron stars? a bayesian approach with correlated uncertainties. **Phys. Rev. Lett.**, American Physical Society, v. 125, p. 202702, Nov 2020. Available at: https://link.aps.org/doi/10.1103/PhysRevLett.125.202702.

DUTRA, M.; cO, O. Louren; AVANCINI, S. S.; CARLSON, B. V.; DELFINO, A.; MENEZES, D. P.; PROVIDÊNCIA, C.; TYPEL, S.; STONE, J. R. Relativistic mean-field hadronic models under nuclear matter constraints. **Phys. Rev. C**, American Physical Society, v. 90, p. 055203, Nov 2014. Available at: https://link.aps.org/doi/10.1103/PhysRevC.90.055203.

DUTRA, M.; cO, O. Louren; MARTINS, J. S. S.; DELFINO, A.; STONE, J. R.; STEVENSON, P. D. Skyrme interaction and nuclear matter constraints. **Phys. Rev. C**, American Physical Society, v. 85, p. 035201, Mar 2012. Available at: https://link.aps.org/doi/10.1103/PhysRevC.85.035201.

DUTRA, M.; LENZI, C. H.; LOURENçO, O. Dark particle mass effects on neutron star properties from a short-range correlated hadronic model. **Monthly Notices of the Royal Astronomical Society**, v. 517, n. 3, p. 4265–4274, 10 2022. ISSN 0035-8711. Available at: https://doi.org/10.1093/mnras/stac2986.

DUTRA, M.; SANTOS, B. M.; LOURENçO, O. Constraints and correlations of nuclear matter parameters from a density-dependent van der waals model. **Journal of Physics G: Nuclear and Particle Physics**, IOP Publishing, v. 47, n. 3, p. 035101, jan 2020. Available at: https://dx.doi.org/10.1088/1361-6471/ab5774.

ELLIS, J.; HUTSI, G.; KANNIKE, K.; MARZOLA, L.; RAIDAL, M.; VASKONEN, V. Phys. rev. d. **Physical Review D**, v. 97, p. 123007, 2018.

FABBRICHESI, M.; GABRIELLI, E.; LANFRANCHI, G. **The Dark Photon**. [*S.l.*]: Springer, 2021. (SpringerBriefs in Physics).

FAN, X.-H.; YANG, Z.-X.; YIN, P.; CHEN, P.-H.; DONG, J.-M.; LI, Z.-P.; LIANG, H. A local-density-approximation description of high-momentum tails in isospin asymmetric nuclei. **Physics Letters B**, Elsevier, 2022.

FISCHER, T.; HUTHER, L.; LOHS, A.; MARTÍNEZ-PINEDO, G. Early protoneutron star deleptonization - consistent modeling of weak processes and equation of state. **Journal of Physics: Conference Series**, IOP Publishing, v. 665, p. 012069, jan 2016. Available at: https://doi.org/10.1088/1742-6596/665/1/012069.

FLACKE, T.; KIM, J. S.; PARK, S. C. Constraining universal extra dimensions at the lhc and beyond. **Journal of High Energy Physics**, Springer, v. 2017, n. 5, p. 189, 2017.

FOGLIZZO, T. Explosion physics of core-collapse supernovae. *In*: Alsabti, A. W.; Murdin, P. (Ed.). **Handbook of Supernovae**. [*S.l.*]: Springer, 2017.

FOMIN, N.; HIGINBOTHAM, D.; SARGSIAN, M.; SOLVIGNON, P. New results on short-range correlations in nuclei. **Annual Review of Nuclear and Particle Science**, v. 67, n. 1, p. 129–159, 2017. Available at: https://doi.org/10.1146/annurev-nucl-102115-044939.

FONSECA, E.; CROMARTIE, H. T.; PENNUCCI, T. T.; RAY, P. S. *et al.* Refined mass and geometric measurements of the high-mass psr j0740+6620. **The Astrophysical Journal Letters**, The American Astronomical Society, v. 915, n. 1, p. L12, jul 2021. Available at: https://dx.doi.org/10.3847/2041-8213/ac03b8.

FONSECA, E. *et al.* Refined Mass and Geometric Measurements of the High-mass PSR J0740+6620. **Astrophys. J. Lett.**, v. 915, n. 1, p. L12, 2021.

GAMBHIR, Y.; RING, P.; THIMET, A. Relativistic mean field theory for finite nuclei. **Annals of Physics**, Elsevier, v. 198, n. 1, p. 132–179, 1990.

GARG, U.; COLò, G. The compression-mode giant resonances and nuclear incompressibility. **Progress in Particle and Nuclear Physics**, v. 101, p. 55–95, 2018. ISSN 0146-6410. Available at: https://www.sciencedirect.com/science/article/pii/S0146641018300322.

GOLDMAN, I.; NUSSINOV, S. Weakly interacting massive particles and neutron stars. **Phys. Rev. D**, American Physical Society, v. 40, p. 3221–3230, Nov 1989. Available at: https://link.aps.org/doi/10.1103/PhysRevD.40.3221.

GONZALEZ-BOQUERA, C.; CENTELLES, M.; NAS, X. V.; RIOS, A. Higher-order symmetry energy and neutron star core-crust transition with gogny forces. **Phys. Rev. C**, American Physical Society, v. 96, p. 065806, Dec 2017. Available at: https://link.aps.org/doi/10.1103/PhysRevC.96.065806.

GONZALEZ-BOQUERA, C.; CENTELLES, M.; NAS, X. V.; ROUTRAY, T. R. Core-crust transition in neutron stars with finite-range interactions: The dynamical method. **Phys. Rev. C**, American Physical Society, v. 100, p. 015806, Jul 2019. Available at: https://link.aps.org/doi/10.1103/PhysRevC.100.015806.

GRABER, V.; ANDERSSON, N.; HOGG, M. Neutron stars in the laboratory. **International Journal of Modern Physics D**, World Scientific, v. 26, n. 08, p. 1730015, 2017.

GRALLA, S. E. On the ambiguity in relativistic tidal deformability. **Classical and Quantum Gravity**, IOP Publishing, v. 35, n. 8, p. 085002, mar 2018. Available at: https://dx.doi.org/10.1088/1361-6382/aab186.

GRIEST, K.; KAMIONKOWSKI, M. Unitarity limits on the mass and radius of dark-matter particles. **Phys. Rev. Lett.**, American Physical Society, v. 64, p. 615–618, Feb 1990. Available at: https://link.aps.org/doi/10.1103/PhysRevLett.64.615.

GUO, W.-M.; LI, B.-A.; YONG, G.-C. Imprints of high-momentum nucleons in nuclei on hard photons from heavy-ion collisions near the fermi energy. **Phys. Rev. C**, American Physical Society, v. 104, p. 034603, Sep 2021. Available at: https://link.aps.org/doi/10.1103/PhysRevC.104.034603.

GUO, W.-M.; LI, B.-A.; YONG, G.-C. Imprints of high-momentum nucleons in nuclei on hard photons from heavy-ion collisions near the fermi energy. **Phys. Rev. C**, American Physical Society, v. 104, p. 034603, Sep 2021. Available at: https://link.aps.org/doi/10.1103/PhysRevC.104.034603.

HANSEN, C. J.; KAWALER, S. D.; TRIMBLE, V. **Stellar interiors: physical principles, structure, and evolution**. [*S.l.*]: Springer Science & Business Media, 2012.

HEN, O.; LI, B.-A.; GUO, W.-J.; WEINSTEIN, L. B.; PIASETZKY, E. Symmetry energy of nucleonic matter with tensor correlations. **Phys. Rev. C**, American Physical Society, v. 91, p. 025803, Feb 2015. Available at: https://link.aps.org/doi/10.1103/PhysRevC.91.025803.

HEN, O.; LI, B.-A.; GUO, W.-J.; WEINSTEIN, L. B.; PIASETZKY, E. Symmetry energy of nucleonic matter with tensor correlations. **Phys. Rev. C**, American Physical Society, v. 91, p. 025803, Feb 2015. Available at: https://link.aps.org/doi/10.1103/PhysRevC.91.025803.

HEN, O.; WEINSTEIN, L. B.; PIASETZKY, E.; MILLER, G. A.; SARGSIAN, M. M.; SAGI, Y. Correlated fermions in nuclei and ultracold atomic gases. **Phys. Rev. C**, American Physical Society, v. 92, p. 045205, Oct 2015. Available at: https://link.aps.org/doi/10.1103/PhysRevC.92.045205.

HEYDE, K. L. The nuclear shell model. *In*: **The Nuclear Shell Model**. [*S.l.*]: Springer, 1994. p. 58–154.

HINDERER, T. Tidal love numbers of neutron stars. **The Astrophysical Journal**, v. 677, n. 2, p. 1216, apr 2008. Available at: https://dx.doi.org/10.1086/533487.

Hong, B.; Ren, Z.; Mu, X.-L. Short-range correlation effects in neutron star's radial and non-radial oscillations. **Chinese Physics C**, v. 46, n. 6, p. 065104, jun. 2022.

Hu, B.; Jiang, W.; Miyagi, T.; Sun, Z.; Ekström, A.; Forssén, C.; Hagen, G.; Holt, J. D.; Papenbrock, T.; Stroberg, S. R.; Vernon, I. Ab initio predictions link the neutron skin of ^{208}Pb to nuclear forces. **Nature Physics**, v. 18, n. 10, p. 1196–1200, out. 2022.

HUANG, K. **Statistical mechanics**. [*S.l.*]: John Wiley & Sons, 2008.

JANKA, H.-T. Explosion mechanisms of core-collapse supernovae. **Annual Review of Nuclear and Particle Science**, Annual Reviews, v. 62, p. 407–451, 2012.

JANKA, H.-T.; MÜLLER, E. Neutrino heating, convection, and the mechanism of type-ii supernova explosions. **Astronomy and Astrophysics**, v. 306, p. 167, 1996.

KAKIZAKI, M.; MATSUMOTO, S.; SATO, R. Phenomenology of universal extra dimensions with bulk masses and brane localized terms. **Physical Review D**, American Physical Society, v. 95, n. 5, p. 055018, 2017.

KARKEVANDI, D. R.; SHAKERI, S.; SAGUN, V.; IVANYTSKYI, O. Constraining dark matter equation of state in neutron stars with gravitational wave observations. **Physical Review D**, v. 105, n. 2, p. 023001, 2022.

KIPPENHAHN, R.; WEIGERT, A.; WEISS, A. **Stellar Structure and Evolution**. [*S.l.: s.n.*], 2013.

KUMAR, M.; KUMAR, S.; THAKUR, V.; KUMAR, R.; AGRAWAL, B. K.; DHIMAN, S. K. Crex- and prex-ii-motivated relativistic interactions and their implications for the bulk properties of nuclear matter and neutron stars. **Phys. Rev. C**, American Physical Society, v. 107, p. 055801, May 2023. Available at: https://link.aps.org/doi/10.1103/PhysRevC.107.055801.

LALAZISSIS, G. A.; KÖNIG, J.; RING, P. New parametrization for the lagrangian density of relativistic mean field theory. **Phys. Rev. C**, American Physical Society, v. 55, p. 540–543, Jan 1997. Available at: https://link.aps.org/doi/10.1103/PhysRevC.55.540.

LATTIMER, J. M. Constraints on nuclear symmetry energy parameters. **Particles**, v. 6, n. 1, p. 30–56, 2023. ISSN 2571-712X. Available at: https://www.mdpi.com/2571-712X/6/1/3.

LI, B.-A.; CAI, B.-J.; XIE, W.-J.; ZHANG, N.-B. Progress in constraining nuclear symmetry energy using neutron star observables since gw170817. **Universe**, v. 7, n. 6, 2021. ISSN 2218-1997. Available at: https://www.mdpi.com/2218-1997/7/6/182.

LI, B.-A.; CHEN, L.-W.; KO, C. M. Recent progress and new challenges in isospin physics with heavy-ion reactions. **Physics Reports**, v. 464, n. 4, p. 113–281, 2008. ISSN 0370-1573. Available at: https://www.sciencedirect.com/science/article/pii/S0370157308001269.

LIGO-CALLTECH. **Latest Update on Start of Next Observing Run (O4)**. 2022. Available at: https://www.ligo.caltech.edu/news/ligo20220617.

LINK, B.; EPSTEIN, R. I.; LATTIMER, J. M. Pulsar constraints on neutron star structure and equation of state. **Phys. Rev. Lett.**, American Physical Society, v. 83, p. 3362–3365, Oct 1999. Available at: https://link.aps.org/doi/10.1103/PhysRevLett.83.3362.

Lopez, A.; Kelly, P.; Dauer, K.; Vitali, E. Fermionic superfluidity: from cold atoms to neutron stars. **European Journal of Physics**, v. 43, n. 6, p. 065801, nov. 2022.

Lourenço, O.; DUTRA, M.; LENZI, C. H.; FLORES, C. V.; MENEZES, D. P. Consistent relativistic mean-field models constrained by gw170817. **Phys. Rev. C**, American Physical Society, v. 99, p. 045202, Apr 2019. Available at: https://link.aps.org/doi/10.1103/PhysRevC.99.045202.

Lourenço, O.; Dutra, M.; Lenzi, C. H.; Biswal, S. K.; Bhuyan, M.; Menezes, D. P. Consistent Skyrme parametrizations constrained by GW170817. **European Physical Journal A**, v. 56, n. 2, p. 32, fev. 2020.

LOURENÇO, O.; DUTRA, M.; LENZI, C. H.; BHUYAN, M.; BISWAL, S. K.; SANTOS, B. M. A density-dependent van der waals model under the gw170817 constraint. **The Astrophysical Journal**, The American Astronomical Society, v. 882, n. 1, p. 67, sep 2019. Available at: https://dx.doi.org/10.3847/1538-4357/ab3122.

LOURENCO, O.; FREDERICO, T.; DUTRA, M. Dark matter component in hadronic models with short-range correlations. **Phys. Rev. D**, American Physical Society, v. 105, p. 023008, Jan 2022. Available at: https://link.aps.org/doi/10.1103/PhysRevD.105.023008.

LOURENÇO, O.; LENZI, C. H.; FREDERICO, T.; DUTRA, M. Dark matter effects on tidal deformabilities and moment of inertia in a hadronic model with short-range correlations. **Phys. Rev. D**, American Physical Society, v. 106, p. 043010, Aug 2022. Available at: https://link.aps.org/doi/10.1103/PhysRevD.106.043010.

LOURENçO, O.; LENZI, C. H.; FREDERICO, T.; DUTRA, M. Dark matter effects on tidal deformabilities and moment of inertia in a hadronic model with short-range correlations. **Phys. Rev. D**, American Physical Society, v. 106, p. 043010, Aug 2022. Available at: https://link.aps.org/doi/10.1103/PhysRevD.106.043010.

LOVELL, A. E.; MOHAN, A. T.; SPROUSE, T. M.; MUMPOWER, M. R. Nuclear masses learned from a probabilistic neural network. **Phys. Rev. C**, American Physical Society, v. 106, p. 014305, Jul 2022. Available at: https://link.aps.org/doi/10.1103/PhysRevC.106.014305.

LU, H.; REN, Z.; BAI, D. Impacts of nucleon-nucleon short-range correlations on neutron stars. **Nuclear Physics A**, v. 1011, p. 122200, 2021. ISSN 0375-9474. Available at: https://www.sciencedirect.com/science/article/pii/S0375947421000658.

MARZOLA, I.; RODRIGUES Éverson H.; COELHO, A. F.; LOURENçO, O. **Strange stars admixed with dark matter: equiparticle model in a two fluid approach**. 2024. Available at: https://arxiv.org/abs/2408.16583.

MIAO, Z.; ZHU, Y.; LI, A.; HUANG, F. Dark matter admixed neutron star properties in the light of x-ray pulse profile observations. **The Astrophysical Journal**, The American Astronomical Society, v. 936, n. 1, p. 69, aug 2022. Available at: https://dx.doi.org/10.3847/1538-4357/ac8544.

MILLER, M. C.; LAMB, F. K.; DITTMANN, A. J.; BOGDANOV, S. *et al.* Psr j0030+0451 mass and radius from nicer data and implications for the properties of neutron star matter. **The Astrophysical Journal Letters**, The American Astronomical Society, v. 887, n. 1, p. L24, dec 2019. Available at: https://dx.doi.org/10.3847/2041-8213/ab50c5.

MILLER, M. C.; LAMB, F. K.; DITTMANN, A. J.; BOGDANOV, S. *et al.* The radius of psr j0740+6620 from nicer and xmm-newton data. **The Astrophysical Journal Letters**, The American Astronomical Society, v. 918, n. 2, p. L28, sep 2021. Available at: https://dx.doi.org/10.3847/2041-8213/ac089b.

Miller, M. C. *et al.* PSR J0030+0451 Mass and Radius from NICER Data and Implications for the Properties of Neutron Star Matter. , v. 887, n. 1, p. L24, dez. 2019.

Mondal, C.; Viñas, X.; Centelles, M.; De, J. N. Structure and composition of the inner crust of neutron stars from Gogny interactions. , v. 102, n. 1, p. 015802, jul. 2020.

Natarajan, P.; WILLIAMS, L. L. R.; BRADAč, M.; GRILLO, C.; GHOSH, A.; SHARON, K.; WAGNER, J. Strong lensing by galaxy clusters. **Space Science Reviews**, v. 220, n. 2, p. 19, 2024. Available at: https://doi.org/10.1007/s11214-024-01051-8.

NEGREIROS, R.; TOLOS, L.; CENTELLES, M.; RAMOS, A.; DEXHEIMER, V. Cooling of small and massive hyperonic stars. **The Astrophysical Journal**, The American Astronomical Society, v. 863, n. 1, p. 104, aug 2018. Available at: https://dx.doi.org/10.3847/1538-4357/aad049.

NELSON, A. E.; REDDY, S.; ZHOU, D. Dark halos around neutron stars and gravitational waves. **Journal of Cosmology and Astroparticle Physics**, v. 2019, n. 07, p. 012, jul 2019. Available at: https://dx.doi.org/10.1088/1475-7516/2019/07/012.

NEUFCOURT, L.; CAO, Y.; GIULIANI, S. A.; NAZAREWICZ, W.; OLSEN, E.; TARASOV, O. B. Quantified limits of the nuclear landscape. **Phys. Rev. C**, American Physical Society, v. 101, p. 044307, Apr 2020. Available at: https://link.aps.org/doi/10.1103/PhysRevC.101.044307.

Oertel, M.; Hempel, M.; Klähn, T.; Typel, S. Equations of state for supernovae and compact stars. **Reviews of Modern Physics**, v. 89, n. 1, p. 015007, jan. 2017.

OERTEL, M.; PROVIDÊNCIA, C.; GULMINELLI, F.; RADUTA, A. R. Hyperons in neutron star matter within relativistic mean-field models. **Journal of Physics G: Nuclear and Particle Physics**, IOP Publishing, v. 42, n. 7, p. 075202, 2015.

OPPENHEIMER, J. R.; VOLKOFF, G. M. On massive neutron cores. **Phys. Rev.**, American Physical Society, v. 55, p. 374–381, Feb 1939. Available at: https://link.aps.org/doi/10.1103/PhysRev.55.374.

OPPENHEIMER, J. R.; VOLKOFF, G. M. On massive neutron cores. **Phys. Rev.**, American Physical Society, v. 55, p. 374–381, Feb 1939. Available at: https://link.aps.org/doi/10.1103/PhysRev.55.374.

PAGE, D.; LATTIMER, J. M.; PRAKASH, M.; STEINER, A. W. Neutrino Emission from Cooper Pairs and Minimal Cooling of Neutron Stars. **Astrophys. J.**, v. 707, p. 1131–1140, 2009.

PATSYUK, M.; HEN, O.; PIASETZKY, E. Exclusive studies on short range correlations in nuclei. **EPJ Web Conf.**, v. 204, p. 01016, 2019.

Pelicer, M. R.; Menezes, D. P.; Dutra, M.; Lourenço, O. Do short range correlations inhibit the appearance of the nuclear pasta? **arXiv e-prints**, p. arXiv:2211.14002, nov. 2022.

PETRAKI, K.; VOLKAS, R. R. Review of asymmetric dark matter. **International Journal of Modern Physics A**, v. 28, n. 19, p. 1330028, 2013. Available at: https://doi.org/10.1142/S0217751X13300287.

Piekarewicz, J. The Nuclear Physics of Neutron Stars. **arXiv e-prints**, p. arXiv:2209.14877, set. 2022.

PIEKAREWICZ, J.; FATTOYEV, F. J. Impact of the neutron star crust on the tidal polarizability. **Phys. Rev. C**, American Physical Society, v. 99, p. 045802, Apr 2019. Available at: https://link.aps.org/doi/10.1103/PhysRevC.99.045802.

Planck Collaboration. Planck 2018 results - I. Overview and the cosmological legacy of Planck. **Astronomy & Astrophysics**, v. 641, p. A1, 2020. Available at: https://doi.org/10.1051/0004-6361/201833880.

POPOLO, A. D.; PACE, F.; DELLIOU, M. L. Constraints to dark matter from relaxed, massive cluster abundances. **Journal of Cosmology and Astroparticle Physics**, v. 2018, n. 2, p. 034, 2018.

POSTNIKOV, S.; PRAKASH, M.; LATTIMER, J. M. Tidal love numbers of neutron and self-bound quark stars. **Phys. Rev. D**, American Physical Society, v. 82, p. 024016, Jul 2010. Available at: https://link.aps.org/doi/10.1103/PhysRevD.82.024016.

POTEKHIN, A. Y.; De Luca, A.; Pons, J. A. Neutron Stars—Thermal Emitters. , v. 191, n. 1-4, p. 171–206, out. 2015.

RAMOS, A.; POLLS, A.; DICKHOFF, W. Single-particle properties and short-range correlations in nuclear matter. **Nuclear Physics A**, Elsevier, v. 503, p. 1–52, 1989.

REED, B. T.; FATTOYEV, F. J.; HOROWITZ, C. J.; PIEKAREWICZ, J. Implications of prex-2 on the equation of state of neutron-rich matter. **Phys. Rev. Lett.**, American Physical Society, v. 126, p. 172503, Apr 2021. Available at: https://link.aps.org/doi/10.1103/PhysRevLett.126.172503.

REINHARD, P. G. The relativistic mean-field description of nuclei and nuclear dynamics. **Reports on Progress in Physics**, v. 52, n. 4, p. 439, apr 1989. Available at: https://dx.doi.org/10.1088/0034-4885/52/4/002.

REINHARD, P.-G.; ROCA-MAZA, X.; NAZAREWICZ, W. Information content of the parity-violating asymmetry in ^{208}Pb. **Phys. Rev. Lett.**, American Physical Society, v. 127, p. 232501, Nov 2021. Available at: https://link.aps.org/doi/10.1103/PhysRevLett.127.232501.

RILEY, T. E.; WATTS, A. L.; BOGDANOV, S.; RAY, P. S. *et al.* A nicer view of psr j0030+0451: Millisecond pulsar parameter estimation. **The Astrophysical Journal Letters**, The American Astronomical Society, v. 887, n. 1, p. L21, dec 2019. Available at: https://dx.doi.org/10.3847/2041-8213/ab481c.

RILEY, T. E.; WATTS, A. L.; RAY, P. S.; BOGDANOV, S. *et al.* A nicer view of the massive pulsar psr j0740+6620 informed by radio timing and xmm-newton spectroscopy. **The Astrophysical Journal Letters**, The American Astronomical Society, v. 918, n. 2, p. L27, sep 2021. Available at: https://dx.doi.org/10.3847/2041-8213/ac0a81.

RING, P.; SCHUCK, P. **The nuclear many-body problem**. [*S.l.*]: Springer Science & Business Media, 2004.

RODRIGUES, E. H.; DUTRA, M.; LOURENçO, O. Recent astrophysical observations reproduced by a short-range correlated van der Waals-type model? **Monthly Notices of the Royal Astronomical Society**, v. 523, n. 4, p. 4859–4868, 06 2023. ISSN 0035-8711. Available at: https://doi.org/10.1093/mnras/stad1783.

ROMANI, R. W.; KANDEL, D.; FILIPPENKO, A. V.; BRINK, T. G.; ZHENG, W. Psr j09520607: The fastest and heaviest known galactic neutron star. **The Astrophysical Journal Letters**, The American Astronomical Society, v. 934, n. 2, p. L17, jul 2022. Available at: https://dx.doi.org/10.3847/2041-8213/ac8007.

ROSZKOWSKI, L.; SESSOLO, E. M.; TROJANOWSKI, S. Wimp dark matter candidates and searches—current status and future prospects. **Reports on Progress in Physics**, IOP Publishing, v. 81, n. 6, p. 066201, may 2018. Available at: https://dx.doi.org/10.1088/1361-6633/aab913.

Rubin, V. C.; Ford, W. K. Rotation of the Andromeda Nebula from a Spectroscopic Survey of Emission Regions. , v. 159, p. 379, fev. 1970.

Rüster, S. B.; Hempel, M.; Schaffner-Bielich, J. Outer crust of nonaccreting cold neutron stars. , v. 73, n. 3, p. 035804, mar. 2006.

RUTHERFORD, N.; RAAIJMAKERS, G.; PRESCOD-WEINSTEIN, C.; WATTS, A. Constraining bosonic asymmetric dark matter with neutron star mass-radius measurements. **Phys. Rev. D**, American Physical Society, v. 107, p. 103051, May 2023. Available at: https://link.aps.org/doi/10.1103/PhysRevD.107.103051.

Sagun, V. V.; Bugaev, K. A.; Ivanytskyi, A. I.; Yakimenko, I. P.; Nikonov, E. G.; Taranenko, A. V.; Greiner, C.; Blaschke, D. B.; Zinovjev, G. M. Hadron resonance gas model with induced surface tension. **European Physical Journal A**, v. 54, n. 6, p. 100, jun. 2018.

SAIKAWA, K.; YANAGIDA, T. T. Stellar cooling anomalies and variant axion models. **Journal of Cosmology and Astroparticle Physics**, v. 2020, n. 03, p. 007, mar 2020. Available at: https://dx.doi.org/10.1088/1475-7516/2020/03/007.

SANTOS, B. M.; DUTRA, M.; cO, O. Louren; DELFINO, A. Correlations between bulk parameters in relativistic and nonrelativistic hadronic mean-field models. **Phys. Rev. C**, American Physical Society, v. 92, p. 015210, Jul 2015. Available at: https://link.aps.org/doi/10.1103/PhysRevC.92.015210.

Sauls, J. A. Superfluidity in the Interiors of Neutron Stars. **arXiv e-prints**, p. arXiv:1906.09641, jun. 2019.

SCHUMANN, M. Direct detection of wimp dark matter: concepts and status. **Journal of Physics G: Nuclear and Particle Physics**, IOP Publishing, v. 46, n. 10, p. 103003, aug 2019. Available at: https://dx.doi.org/10.1088/1361-6471/ab2ea5.

SHEN, S.-H.; HU, J.-N.; LIANG, H.-Z.; MENG, J.; RING, P.; ZHANG, S.-Q. Relativistic brueckner—hartree—fock theory for finite nuclei. **Chinese Physics Letters**, IOP Publishing, v. 33, n. 10, p. 102103, oct 2016. Available at: https://doi.org/10.1088/0256-307x/33/10/102103.

Shlomo, S.; Kolomietz, V. M.; Colò, G. Deducing the nuclear-matter incompressibility coefficient from data on isoscalar compression modes. **European Physical Journal A**, v. 30, n. 1, p. 23–30, out. 2006.

SILVA, J.; LOURENçO, O.; DELFINO, A.; MARTINS, J. S.; DUTRA, M. Critical behavior of mean-field hadronic models for warm nuclear matter. **Physics Letters B**, v. 664, n. 4, p. 246–252, 2008. ISSN 0370-2693. Available at: https://www.sciencedirect.com/science/article/pii/S0370269308006175.

SKYRME, T. The effective nuclear potential. **Nuclear Physics**, Elsevier, v. 9, n. 4, p. 615–634, 1958.

Souza, L. A.; Dutra, M.; Lenzi, C. H.; Lourenço, O. Effects of short-range nuclear correlations on the deformability of neutron stars. , v. 101, n. 6, p. 065202, jun. 2020.

SOUZA, L. A.; DUTRA, M.; LENZI, C. H.; cO, O. Louren. Effects of short-range nuclear correlations on the deformability of neutron stars. **Phys. Rev. C**, American Physical Society, v. 101, p. 065202, Jun 2020. Available at: https://link.aps.org/doi/10.1103/PhysRevC.101.065202.

STONE, J. R.; STONE, N. J.; MOSZKOWSKI, S. A. Incompressibility in finite nuclei and nuclear matter. **Phys. Rev. C**, American Physical Society, v. 89, p. 044316, Apr 2014. Available at: https://link.aps.org/doi/10.1103/PhysRevC.89.044316.

THAKUR, P.; MALIK, T.; DAS, A.; JHA, T. K.; PROVIDÊNCIA, C. m. c. Exploring robust correlations between fermionic dark matter model parameters and neutron star properties: A two-fluid perspective. **Phys. Rev. D**, American Physical Society, v. 109, p. 043030, Feb 2024. Available at: https://link.aps.org/doi/10.1103/PhysRevD.109.043030.

TOLMAN, R. C. Static solutions of einstein's field equations for spheres of fluid. **Phys. Rev.**, American Physical Society, v. 55, p. 364–373, Feb 1939. Available at: https://link.aps.org/doi/10.1103/PhysRev.55.364.

TOLMAN, R. C. Static solutions of einstein's field equations for spheres of fluid. **Phys. Rev.**, American Physical Society, v. 55, p. 364–373, Feb 1939. Available at: https://link.aps.org/doi/10.1103/PhysRev.55.364.

TOLOS, L.; CENTELLES, M.; RAMOS, A. Equation of state for nucleonic and hyperonic neutron stars with mass and radius constraints. **Publications of the Astronomical Society of Australia**, v. 34, p. e065, 2017.

TOLOS, L.; CENTELLES, M.; RAMOS, A. The equation of state for the nucleonic and hyperonic core of neutron stars. **Publications of the Astronomical Society of Australia**, Cambridge University Press, v. 34, p. e065, 2017.

TONG, H.; WANG, C.; WANG, S. Nuclear matter and neutron stars from relativistic brueckner–hartree–fock theory. **The Astrophysical Journal**, IOP Publishing, v. 930, n. 2, p. 137, 2022.

TSANG, C.; TSANG, M.; DANIELEWICZ, P.; FATTOYEV, F.; LYNCH, W. Insights on skyrme parameters from gw170817. **Physics Letters B**, v. 796, p. 1–5, 2019. ISSN 0370-2693. Available at: https://www.sciencedirect.com/science/article/pii/S0370269319304575.

VAUTHERIN, D.; BRINK, D. M. Hartree-fock calculations with skyrme's interaction. i. spherical nuclei. **Phys. Rev. C**, American Physical Society, v. 5, p. 626–647, Mar 1972. Available at: https://link.aps.org/doi/10.1103/PhysRevC.5.626.

Viñas, X.; Gonzalez-Boquera, C.; Centelles, M.; Mondal, C.; Robledo, L. M. Unified Equation of State for Neutron Stars Based on the Gogny Interaction. **Symmetry**, v. 13, n. 9, p. 1613, set. 2021.

VOVCHENKO, V. Equations of state for real gases on the nuclear scale. **Phys. Rev. C**, American Physical Society, v. 96, p. 015206, Jul 2017a. Available at: https://link.aps.org/doi/10.1103/PhysRevC.96.015206.

VOVCHENKO, V.; ANCHISHKIN, D. V.; GORENSTEIN, M. I. Particle number fluctuations for the van der waals equation of state. **Journal of Physics A: Mathematical and Theoretical**, IOP Publishing, v. 48, n. 30, p. 305001, jul 2015a. Available at: https://dx.doi.org/10.1088/1751-8113/48/30/305001.

VOVCHENKO, V.; ANCHISHKIN, D. V.; GORENSTEIN, M. I. Van der waals equation of state with fermi statistics for nuclear matter. **Phys. Rev. C**, American Physical Society, v. 91, p. 064314, Jun 2015b. Available at: https://link.aps.org/doi/10.1103/PhysRevC.91.064314.

Vovchenko, V.; Gorenstein, M. I.; Stoecker, H. Modeling baryonic interactions with the Clausius-type equation of state. **European Physical Journal A**, v. 54, n. 2, p. 16, fev. 2018.

VOVCHENKO, V.; MOTORNENKO, A.; ALBA, P.; GORENSTEIN, M. I.; SATAROV, L. M.; STOECKER, H. Multicomponent van der waals equation of state: Applications in nuclear and hadronic physics. **Phys. Rev. C**, American Physical Society, v. 96, p. 045202, Oct 2017b. Available at: https://link.aps.org/doi/10.1103/PhysRevC.96.045202.

Walecka, J. D. A theory of highly condensed matter. **Annals of Physics**, v. 83, p. 491–529, jan. 1974.

XIANG, Q.-F.; JIANG, W.-Z.; ZHANG, D.-R.; YANG, R.-Y. Effects of fermionic dark matter on properties of neutron stars. **Phys. Rev. C**, American Physical Society, v. 89, p. 025803, Feb 2014. Available at: https://link.aps.org/doi/10.1103/PhysRevC.89.025803.

Xu, J.; Chen, L.-W.; Li, B.-A.; Ma, H.-R. Nuclear Constraints on Properties of Neutron Star Crusts. , v. 697, n. 2, p. 1549–1568, jun. 2009.

YOUNG, B.-L. A survey of dark matter and related topics in cosmology. **Frontiers of Physics**, v. 12, n. 2, p. 121201, 2016. ISSN 2095-0470. Available at: https://doi.org/10.1007/s11467-016-0583-4.

ZHANG, J.; LIU, H.-M.; LI, Z.; BURGIO, G. F.; SCHULZE, H. Nuclear liquid-gas phase transition within a brueckner-hartree-fock approach. **Chinese Physics C**, 2022. Available at: http://iopscience.iop.org/article/10.1088/1674-1137-/ac82e2http://iopscience.iop.org/article/10.1088/1674-1137/ac82e2.

ZHANG, Z.; CHEN, L.-W. Extended skyrme interactions for nuclear matter, finite nuclei, and neutron stars. **Phys. Rev. C**, American Physical Society, v. 94, p. 064326, Dec 2016. Available at: https://link.aps.org/doi/10.1103/PhysRevC.94.064326.

ZHANG, Z.; CHEN, L.-W. **Bayesian Inference of the Symmetry Energy and the Neutron Skin in ^{48}Ca and ^{208}Pb from CREX and PREX-2**. 2022.

ZUREK, K. M. Asymmetric dark matter: Theories, signatures, and constraints. **Physics Reports**, v. 537, n. 3, p. 91–121, asymmetric Dark Matter: Theories, signatures, and constraints, 2014. ISSN 0370-1573. Available at: https://www.sciencedirect.com/science/article/pii/S0370157313004341.

ZWICKY, F. On the Masses of Nebulae and of Clusters of Nebulae. , v. 86, p. 217, out. 1937.

Appendix A - Relativistic mean field models

The relativistic mean field model has its foundations in the model first proposed by Walecka (1974). In the original form, the model was proposed based on the Quantum Field Theory. It was composed of protons and neutrons interacting through the exchange of two kinds of mesons, the scalar mesons σ and vectorial mesons $\omega$with masses m_σ and m_ω, respectively. The exchange of the scalar mesons σ would be responsible for the attractive interaction. In contrast, the exchange of vectorial mesons would generate the repulsive part of the interaction.

The model is constructed from a Lorentz invariant Lagrangian, which gives to it a relativistic nature. Starting from the Lagrangian, after using a fields theory formalism, one can obtain thermodynamics quantities such as pressure and energy density, and in addition, characteristic quantities from the nuclear matter, such as saturation density and binding energy. For the pure Walecka model, the final form of the potential is (Walecka, 1974)

$$V(r) = -\frac{g_\sigma}{4\pi}\frac{e^{-m_\sigma r}}{r} + \frac{g_\omega}{4\pi}\frac{e^{-m_\omega r}}{r} \tag{A.1}$$

with g_σ and g_ω being choosen to fit nuclear matter observables quantities.

The model proposed by Walecka fails to reproduce some of the bulk parameter quantities such as the incompressibility of the nuclear matter in the saturation density and the effective nucleon mass. However, the model first proposed by Walecka has received many adjustments through the years, with several terms being added to apply this kind of description in different contexts. The modifications led the relativistic mean field models (RMF) to reproduce successfully many modern experimental data, from finite nuclei to nuclear matter in stellar environments. This fact has raised the RMF models to the most used and powerful descriptions in nuclear theory.

In a general way, one could write the Lagrangian considering several mesonic fields. Another possibility is to consider the mesonic field as sensitive to the medium, allowing

one to write density-dependent models.

For a detailed description, one could check Dutra *et al.* (2014) and references wherein. For practical purposes, we will consider a model with four mesonic fields, two vectorial and two scalar fields. The Lagrangian represented by

$$\mathcal{L} = \mathcal{L}_{mn} + \mathcal{L}_{\sigma} + \mathcal{L}_{\omega} + \mathcal{L}_{\rho} + \mathcal{L}_{\sigma\omega\rho} \tag{A.2}$$

with

$$\begin{aligned}
\mathcal{L}_{mn} &= \overline{\psi}[\gamma_{\mu}(i\partial^{\mu} - g_{\omega}\omega^{\ \mu} - g_{\rho}\vec{\rho}^{\ \mu}\ \vec{\tau}) - (M - g_{\sigma}\sigma)]\psi, \\
\mathcal{L}_{\sigma} &= -\frac{1}{2}m_{\sigma}^{2}\sigma^{2} + \frac{1}{2}\partial_{\mu}\sigma\partial^{\mu}\sigma - \frac{A}{3}\sigma^{3} - \frac{B}{4}\sigma^{4}, \\
\mathcal{L}_{\omega} &= +\frac{1}{2}m_{\omega}^{2}\ \omega_{\mu}\omega^{\mu} - \frac{1}{4}\omega_{\mu\nu}\omega^{\mu\nu} + \frac{C}{4}(g_{\omega}^{2}\omega_{\mu}\omega^{\mu})^{2}, \\
\mathcal{L}_{\rho} &= +\frac{1}{2}m_{\rho}^{2}\ \vec{\rho}_{\mu}\vec{\rho}^{\ \mu} - \frac{1}{4}\vec{\rho}_{\mu\nu}\vec{\rho}^{\ \mu\nu}, \\
\mathcal{L}_{\sigma\omega\rho} &= +\frac{1}{2}g_{\rho}^{2}\ \vec{\rho}_{\mu}\vec{\rho}^{\ \mu}\ \Lambda_{V}\ g_{\omega}^{2}\ \omega_{\mu}\omega^{\mu}.
\end{aligned} \tag{A.3}$$

The two last terms in $\mathcal{L}_{\sigma}$ are sometimes also written as

$$U(\sigma) = \frac{A}{3}\sigma^{3} + \frac{B}{4}\sigma^{4} = b_{\sigma}\frac{M(g_{\sigma}\sigma)^{3}}{3} + c_{\sigma}\frac{(g_{\sigma}\sigma)^{4}}{4}. \tag{A.4}$$

In the equation for $\mathcal{L}_{\omega}$ we have $C = c_{\omega}/g_{\omega}^{2}$. We also have that $\omega_{\mu\nu} = \partial_{\mu}\omega_{\nu} - \partial_{\nu}\omega_{\mu}$ and $\vec{\rho}_{\mu\nu} = \partial_{\mu}\vec{\rho}_{\nu} - \partial_{\nu}\vec{\rho}_{\mu}$ being the strength tensors for the fields ω and ρ. The mesons ψ stand for the nucleon field, σ and ω stand for the scalar and vectorial parts of the isoscalar field, and at last, $\vec{\rho}$ stand for the vectorial isovector field. It is worth mentioning that the Lagrangian $\mathcal{L}_{mn}$ concentrate the terms related to the interaction between the nucleons and the mesons. The lagrangians written as $\mathcal{L}_{j}$, with $j = \sigma, \omega, \rho$ bring the free and self-interacting terms of the mesons. The lagrangian with more than one greek subscript brings the terms due to crossed interactions between the meson fields.

Once composed the Lagrangian with the desired mesonic fields, one could write down the field equations by using the Euler-Lagrange equations (EL). However, that can not be immediately done. If one just uses the EL equations, the fields will be treated fully as quantum fields, which means considering the quantum fluctuations and the particle correlations. These effects will, many times, complicate considerably or even make impossible to calculate interesting quantities for nuclear physics in many nucleon systems. Therefore, the first required artifice is the mean-field approximation (MFA).

Within the mean-field approximation, all the quantum fluctuations disappear, since

it only uses the mean value of the field. This approach provides another simplification, since, in this approximation, the fields act on single nucleons independently (REINHARD, 1989).

The second approximation usually adopted in the RMF models is the no-sea approximation. In this case, the effects becoming from the Dirac sea are not taken into account. This approximation restrains the summation of the state's density to occupied particle states only, freeing one from calculating the vacuum polarisation effects by ignoring the antiparticle states. (REINHARD, 1989; GAMBHIR *et al.*, 1990).

Then, taking into account those approximations, one could write

$$\begin{aligned} &\sigma \to \langle\sigma\rangle \equiv \sigma, \qquad \omega_\mu \to \langle\omega_\mu\rangle \equiv \omega_0, \\ &\vec{\rho_\mu} \to \langle\vec{\rho_\mu}\rangle \equiv \overline{\rho}_0^{(3)}, \end{aligned} \tag{A.5}$$

The superscript (3) represents the third isospin component and the subscript 0 is the zeroth four-vector component.

From considerations (A.5), one can write the mean-field equations. One of the field equations, specifically the one deduced from the Lagrangian $\mathcal{L}_{mn}$, will be equivalent to the Dirac equation for a nucleon of effective mass $M^\star$. For our system, the effective mass will be $M^\star = M - g_\sigma\overline{\sigma}$, being M the nucleon mass. Furthermore, the field equations provide the relations needed to calculate the energy-momentum tensor $\mathcal{T}_{\mu\nu}$

$$\mathcal{T}_{\mu\nu} = -g_{\mu\nu}\mathcal{L} + \sum_i \frac{\partial\mathcal{L}}{\partial(\partial_\mu Q_i)}\partial_\nu Q_i. \tag{A.6}$$

In the MFA, the mean value of the time component $\mathcal{T}_{00}$ is the total energy density of the system, so $\langle\mathcal{T}_{00}\rangle = \epsilon$. Additionally, the total pressure is given by the mean value of the spatial component of $\langle\mathcal{T}_{ii}/3\rangle = P$.

For the Lagrangian (A.2), the pressure and energy density are

$$\begin{aligned} P = P^n_{kin} + P^p_{kin} - \frac{1}{2}\left[m_\sigma^2\overline{\sigma}^2 - m_\omega^2\overline{\omega_0}^2 - m_\rho^2(\overline{\rho}_0^{(3)})^2\right] - \frac{1}{3}b_\sigma(g_\sigma\overline{\sigma})^3 - \frac{1}{4}c_\sigma(g_\sigma\overline{\sigma})^4 + \frac{1}{4}c_\omega(g_\omega\overline{\omega}_0)^4 \\ + \frac{1}{2}(g_\rho\overline{\rho}_0^{(3)})^2\Lambda_V(g_\omega\overline{\omega_0})^2 \end{aligned} \tag{A.7}$$

and

$$\epsilon = \epsilon^n_{kin} + \epsilon^p_{kin} + \frac{1}{2}\left[m_\sigma^2\overline{\sigma}^2 + m_\omega^2\overline{\omega_0}^2 + m_\rho^2(\overline{\rho}_0^{(3)})^2\right] + \frac{1}{3}b_\sigma(g_\sigma\overline{\sigma})^3 + \frac{3}{4}c_\sigma(g_\sigma\overline{\sigma})^4 + \frac{1}{4}c_\omega(g_\omega\overline{\omega}_0)^4 + \frac{3}{2}(g_\rho\overline{\rho}_0^{(3)})^2\Lambda_V(g_\omega\overline{\omega_0})^2. \tag{A.8}$$

With the terms ϵ^j_{kin} being the kinetic part of the energy density and P^j_{kin} being the analogous quantity for the pressure. Once obtained the energy and pressure, other quantities such as the symmetry energy, the binding energy and the incompressibility can be equally found. These quantities can be compared to experimental data to establish values for the system parameters.

Expression (A.8) and (A.7) are a direct consequence of the Lagrangian construction. The RMF models are very heterogenous and changes in the Lagrangian constituents can change dramatically the form of the density energy and pressure. In this chapter, we have chosen the Lagrangian (A.2) due to the extensive analysis already done with it. As an example, one can cite the theoretical study about the symmetry energy done by (CAI; LI, 2016c). Another imperative work is the one by (Souza *et al.*, 2020) in which the model was also applied to the neutron stellar environment, reproducing satisfactorily several physical quantities. Both works have been used the described RMF model with the inclusion of SRC.

Appendix B - Short-range correlation foundations

The short-range correlation will promote the apparition of a high momentum tail in the fermions system. In this tail, the fermions will have momentum above the Fermi one. Thence, the particle distribution will change. The modified fermi distribution n_k^J has been extensively discussed in the past few years in the literature (CAI; LI, 2015a; HEN *et al.*, 2015b; CAI; LI, 2016a)

$$n_k^J(\rho, y) = \begin{cases} \Delta_J + \beta_j \ I(|\mathbf{k}/k_F^J|), & 0 < |\mathbf{k}| < k_F^J \\ C_J \ (k_F^J/|\mathbf{k}|)^4, & k_F^J < |\mathbf{k}| < \phi_J k_F^J \end{cases} \tag{B.1}$$

Inside the interval $0 < k < \infty$, it is expected to find all the nucleons. So, if one uses this normalization condition, one will found that

$$\frac{1}{(\pi)^2}\int_0^\infty n_k^J(\rho, y)k^2dk = \frac{1}{(\pi)^2}\left[\int_0^{k_F^J}[\Delta_J + \beta_j \ I(k/k_F^J)] \ k^2dk + \int_{k_F^J}^{\phi_J k_F^J}(k_F^J/k)^4 \ k^2dk\right] = \rho_J. \tag{B.2}$$

Using that the density is $\rho_j = (k_F^J)^3/3\pi^2$ and will result

$$\begin{gathered} \frac{1}{(\pi)^2}\left[\int_0^{k_F^J}[\Delta_J + \beta_j \ I(k/k_F^J)] \ k^2dk + \int_{k_F^J}^{\phi_J k_F^J}(k_F^J/|\mathbf{k}|)^4 \ k^2dk\right] = \frac{(k_F^J)^3}{3\pi^2} \\ \Delta_J + \frac{3\beta_J}{(k_F^J)^3}\int_0^{k_F^J}[\ I(k/k_F^J)] \ k^2dk + 3C_J\left(\frac{\phi_J - 1}{\phi_J}\right) = 1 \end{gathered} \tag{B.3}$$

The last term in (B.5) is the function that gives the fraction of nucleons with momentum higher than the Fermi one and is described by

$$\chi_J^{HMT} = \frac{3}{(k_F^J)^3}\int_{k_F^J}^{\phi_J k_F^J}(k_F^J/k)^4 \ k^2dk = 3C_J\left(\frac{\phi_J - 1}{\phi_J}\right). \tag{B.4}$$

The parameter β_J measures how intensively the depletion depends upon the momentum

near the Fermi surface. This factor promotes a very small alteration in the energy per nucleon and it can be taken as zero.

Now only two terms remain in (B.5). Isolating the Δ_J one will find the depletion as

$$\Delta_J = 1 - 3C_J \left(\frac{\phi_J - 1}{\phi_J} \right). \tag{B.5}$$

Now considering that investigations using the Bruenecker-Hartree-Fock have found that the energy must be linear with $\delta = 1 - 2y$, so the four parameters are expanded as $L^J = L_0^J(1 + L_0^J\delta)$. Considering the kinetic energy and the fact the linear part of it with δ must vanish, the relation $\Delta^n = -\Delta^p$, $C_n = C_p$ and $\phi_1 = \phi_0$. This information, linked to the generic form of the expansion $L^J = L_0^J(1 + L_0^J\delta)$ results for the cut-off parameters

$$\begin{aligned} \phi_n &= \phi_0(1 + \phi_1(1 - 2y)), \\ \phi_p &= \phi_0(1 - \phi_1(1 - 2y)), \end{aligned} \tag{B.6}$$

and for the amplitude

$$\begin{aligned} C_n &= C_0(1 + C_1(1 - 2y)), \\ C_p &= C_0(1 - C_1(1 - 2y)). \end{aligned} \tag{B.7}$$

The short-range correlation will also change the thermodynamic quantities of the system. In a free Fermi gas, pressure and energy density are calculated through an integration of the particle's momentum. If one is treating a system without the inclusion of SRC, the integral will be from the lower possible momentum, zero, to maximum one, k_F^J. But, as argued, now a fraction of the gas particles are in a correlated state with momentum higher than the Fermi momentum, $k_F^J\phi_J$.

In a general way, the modification induced by the SRC is of the form

$$\int_0^{k_F^J} n_{\mathbf{k}}^{J(FFG)} f d\mathbf{k} \rightarrow \int_0^{k_F^J\phi_J} n_{\mathbf{k}}^{J(HMT)} f d\mathbf{k} \tag{B.8}$$

where f is any quantity, $n_{\mathbf{k}}^{J(FFG)}$ is the step function that defines the distribution of the free Fermi gas, and $n_{\mathbf{k}}^{J(HMT)}$ is the distribution with the inclusion of SRC.

Directly, for a model such as the one described by (A.2), the kinetic part of the pressure becomes:

$$P_{kin}^J = \frac{\gamma\Delta_J}{6\pi^2} \int_0^{k_F^J} dk \, \frac{k^4}{\sqrt{M^{\star 2} + k^2}} + \frac{\gamma C_J}{6\pi^2} \int_{k_F^J}^{\phi_J k_F^J} dk \, \frac{(k_F^J)^4}{k^4\sqrt{M^{\star 2} + k^2}} \tag{B.9}$$

and the kinetic part of the energy density:

$$\epsilon^{J}_{kin} = \frac{\gamma\Delta_J}{2\pi^2}\int_0^{k_f^J} dk\ k^2\sqrt{M^{\star 2}+k^2}\ + \frac{\gamma C_J}{2\pi^2}\int_{k_f^J}^{\phi_J k_f^J} dk\ \frac{(k_f^J)^4}{k^2}\sqrt{M^{\star 2}+k^2}. \tag{B.10}$$

Additionally, the scalar density will also change in the exact same way that happens for (B.10) and (B.9). The modification in those quantities has a powerful effect on many characteristics of the system and even changes some structural properties of the NS, if one is considering this medium.

The seminal work by Pelicer *et al.* (2022), using the RMF IUFSU model has investigated the effects of the SRC in nuclear pasta. The authors were able to conclude, in this scope, that if one considers the SRC, the presence of nuclear pasta becomes highly related to the temperature. For a small change in temperature, no pasta phase will be found in the inner crust, whereas for a model without SRC pasta certainly exists in that region.

In addition, SRC also could affect the NS oscillations. Hong *et al.* (2022) have demonstrated that the inclusion of the SRC in the RMF theory using coupling parameters given by $SU(3)$ group changes the frequency of both oscillations: radial and non-radial. For the non-radial oscillation, the f-mode frequency decreases with the inclusion of SRC by a factor of $7.35\% \sim 11.57\%$. At this point, is worth mentioning that the f-mode is the main information source about non-radial oscillations of the NS received by the ground-based interferometers. For the radial oscillations, the authors have found a reduction in the frequency of approximately 22% for low massive NS ($1.4M_{\odot}$). Due to this huge alteration, the authors argue that the future Einstein Telescope and Cosmic Explorer detectors could directly test the SRC in NS.

Appendix C - High orders short-range correlations

High powers in short-range-correlation

The preeminence of the SRC has also led to studies of how modifications in the functional form of this phenomenon alter its effects. As argued by many papers in the first years following the observation of the SRC, the function that describes the HMT is usually of quartic form (HEN *et al.*, 2015b; CAI; LI, 2015a). However, the restriction over the form of the tail is very unfettered, as long as the number of observed high momentum nucleons stays next to the observed 20 to 25% of the total of nucleons (HEN *et al.*, 2015c; COLLE *et al.*, 2015).

In fact, a notable work by Guo *et al.* (2021a) has investigated the effects that the different shapes of SRC will promote in the production of hard photons. The authors have studied three different shapes for the SRC HMT: k^4, k^6 and k^9. The analysis done by the authors was concentrated in the hard photons emissions due to the reactions $^{14}\mathrm{N} + ^{12}\mathrm{C}$ and $^{48}\mathrm{Ca} + ^{124}\mathrm{Se}$ at beam energies around the Fermi energy. From the reactions, they analyzed the yields, angular distribution and energy spectra of the hard photons, leading them to important conclusions.

The first is related to the yields, which increase equally for all different powers of k in (B.2). The second is that the shape of the HMT does not affect the angular distribution of the produced hard photons. In this way, if one looks only at the yields of production or at the angular distribution, the shape seems not to be relevant.

The two first conclusions make the third one the most meaningful. The authors have calculated the effects of the HMT shape in the hard photons spectra, finding that this effect is considerable and should not be ignored. The effects are greater as greater are the energy of the photons (GUO *et al.*, 2021a).

Therefore, if one considers an NS environment, it is reasonable to consider that the shape of the HMT could promote relevant changes in the macrophysics of the NS. More

than that, some observables from NS could help to test the influence of the HMT, even if its microphysics is unknown. Motivated by that, we have calculated in the context of the RMF model, the pressure and energy density of HMT for shapes k^6, k^9 and for a generic shape k^m, all of that using the model (A.2).

From references where the quartic form of the HMT was studied (CAI; LI, 2015a; Souza *et al.*, 2020) one may notice that the change in the pressure and density energy happens only in the kinetic part of (A.7) and (A.8). Its calculations are straightforward, being necessary only to change the power of the last term to the shape of interest. The puzzling part is to calculate the coefficients of cut-off, amplitude and depletion. These coefficients C_n, ϕ_n and Δ_n, depends upon the constants C_0, C_1, ϕ_0 and ϕ_1. All these constants are determined using the normalization condition and the expression for the fraction of nucleons in the HMT, both clearly change with the shape. Considering this, we have calculated the modified constants C_0, C_1, ϕ_0 and ϕ_1. inasmuch as the cases k^6 and k^9 are specific forms for the most general k^m, we will do only this one.

The function that gives the nucleons fraction in HMT, for distribution of the kind

$$n_k^J(\rho, y) = \begin{cases} \Delta_J + \beta_j \; I(|\mathbf{k}/k_F^J|), & 0 < |\mathbf{k}| < k_F^J \\ C_J \; (k_F^J/|\mathbf{k}|)^m, & k_F^J < |\mathbf{k}| < \phi_J k_F^J \end{cases} \tag{C.1}$$

is

$$\begin{aligned} \chi_J^{HMT} &= \frac{3}{(k_F^J)^3} \int_{k_F^J}^{\phi_J k_F^J} (k_F^J/k)^m \; k^2 dk \\ &= \frac{C_J \; \left(1 - \phi_J^{3-m}\right)}{(m-3)}. \end{aligned} \tag{C.2}$$

what is the same as

$$\phi_J = \left(1 - \frac{\chi_J^{HMT}}{3C_J}(m-3)\right)^{1/(m-3)}. \tag{C.3}$$

From the above equation, one may notice that the C_J and ϕ_J are related by the fraction χ_J^{HMT}. If one considers the symmetric nuclear matter, equations (B.7) show that $C_n = C_p = C_0$. Furthermore, the cutoff parameter ϕ_0 is defined as $\phi_0 = 2.38$(CAI; LI, 2015a;

GUO *et al.*, 2021a). So

$$\begin{aligned}\phi_0 &= \left(1 - \frac{\chi_{SNM}^{HMT}}{3C_0}(m-3)\right)^{1/(m-3)} \\ C_0 &= \frac{\chi_{SNM}^{HMT}}{3(1-\phi_0^{(m-3)})}(m-3)\end{aligned} \tag{C.4}$$

where the fraction $\chi_{SNM}^{HMT} = 0.28$ (HEN *et al.*, 2015b; COLLE *et al.*, 2015; HEN *et al.*, 2015c). So, for any power m chosen, the term ϕ_0 is uniquely determined. To determine the constant C_1 one may consider again equations (B.7) but now in the pure neutron matter regime. That means $y = 0$, so $C_n^{PNM} = C_0(1 + C_1)$. But $C_n^{PNM} \approx 0.12$ (CAI; LI, 2015a) so

$$\begin{aligned}C_1 &= \frac{C_n^{PNM}}{C_0} - 1 \\ C_1 &= 3C_n^{PNM}\frac{(1-\phi_0^{(m-3)})}{\chi_{SNM}^{HMT}(m-3)}\end{aligned} \tag{C.5}$$

Another experimental constraint states that in pure neutron matter, only 1.5% of the neutrons correlate between themselves in high momentum pairs, so $\chi_{PNM}^{HMT} = 0.015$ (HEN *et al.*, 2015b). The expression for ϕ_n^{PNM}

$$\phi_n^{PNM} = \left(1 - \frac{\chi_{PNM}^{HMT}}{3C_n}(m-3)\right)^{1/(m-3)} \tag{C.6}$$

At last, using the expression (B.6) and (C.6), ϕ_1 is also determined

$$\begin{aligned}\phi_1 &= \frac{\phi_n^{PNM}}{\phi_0} - 1 \\ \phi_1 &= \frac{1}{\phi_0}\left(1 - \frac{\chi_{PNM}^{HMT}}{3C_n}(m-3)\right)^{1/(m-3)} - 1.\end{aligned} \tag{C.7}$$

In the table C.1, we have expressed the values for the calculated constants for the shapes k^4, k^6 and k^9. The first line $k^{4\dagger}$ brings values found using the calculation for a generic m of this work, which gives back the values of (CAI; LI, 2015a) for $m = 4$. They are disposed only to show consistency and for comparison purposes. The other two lines show the original and unpublished results, coming from this work.

TABLE C.1 – Constant values for different shapes

	ϕ_1	C_0	C_1
$k^{4\dagger}$	-0.561	0.160	-0.254
k^6	-0.560	0.302	-0.603
k^9	-0.559	0.563	-0.786

With the calculated coefficients one can easily write the energy density and pressure for any desired shaping power. We have calculated both quantities again for a generic shape m.

Beginning with the energy density, the integral

$$\epsilon^J_{kin} = \frac{\gamma\Delta_J}{2\pi^2}\int_0^{k_f^J} dk\ k^2\sqrt{M^{\star 2}+k^2}\ + \frac{\gamma C_J}{2\pi^2}\int_{k_f^J}^{\phi_J k_f^J} dk\ \frac{(k_f^J)^m}{k^{m-2}}\sqrt{M^{\star 2}+k^2}, \tag{C.8}$$

the next step was to evaluate this integral. Using concepts of mathematical physics (ARFKEN *et al.*, 2013; ABRAMOWITZ; STEGUN, 1964), one may recognize the second term in C.8 as a hypergeometric function. So the integration results in

$$\begin{aligned}\epsilon^J_{kin} = {} & \frac{C_J(k_F^J)^4}{\pi^2(m-4)} \\ & \times\left[\ {}_2F_1\left(-\frac{1}{2},\frac{m-4}{2};\frac{m-2}{2};-\frac{M^{\star 2}}{(k_F^J)^2}\right) - \phi_J^{4-m}\ {}_2F_1\left(-\frac{1}{2},\frac{m-4}{2};\frac{m-2}{2};-\frac{M^{\star 2}}{(k_F^J)^2\phi_J^2}\right)\right] \\ & + \frac{\Delta}{8\pi^2}\left[(k_F^J)\left(2(k_F^J)^2+M^{\star 2}\right)\sqrt{(k_F^J)^2+M^{\star 2}} + M^{\star 4}\log\left(\frac{\mathrm{Ms}}{\sqrt{(k_F^J)^2+M^{\star 2}}+(k_F^J)}\right)\right].\end{aligned} \tag{C.9}$$

Similarly, the pressure

$$P^J_{kin} = \frac{\gamma\Delta_J}{6\pi^2}\int_0^{k_F^J} dk\ \frac{k^4}{\sqrt{M^{\star 2}+k^2}} + \frac{\gamma C_J}{6\pi^2}\int_{k_F^J}^{\phi_J k_F^J} dk\ \frac{(k_F^J)^m}{k^{m-4}\sqrt{M^{\star 2}+k^2}} \tag{C.10}$$

results in

$$
\begin{aligned}
P^J_{kin} =& \frac{C_J (k_F^J)^4}{3\pi^2 (m-4)} \\
&\times \left[{}_2F_1\left(\frac{1}{2}, \frac{m-4}{2}; \frac{m-2}{2}; -\frac{M^{\star 2}}{(k_F^J)^2}\right) - \phi^{4-m}\, {}_2F_1\left(\frac{1}{2}, \frac{m-4}{2}; \frac{m-2}{2}; -\frac{M^{\star 2}}{(k_F^J)^2\phi^2}\right)\right] \\
&+ \frac{1}{24\pi^2}\left[\Delta_J k_F^J \left(2(k_F^J)^2 - 3M^{\star 2}\right)\sqrt{(k_F^J)^2 + M^{\star 2}} + 3\Delta_J M^{\star 4} \tanh^{-1}\left(\frac{k_F^J}{\sqrt{(k_F^J)^2 + M^{\star 2}}}\right)\right].
\end{aligned}
\tag{C.11}
$$

In the denominator of (C.11) and (C.9) there is a $(m-4)$ term. Due to this fact, it seems that there is a divergence if $m = 4$. However, in the limit of $m \to 4$ the subtraction of the hypergeometric functions also go to zero. So, applying the L'Hospital rule, the result found is exactly the results present in the literature (CAI; LI, 2015a; GUO *et al.*, 2021a).

The generalizations in this section allow one to choose any convenient shape for m. The generic expressions used to find the numerical values for the C_0 , C_1, ϕ_0, and ϕ_1 could be used to construct the cut-off parameters, the amplitude, and depletion.

This versatility is required since the exact shape of the SRC HMT is not exactly known, and the SRC effect have been recently under deep scrutiny. For example, experiments to investigate the contribution of the SRC in several nuclei including light nuclei such as ^{4}He, ^{6}Li, and ^{12}C (ARRINGTON *et al.*, 2022). The CLAS-12 collaboration aims to increase the data collection rate (PATSYUK *et al.*, 2019). In the Joint Institute for Nuclear Research in Dubna, an innovative inverse kinematics experiment has begun the measurements, from which sensitive information about knocked-out nucleons is expected to come.

Furthermore, the generalization done for the pressure and energy density never has been done in the literature. So, the pioneering calculations open ways to apply these quantities into the NS environments, testing in such medium every possible shape for the SRC. Also, we expect to guide future works with more complex models or with different effects included.

As future prospects, we expect to conclude the calculation of thermodynamics quantities by finding the scalar density, chemical potential, and incompressibility. From that point, we should be able to also find the symmetry energy, which is the last step before starting the application of this formalism to the stellar matter.

FOLHA DE REGISTRO DO DOCUMENTO

1. CLASSIFICAÇÃO/TIPO	2. DATA	3. DOCUMENTO Nº	4. Nº DE PÁGINAS
TD	10 de setembro de 2024	DCTA/ITA/TD-050/2024	96

5. TÍTULO E SUBTÍTULO:

Effects of dark matter and short-range correlations in neutron stars

6. AUTOR(ES):

Everson Henrique Rodrigues

7. INSTITUIÇÃO(ÕES)/ÓRGÃO(S) INTERNO(S)/DIVISÃO(ÕES):

Instituto Tecnológico de Aeronáutica – ITA

8. PALAVRAS-CHAVE SUGERIDAS PELO AUTOR:

Neutron Stars. Short-Range Correlations. Dark Matter. Nuclear Physics.

9. PALAVRAS-CHAVE RESULTANTES DE INDEXAÇÃO:

Estrelas de nêutrons; Matéria obscura; Correlação; Física nuclear; Física.

10. APRESENTAÇÃO: (**X**) **Nacional** ( ) **Internacional**

ITA, São José dos Campos. Curso de Doutorado. Programa de Pós-Graduação em Física. Área de Física Nuclear. Orientador: Prof. Dr. Odilon Lourenço da Silva Filho. Defesa em 22/10/2024. Publicada em 2024.

11. RESUMO:

In this study, we investigate the impact of dark matter (DM) and short-range correlations (SRC) on the physical properties of neutron stars (NS). In the second chapter we enhance a van der Waals-type model by incorporating the effects of short-range correlations (SRC). The attractive and repulsive components of the nucleon-nucleon interaction are treated as density-dependent functions. Specifically, we adopt the Carnahan–Starling (CS) approach for the repulsive term and employ a suitable expression for the attractive term to replicate the Clausius (C) real gas model structure. The resulting model, referred to as the Clausius–Carnahan–Starling (CCS)-SRC model, demonstrates its capability to reproduce the flow constraint at high-density regimes of symmetric nuclear matter, with incompressibility values within the range of $K_0 = (240 \pm 20)$ MeV.

In the context of stellar matter, the CCS-SRC model shows good agreement with recent astrophysical observations, including mass-radius contours and dimensionless tidal deformability constraints obtained from gravitational wave data associated with the GW170817 and GW190425 events, as well as observations from NASA's Neutron Star Interior Composition Explorer (NICER) mission. Furthermore, the slope of the symmetry energy (L_0) predicted by this model aligns with recent results, consistent with those reported by the updated Lead Radius Experiment (PREX-2) collaboration. Our findings indicate that higher values of L_0 are preferred for ensuring simultaneous compatibility with astrophysical data, while lower values of L_0 fail to meet this criterion.

In the third chapter, we incorporate dark matter (DM) and SRC into the relativistic mean-field model FSU2R using the fermionic and bosonic dark matter models. Both models include a repulsive vector interaction, which is particularly crucial for the bosonic model, as it prevents the collapse of the star in the absence of degeneracy pressure. We explore its effects on the mass-radius (MR) diagram. Our findings show that both fermionic and bosonic DM models influence the MR diagram in a similar manner. The inclusion of SRC results in a notable increase in the maximum mass of NS balancing the reduction yielded by the inclusion of DM. Our findings suggest the existence of potentially stable configurations of neutron stars that are consistent with observations from PSR J0030+0451, PSR J0740+6620 and NICER.

12. GRAU DE SIGILO:

(**X**) **OSTENSIVO** ( ) **RESERVADO** ( ) **SECRETO**